CONTAMINATION EFFECTS ON LIQUID RUBIDIUM AND LIQUID LITHIUM SYSTEMS

TECHNICAL DOCUMENTARY REPORT NO. ASD-TDR-63-413
May 1963

Air Force Aero Propulsion Laboratory
Aeronautical Systems Division
Air Force Systems Command
Wright-Patterson Air Force Base, Ohio

Project No. 8169, Task No. 816902

(Prepared under Contract No. AF 33(657)-8657
by Southwest Research Institute, San Antonio, Texas
W. D. Weatherford, Jr., Robert K. Johnston,
M. L. Valtierra, and J. W. Rhoades, authors).

NOTICES

When Government drawings, specifications, or other data are used for any purpose other than in connection with a definitely related Government procurement operation, the United States Government thereby incurs no responsibility nor any obligation whatsoever; and the fact that the Government may have formulated, furnished, or in any way supplied the said drawings, specifications, or other data, is not to be regarded by implication or otherwise as in any manner licensing the holder or any other person or corporation, or conveying any rights or permission to manufacture, use, or sell any patented invention that may in any way be related thereto.

Qualified requesters may obtain copies of this report from the Armed Services Technical Information Agency, (ASTIA), Arlington Hall Station, Arlington 12, Virginia.

This report has been released to the Office of Technical Services, U. S. Department of Commerce, Washington 25, D. C., for sale to the general public.

Copies of this report should not be returned to the Aeronautical Systems Division unless return is required by security considerations, contractual obligations, or notice on a specific document.

FOREWORD

The work described in this report was performed at Southwest Research Institute, San Antonio, Texas, under USAF Contract 33(657)-8657 Project 8169, Task 816902, and administered by the Air Force Aero Propulsion Laboratory, Aeronautical Systems Division, Air Force Systems Command, Wright-Patterson Air Force Base, Ohio. Mr. R. H. Herald of the Air Force Aero Propulsion Laboratory was the project engineer.

This report summarizes the work performed in the period of May 1, 1962 through April 15, 1963.

The authors wish to acknowledge the aid of E. L. Anderson, J. K. Campbell, R. D. Dietert, L. H. Krough, L. W. Lew, and W. A. Mallow who participated in various phases of the experimental program, and of C. C. Skipper who aided in the mechanical design of the experimental equipment.

ABSTRACT

A research program directed toward the goal of developing an improved understanding of contamination effects on liquid rubidium and liquid lithium systems is described. Experimental measurements were conducted on the vapor pressure of pure rubidium, the melting point of pure and oxygen-contaminated rubidium, and the melting point of pure and nitrogen-contaminated lithium. The results of this phase of the experimental program confirmed recently reported rubidium vapor pressure data, established that oxygen contaminant exists in rubidium as soluble rubidium monoxide, and revealed that lithium nitride precipitates from supersaturated lithium at relatively slow rates. A capillary viscometer was designed and constructed, and extensive viscosity data were measured for pure and oxygen-contaminated rubidium from less than 200°F to about 1200°F. The results revealed that oxygen contamination in rubidium can lead to significant viscosity increases, particularly in the region of the normal melting point, but to a much less extent at higher temperatures. Pumping experiments in an isothermal loop revealed that oxygen contamination is quite deleterious to the electromagnetic pumping characteristics of rubidium. A new method was developed for the analysis of carbon in rubidium, and it was shown that the butyl bromide method for oxygen analysis is not applicable to rubidium. An alternate oxygen-analysis procedure for rubidium, based upon melting-point measurements, is proposed. On the basis of the results and observations of this program regarding handling problems and contamination effects entering into reliability considerations, it is concluded that rubidium appears more promising than lithium (and possibly than potassium and sodium) for use as a working fluid in space power plants.

This technical documentary report has been reviewed and is approved.

H. E. GAMLI
Chief, Support Techniques Division
AF Aero Propulsion Laboratory

(138 pp) (52 fig.) (17 tbls..) (101 ref.)

TABLE OF CONTENTS

TABLE OF CONTENTS (Cont'd)

TABLE OF CONTENTS (Cont'd)

LIST OF ILLUSTRATIONS

LIST OF ILLUSTRATIONS (Cont'd)

LIST OF ILLUSTRATIONS (Cont'd)

LIST OF ILLUSTRATIONS (Cont'd)

LIST OF TABLES

I. INTRODUCTION

The anticipated uses of alkali metals as heat-transfer and energy-conversion fluids in nuclear and space applications have resulted in significant progress in alkali-metal technology. Several alkali-metal research programs are in progress, with their objectives being to establish reliable data on thermophysical properties, corrosion characteristics, lubrication performance, and working fluid capabilities. As such applications are developed, the need for specific fluid-systems support facilities and techniques will materialize. In order for such support to be most effective, improved knowledge of the role of contamination in alkali-metal fluids must be developed.

The program of research described in this report has been directed toward the goal of developing such an improved understanding of contamination effects on liquid rubidium and liquid lithium systems. This program has approached the problem along several parallel lines in order to bring the potential problem areas into better focus. Particular attention has been given to the influence of selected contaminants on properties such as melting point, viscosity, and electromagnetic pumping characteristics. It is the purpose of this report to review this experimental program, presenting the developed experimental data, and to further clarify the role of contamination in liquid rubidium and liquid lithium systems in the light of the experimental observations.

Manuscript released by authors April 1963 for publication as an ASD Technical Documentary Report.

II. BACKGROUND INFORMATION

A. Summary of Properties of Pure Rubidium and Pure Lithium

The following property information[90,91] is presented to serve as a basis for subsequent discussion and to emphasize the differences between rubidium and lithium. Recommended best values of rubidium and lithium property data are summarized in Tables 1 and 2.

Rubidium is a soft, silver-white alkali metal which is intermediate between cesium and potassium in its chemical and physical properties. It ignites spontaneously in dry air and also reacts violently with water, igniting the liberated hydrogen. Because of its chemical reactivity, it is usually immersed in a dry saturated hydrocarbon liquid or an inert gas atmosphere during storage and handling.

Lithium also is a silver-white alkali metal. It is the hardest, least volatile, and the least dense alkali metal. Among the alkali metals, it is the least reactive with oxygen and water, but the most reactive with nitrogen and hydrogen, and in some of its properties, lithium resembles the alkaline-earth metals, calcium, barium, and strontium. It is not tarnished by dry air below 100°C, but it reacts with moist nitrogen at ordinary temperatures to form a black deposit. As in the case of other alkali metals, lithium is immersed in a dry hydrocarbon liquid or inert gas atmosphere during storage and handling.

B. Survey of Handling and Uses of Rubidium and Lithium

As part of this program, visits were made to eight organizations to survey present practices and experiences regarding the role of contamination in liquid rubidium and liquid lithium systems. These organizations ranged from industrial and Government laboratories, having experience with the handling and uses of these fluids, through typical suppliers of rubidium and lithium. This survey yielded many comments and suggestions, and several of these are summarized in the following paragraphs.

1. Rubidium

It has been observed qualitatively that the viscosity of rubidium may be increased appreciably by the presence of contaminants. Moreover, it is believed that the saturation solubility of oxygen in rubidium is sufficiently great that saturation rarely will be encountered in practice. Plugging of system

TABLE 1. SUMMARY OF PROPERTIES OF RUBIDIUM

Property	Value	Temp(°F)	Data Basis
Physical:			
Atomic Weight	85.48	--	Experimental
Melting Point, °F	102.9	--	Experimental
Boiling Point, °F	1266	--	Experimental
Critical Point, atm	188	3480	Estimated
Density of Solid, lb/ft^3	95.518	68	Handbook
Density of Liquid, lb/ft^3	94.3	M.P.	Experimental
Density of Vapor, lb/ft^3	0.0708	B.P.	Theoretical
Viscosity of Liquid, lb/ft hr	1.64	M.P.	Experimental
Viscosity of Vapor, lb/ft hr	0.061	B.P.	Theoretical
Surface Tension, lb/ft	0.0053	M.P.	Experimental
Thermal:			
Thermal Conductivity of Liquid, BTU/hr ft °F	11.65	B.P.	Unknown
Thermal Conductivity of Vapor, BTU/hr ft °F	0.00482	B.P.	Estimated
Specific Heat of Liquid, BTU/lb°F	0.0877	B.P.	Estimated
Specific Heat of Vapor, BTU/lb °F	0.0578	B.P.	Theoretical
Latent Heat of Fusion, BTU/lb	11.79	M.P.	Survey
Latent Heat of Vaporization, BTU/lb	347.8	B.P.	Theoretical
Electrical and Magnetic:			
Resistivity, μ ohm-inch	9.1	M.P. liq	Experimental
Ionization Potential, volts	4.126		Experimental
Magnetic Susceptibility, fps electromagnetic units/unit mass	0.0379	64.4 sol	Handbook

TABLE 2. SUMMARY OF PROPERTIES OF LITHIUM

Property	Value	Temp (°F)	Data Basis
Physical:			
Atomic Weight	6.94	--	Experimental
Melting Point, °F	359.2	--	Experimental
Boiling Point, °F	2430	--	Theoretical
Critical Point, atm	--	6940	Estimated
Density of Solid, lb/ft^3	33.338	68	Handbook
Density of Liquid, lb/ft^3	31.8	M.P.	Experimental
Density of Vapor, lb/ft^3	0.00375	B.P.	Theoretical
Viscosity of Liquid, lb/ft hr	1.45	M.P.	Experimental
Viscosity of Vapor, lb/ft	0.0473	B.P.	Theoretical
Surface Tension, lb/ft	0.027	M.P.	Experimental
Thermal:			
Thermal Conductivity of Liquid, BTU/hr ft °F	26.54	M.P.	Extrapolated
Thermal Conductivity of Vapor, BTU/hr ft °F	0.0459	B.P.	Estimated
Specific Heat of Liquid, BTU/lb °F	0.979	B.P.	Extrapolated
Specific Heat of Vapor, BTU/lb °F	0.708	B.P.	Theoretical
Latent Heat of Fusion, BTU/lb	186	M.P.	Calculated
Latent Heat of Vaporization, BTU/lb	8338	B.P.	Theoretical
Electrical and Magnetic:			
Resistivity, μ ohm-inch	9.5	M.P. liq	Experimental
Ionization Potential, volts	5.39	--	Experimental
Magnetic Susceptibility, fps electromagnetic units/unit mass	1.0198	367 liq	Survey
Thermal Neutron Cross Section (2200 m/s)			
Absorption, barns	71.0 ± 1.0	--	Handbook
Scattering, barns	1.4 ± 0.3	--	Handbook

components such as that commonly experienced with sodium and potassium has not been encountered with rubidium under similar conditions. This observation suggests that the oxides of rubidium are much more soluble in rubidium than are the oxides of potassium in potassium.

An example of the changes in trace metals content in rubidium following exposure to type 316 stainless steel indicated only slight changes in most components. However, the exposed rubidium appeared to have picked up some silicon, copper, and chromium while losing some aluminum, nickel, tin, lead, and beryllium. The total concentration of transition metals in unfiltered samples of as-received rubidium is usually less than 50 ppm.

A suitable purification technique recommended for rubidium involves distillation over 50-50 titanium-zirconium chips at 1000-1100°F during a period of about 24 hours. Oxygen determination procedures include mercury amalgamation method, n-butyl bromide method, and neutron activation analysis. However, the absolute accuracy of these methods has not been established for rubidium. It is suspected that the mercury amalgamation method may suffer because of the possibly appreciable solubility of rubidium oxide in mercury. In fact, difficulties have been experienced in the application of this method to the analysis of cesium where impossibly low oxygen contents of 0.0 ppm have been obtained. It is believed that neutron activation analysis of rubidium should be satisfactory for oxygen contents in excess of about 50 ppm. Nitrogen content may be measured by more-or-less standard Kjeldahl procedures, and analysis for carbon may be achieved by combustion followed by measurement of carbon dioxide.

2. Lithium

It has been observed that low-carbon lithium may extract carbon from high-carbon alloys. In fact, evolution of acetylene gas when lithium is reacted with water occurs only when the lithium contains carbide carbon which has been thus extracted from container alloys. The garlic odor usually attributed to acetylene formation has been observed when no carbon is present in the lithium, and it is now believed that this odor results from minute traces of phosphorous compounds.

Lithium has not been observed to experience nitriding at its melting point in air in the absence of water, although it does undergo some oxidation. On the other hand, the presence of water appears to catalyze the nitriding and oxidizing reactions. It has been observed also that the presence of as little as 0.1% sodium renders lithium about 100 times more reactive toward moisture than is pure lithium. Reactor grade lithium, containing 50-60 ppm sodium, is not very reactive.

It was recommended that contact of lithium with organic compounds should be avoided. Purified inert gases such as argon or helium should be used for blanketing purposes, and all manipulations should be conducted in a dry box. Lithium may be handled briefly in air, and the resulting surface contamination may be removed simply by rinsing with water. It was observed in some cases that positive-flow cold traps appear to reduce the nitrogen content of liquid lithium systems. Vacuum distillation also has been observed to reduce the nitrogen content of lithium containing less than 300 ppm of nitrogen.

The n-butyl bromide method of analysis for oxygen content is not applicable to lithium. It was suggested that the mercury amalgamation method could be adapted for use with lithium by applying an appropriate correction for nitrogen content. However, lithium does not amalgamate as well as do the other alkali metals, and such a procedure would be a nonroutine method requiring a professional operator. It is believed that neutron activation analysis represents the only method presently available for measurement of oxygen in lithium. A modified Kjeldahl method is commonly employed for nitrogen analysis in lithium and the combustion method is used for carbon analysis. Polyethylene containers are employed in wet analysis of lithium in order to avoid adsorption or reaction with glass during dissolution.

C. Production and Purification Methods for Rubidium and Lithium

Four types of processes are commonly employed for producing alkali metals. These include: electrolytic, reduction, metal displacement, and thermal decomposition. Electrolytic methods involving the chloride salt are commonly employed for lithium. Thermal reduction with carbon or carbides and metal displacement reactions, dependent upon equilibrium being shifted by the selective vaporization of the more volatile alkali metal, are more common for rubidium preparation.

Rubidium is commonly associated as a minor constituent with potassium in micas, feldspars, and other pegmatitic minerals[5]. Although rubidium does not occur as an essential constituent in any known mineral, it is present as a minor component in many minerals, and it is more abundant than lead. Rubidium is produced from the lithium mineral, lepidolite, and as a by-product of other mineral refining processes.

Lithium chloride concentrate is prepared from various ores by high temperature substitution reactions. Lithium occurs in typical ores as phosphates and aluminum silicates. Spodumene (lithium aluminum silicate) represents the most abundant lithium-containing mineral. It and lepidolite (lithium fluoro potassium aluminum silicate-i.e., lithium potassium mica) are the

most commonly employed lithium ores[32, 71]. Typical reagents employed in winning lithium from various ores are sulfuric acid, limestone (calcium carbonate), potassium bisulfate, and calcium chloride. Lithium salts other than the chloride thus produced are extracted with water and converted to the carbonate with soda ash (sodium carbonate) or carbon dioxide. The purified carbonate is converted to the chloride with hydrochloric acid. Before electrolysis, dried lithium chloride is mixed with potassium to form a low-melting chloride eutectic (~850°F), and this eutectic mixture is electrolyzed to produce metallic lithium.

In alkali metal oxides, the ratio of oxygen to metal in the most stable form increases with increasing molecular weight[81]. Accordingly, lithium monoxide is the most stable of the lithium oxides whereas rubidium superoxide is the most stable form of rubidium oxides. In the case of rubidium, oxide contaminant may be removed by hot gettering with substances such as titanium or zirconium. The efficacy of such gettering processes stems from the favorable free energy relationships of the gettering material oxides relative to the oxides of rubidium[35]. In the case of lithium, however, both nitrogen and oxygen impurities are significant. Although titanium and zirconium should be effective for removing nitrogen, free energy relationships favor their losing oxygen to lithium rather than gettering oxygen from lithium oxide[35]. Investigations are being conducted in other laboratories of the possible use of yttrium for gettering both oxygen and nitrogen in lithium, and preliminary results appear encouraging. However, before such a method can be accepted as practical, further study of the solubility of yttrium in lithium should be undertaken.

Conflicting results have been reported for the efficacy of vacuum distillation for the purification of lithium. However, it appears that such distillation at pressures less than 10^{-4} torr, in the presence of appropriate gettering material, should be effective for reducing the oxygen, nitrogen, and carbon content to low levels[4, 34, 35].

Previous experimental studies of lithium purification by cold trapping have not clearly established the efficacy of such techniques for the removal of oxygen and nitrogen[4, 34, 35]. In fact, solubility data which are presented in Figures 1 and 2 indicate that lithium nitride may be appreciably soluble in lithium at the melting point and that lithium monoxide is not.

D. Role of Contamination in Liquid Rubidium and Liquid Lithium Systems

The presence of contaminants in alkali metals may exert deleterious effects on thermophysical properties, corrosivity, and handling characteristics. It is conceivable that low concentrations of certain contaminants could be beneficial at low temperatures whereas the same degree of contamination

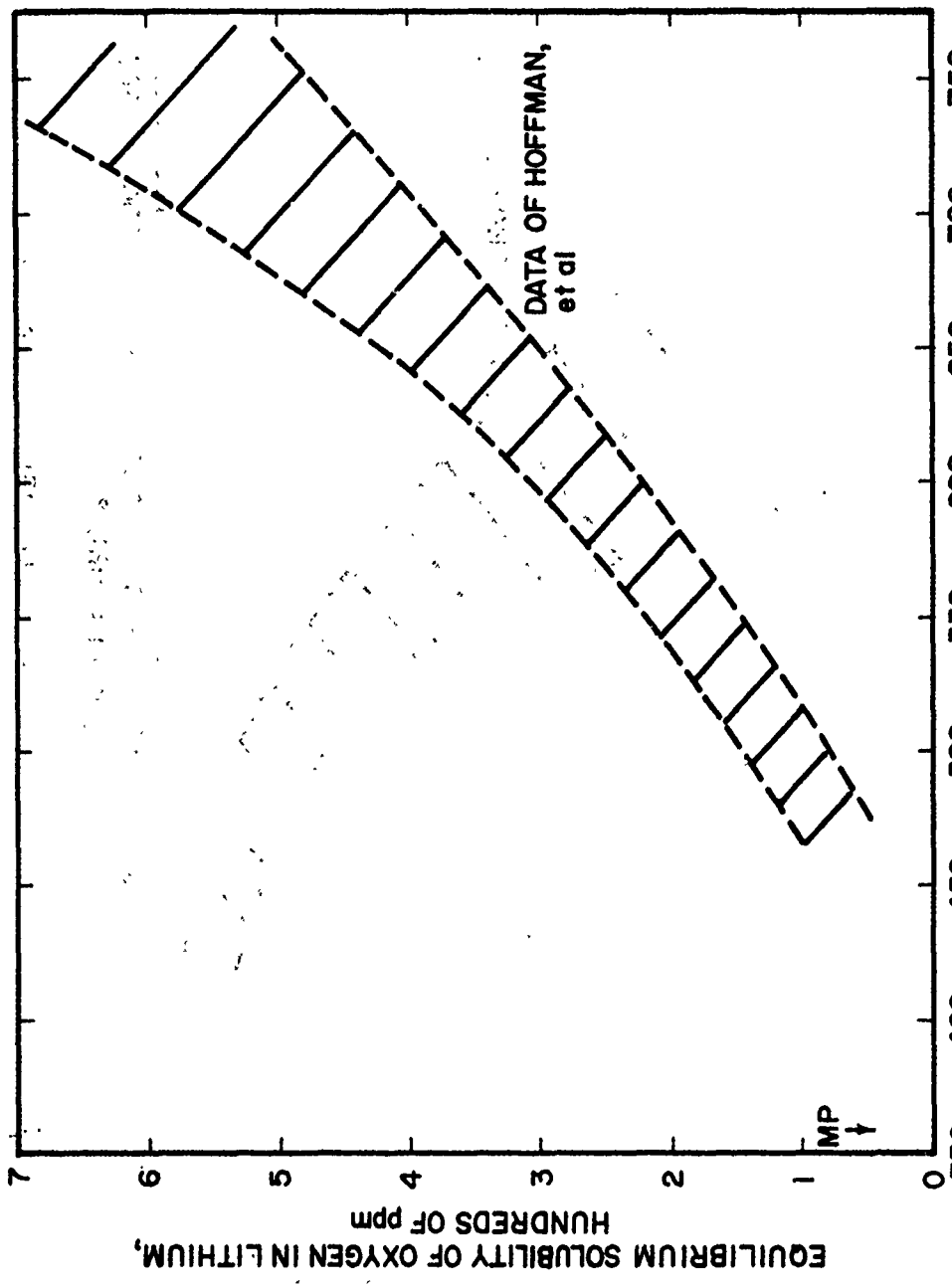

FIGURE 1. SOLUBILITY OF OXYGEN IN LITHIUM

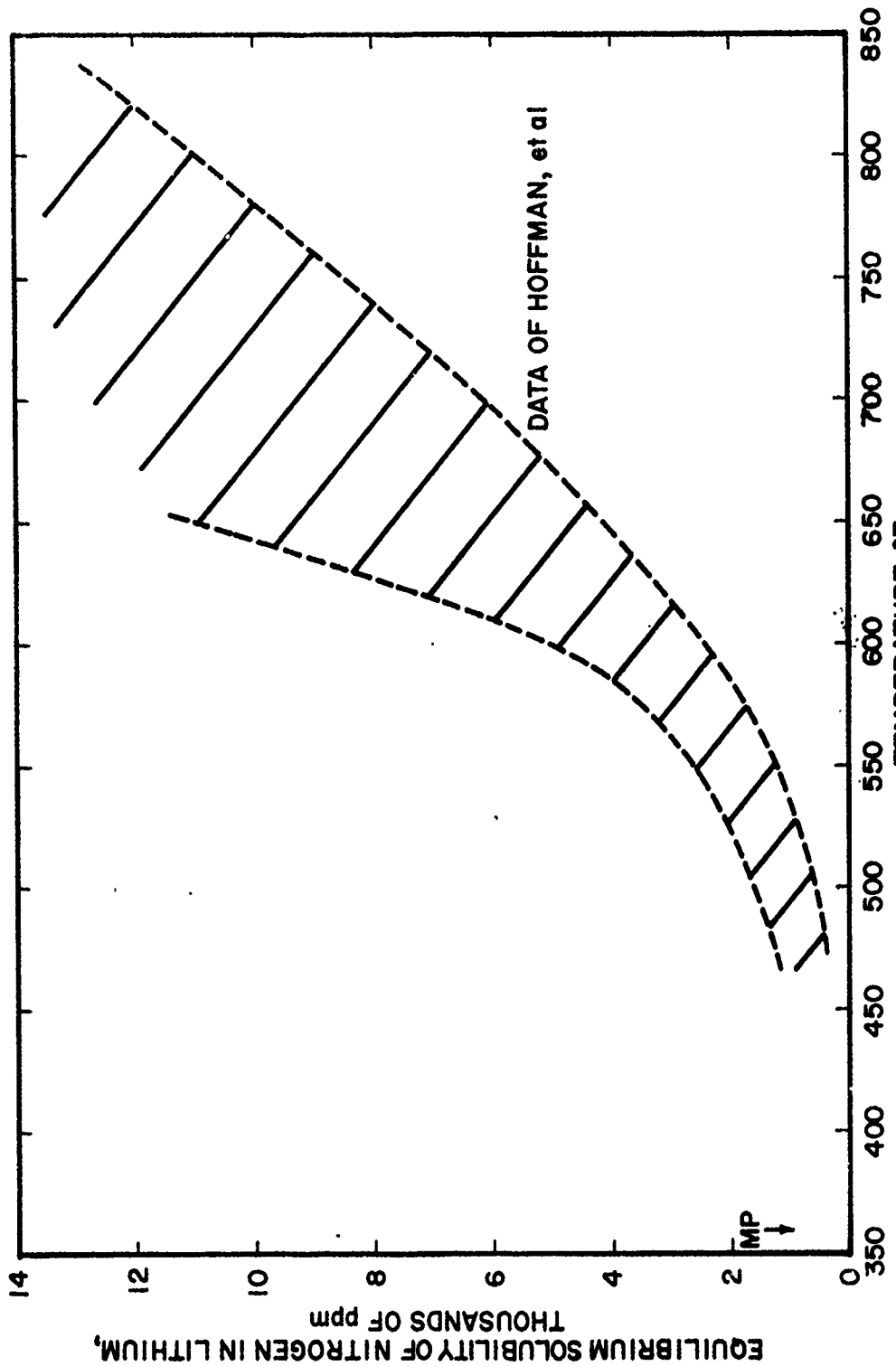

FIGURE 2. SOLUBILITY OF NITROGEN IN LITHIUM

could prove deleterious at higher temperatures. As a case in point, it has been observed that low concentrations of certain contaminants depress the melting point of rubidium and thereby may reduce room-temperature handling problems. Moreover, it is believed that low concentrations of oxygen in rubidium could provide a benficial additive effect in low-temperature bearing lubrication applications. On the other hand, even low concentrations of oxygen in rubidium are known to magnify corrosion problems in high-temperature applications.

Extensive investigation is required in order to fully establish the influence of contamination on thermophysical and handling properties. The experimental investigation discussed in this report has been directed toward determining some of these contamination effects.

1. Contamination Mechanisms and Kinetics

Contamination of alkali-metal fluids may stem from several sources. The presence of extraneous constituents in the raw materials and the introduction of contaminants during manufacture represent two distinct categories of contamination sources. Substances which may be dissolved or dislodged from alkali-metal storage, handling, or application systems represent a third contamination-source category. Constituents of the atmosphere provide a fourth source of contamination. Control of contamination from the first two categories is inherently dependent upon the state of manufacturing technology and the specified purity requirements for a particular application. System-derived contamination may result from inadequate or improper cleaning and preparation procedures, or from corrosion or erosion processes within the system. In the latter case, liquid alkali metals are noted for their tendencies to dissolve or attack container materials, particularly at high temperatures. However, such corrosion problems can be minimized in many cases by appropriate selection of container materials and fluid-purity requirements. Atmospheric-source contamination, on the other hand, represents an ever-present vulnerability of terrestrial alkali-metal storage, handling, and application systems. Accidental occurrences, equipment failures, or improper techniques can rapidly and effectively poison an alkali metal for its intended use. In such cases, the attendant delays and expense of reprocurement or repurification could adversely affect the success of the intended application.

At the present state of the art, very little quantitative information is available regarding the rate of absorption or reaction of various contaminants with liquid rubidium or lithium. In most cases, such contamination rates are extremely rapid, as is illustrated by the following discussion of rubidium oxidation.

Because of the extreme chemical reactivity of rubidium, the rate at which contaminants such as oxygen may be absorbed is apparently limited

only by nonchemical processes. Physical processes such as fluid friction, diffusion through a stagnant nonreactive gas, or diffusion through reaction products may contribute significant inhibition to contamination rates. However, diffusion of a gaseous contaminant such as oxygen through solid or liquid reaction products appears to be extremely rapid. During one portion of this study, a stream of pure oxygen was admitted to a glass ampoule containing several grams of solid rubidium at room temperature. The oxygen was absorbed as rapidly as it could be supplied, and a thermocouple, cemented to the base of the ampoule, indicated temperatures in excess of 600°F within several seconds. In other experiments, it was found impossible to achieve a significant pressure of oxygen in a previously evacuated system containing rubidium. In this case, the rate of oxygen addition appeared to be controlled by the pressure drop in the lines leading into the apparatus. In fact, the pressure returned to the original vacuum conditions as soon as oxygen admission was terminated.

In view of the foregoing observations, it is apparent that specialized kinetic equipment would be necessary for conducting meaningful studies of the chemical kinetics of oxygen-rubidium reactions. On the other hand, reasonable theoretical estimates of absorption rates may be made in cases where rate-controlling physical processes are evident. The following hypothetical case illustrates the prediction of such absorption-rate information.

Consider the storage of liquid rubidium in a container such as that illustrated in the sketch of Figure 3. The fill-pipe (or vent) contains an inert gas, such as argon, at atmospheric pressure, and the liquid level is near the bottom of this pipe. If the fill-pipe closure is removed, the rate at which atmospheric oxygen will diffuse through the inert gas blanket to the rubidium interface may be calculated with well established gaseous diffusion theory. For this case, it is assumed that oxygen reacts instantaneously upon contact with rubidium and that diffusional processes in the condensed phase are not rate-limiting. The molecular concentrations of carbon dioxide and water in the atmosphere are significantly lower than those of oxygen; therefore, contamination by these atmospheric constituents is neglected in this example.

The oxygen absorption rate, predicted on this basis, is presented in Figure 3. For purposes of this presentation, the length of empty tube, L, its cross-sectional area, A, and the total inventory of liquid, Q, are grouped together as one parameter. Consequently, this graph provides a generalized correlation for estimating possible rates of contamination of stored liquid rubidium by atmospheric oxygen when a fill-pipe or vent is accidentally opened to the atmosphere. It cannot be over-emphasized at this point that the described hypothetical case represents a potentially hazardous situation. In such a case, it is quite probable that hydrogen gas would accumulate in the vent as a result of

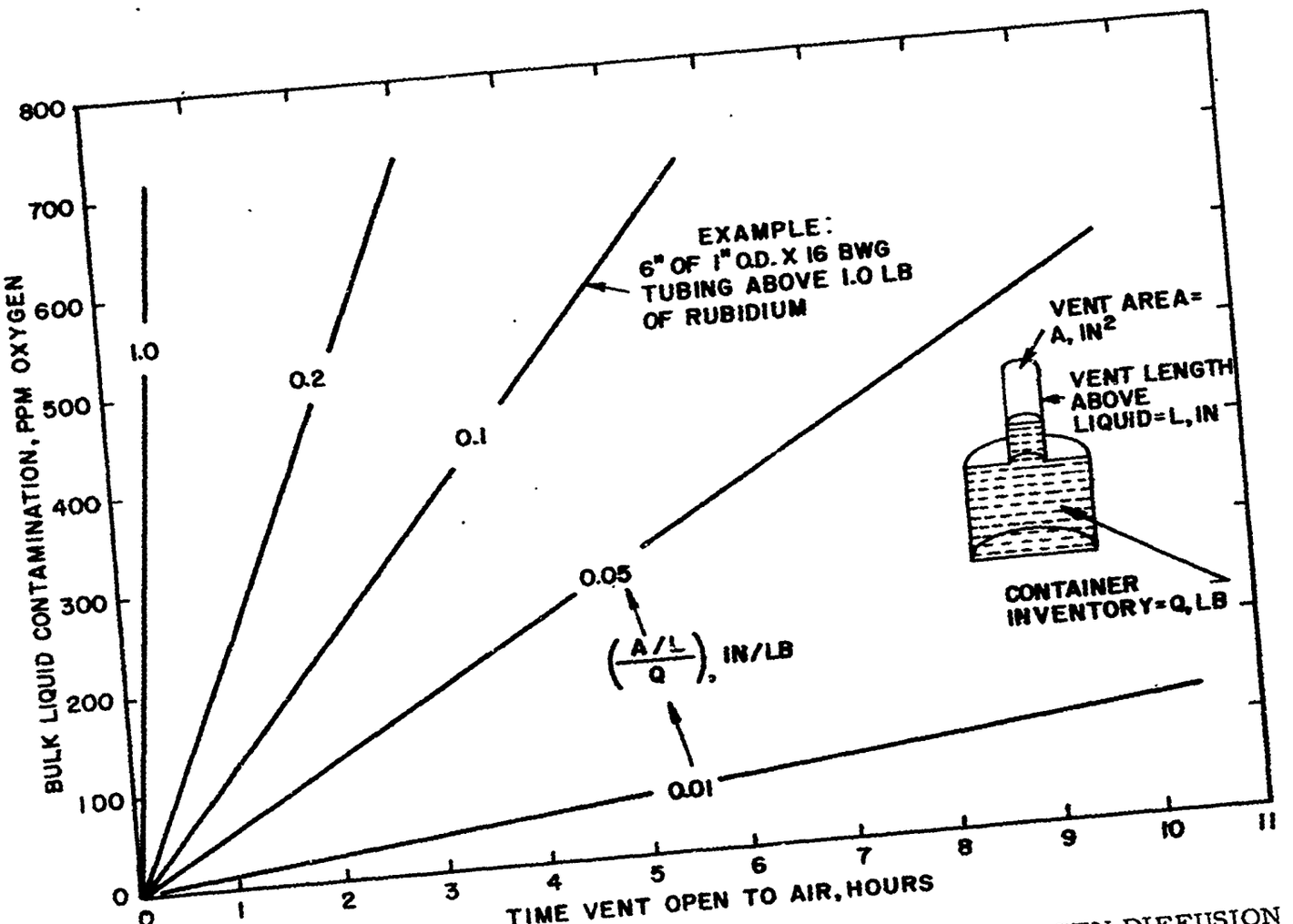

FIGURE 3. RATE OF CONTAMINATION OF RUBIDIUM BY OXYGEN DIFFUSION THROUGH VENT OPEN TO DRY, CO_2-FREE AIR

the reaction of atmospheric moisture with the rubidium, and an explosion could be ignited by the high interfacial temperature generated by the contamination reactions. If the resulting hydrogen-oxygen detonation wave should rupture the vent or container, an extremely hazardous conflagration could result.

When liquid lithium is exposed to ambient moist air, water vapor, moist argon, moist oxygen, or moist nitrogen, the metal surface turns black, It has been observed that the black coating contains anhydrous lithium hydroxide. It is currently believed that the black color represents amorphous lithium metal covered by a transparent film of lithium hydroxide (in the past, it has been assumed that the black color was due solely to lithium nitride).[51]

A recent experimental publication on the kinetics of nitridation of lithium[54] has shown that the rate of absorption of nitrogen by liquid lithium is independent of the nitrogen pressure. Moreover, these data reveal that the rate of nitrogen absorption is inversely proportional to the cumulative quantity of nitrogen absorbed (parabolic law). These results indicate that diffusion of lithium metal through a film of lithium nitride is the rate controlling step in the absorption of nitrogen gas. Additional calculations have been made with the reported experimental data, *and the results indicate that the rate constant for the absorption at 650°F is about 3×10^{-7} grams of nitrogen gas absorbed (squared) per square centimeter of nitriding surface (squared) per second, i.e.-- 3×10^{-7} $(gm/cm^2)^2/sec$.

2. Sources and Extent of Contamination

Critical reviews of the literature and of current alkali-metal production and handling practices have revealed several most probable sources of contaminants (see References). Typical sources are summarized in Table 3, and typical concentration ranges for common contaminants present in rubidium and lithium after manufacture are illustrated in Table 4.

---

*The published rate-constant data cannot be used because these rate constants and the resulting activation energy are erroneous. Wrong-order rate constants were correlated in determining the activation energy.

TABLE 3. TYPICAL CONTAMINANT SOURCES

Fluid	Contaminant	Probable Sources
rubidium	lithium	mineral
	sodium	mineral or glassware
	potassium	mineral
	cesium	mineral
	silicon	mineral or glassware
	heavy metals	mineral or corrosion products
	carbon	protective hydrocarbon or atmosphere
	oxygen	atmosphere
lithium	sodium	mineral
	chlorine	electrolyte*
	iron	cathode*
	iron and other heavy metals	mineral or corrosion products
	carbon	anode*
	oxygen and nitrogen	atmosphere

*LiCl electrolytic reduction cell

TABLE 4. TYPICAL CONTAMINANT CONCENTRATION RANGES

Fluid	Contaminant	Concentration Range, ppm
rubidium	lithium	20 - <50
	sodium	100 - 900
	potassium	<200 - 1400
	cesium	216 - 7300
	silicon	31 - 950
	iron	<5 - 24
	nickel	<4
	chromium	<3
	oxygen	16 - >500
lithium	sodium	50 - 1500
	potassium	70 - 1000
	calcium	1 - 500
	chlorine	20 - 2000
	aluminum	10 - 100
	iron	5 - 400
	nickel	10 - 165
	chromium	<6 - 115
	silicon	10 - 150
	nitrogen	10 - 310

III. EXPERIMENTAL PROGRAM

A. Experimental Facilities

1. Laboratory Facilities

This experimental program was performed in a laboratory designed especially for this purpose. The laboratory and some of its facilities are illustrated in Figures 4 and 5. It is provided with an argon inerting system, capable of serving the various experimental devices.

Two evacuatable, stainless steel glove boxes were developed for use on this program, one for the liquid metals laboratory and one for the analytical chemistry laboratory. This glove box, which is illustrated in Figures 6 and 7, is provided with a hemispherical plastic dome [similar to that used by ORNL[35]], three glove ports, and a gas-lock chamber. It is also equipped with electrical and inert-gas utility connections.

An enclosed cell is provided for alkali-metal pumping operations. This cell contains a separate ventilation system and a safety blow-out panel in an exterior wall. A remote-control panel is located adjacent to this cell. Pressurized alkali-metal fire extinguishers and separate hand dispensing fire-extinguisher cartons are located centrally for use in coping with possible alkali-metal fires. A forced-ventilation storage vault (converted refrigerator) is provided outside of and adjacent to the liquid metals laboratory. A disposal pit suitable for the burning of large quantities of alkali-metals is located nearby. First aid supplies and complete instructions for their use are located conveniently in the laboratory.

2. Handling

In view of the fact that this experimental program has been directed toward studying the influences of contamination, extreme precautions have been taken in order to minimize the possibility of unintentional contamination during handling operations. Consequently, detailed operating procedures have been enumerated for use as standard laboratory procedures, and these procedural details are presented in the Appendix. A simple transfer vessel which has been employed extensively in this study is illustrated in Figure 8. Techniques have been devised for transferring alkali metals which are liquid or solid at room temperature in the glove box. Solid sodium and

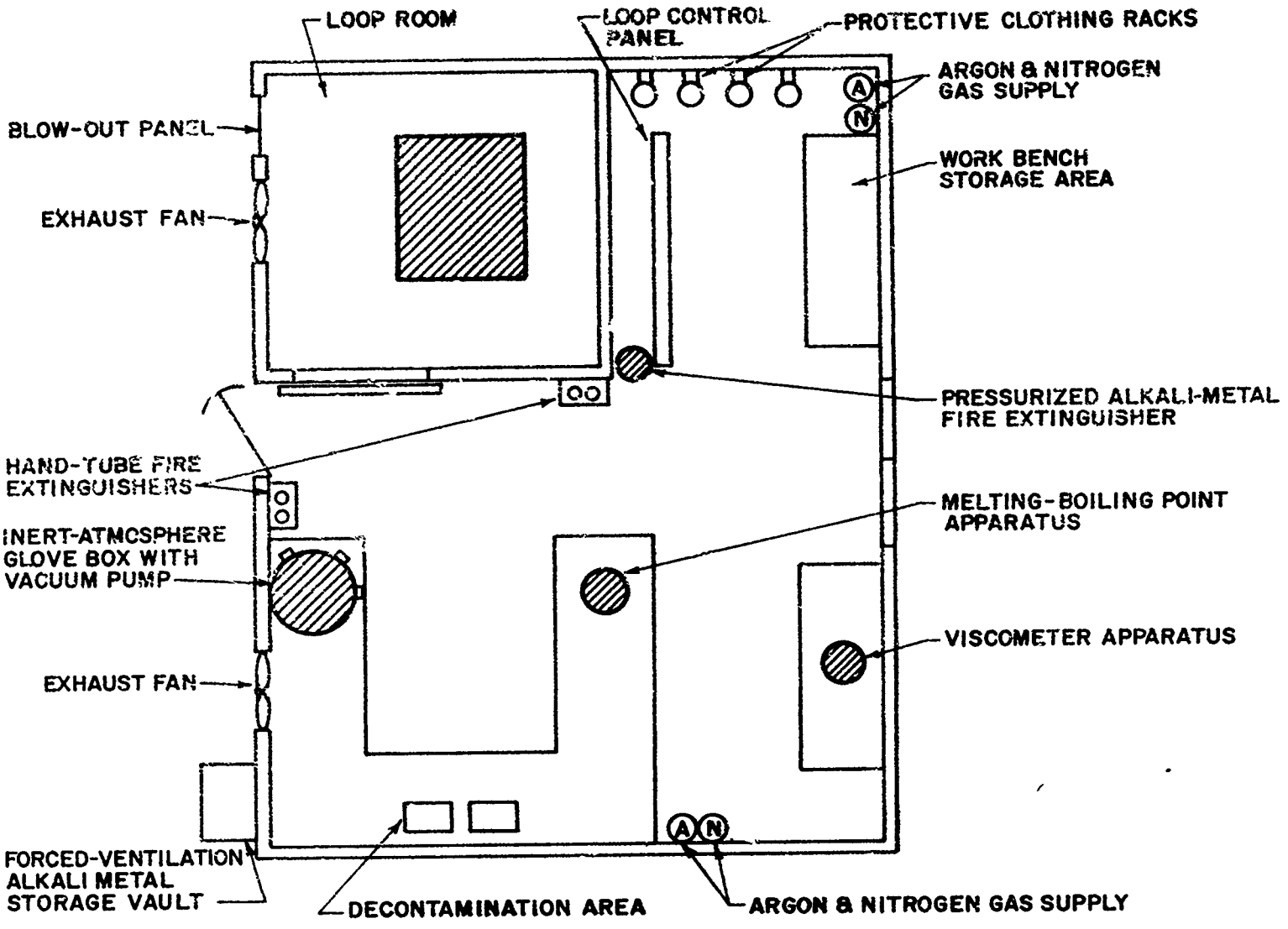

FIGURE 4. LIQUID-METALS LABORATORY

FORCED-VENTILATION, WEATHERPROOF ALKALI-METAL STORAGE VAULT

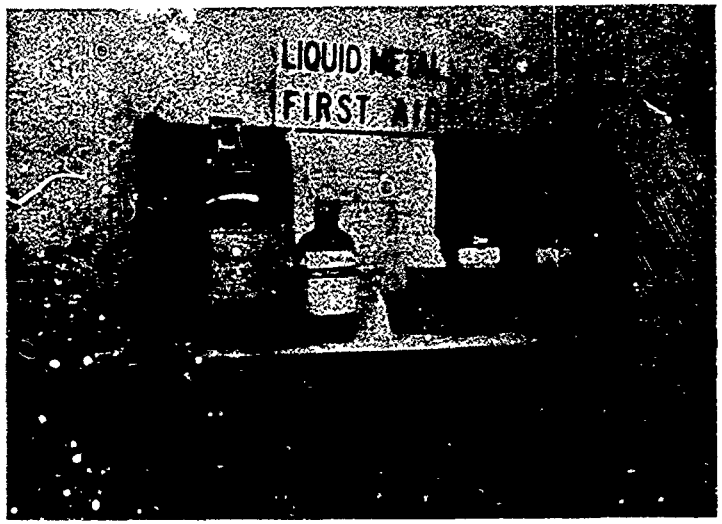

CENTRALIZED ALKALI-METAL FIRST AID SUPPLIES

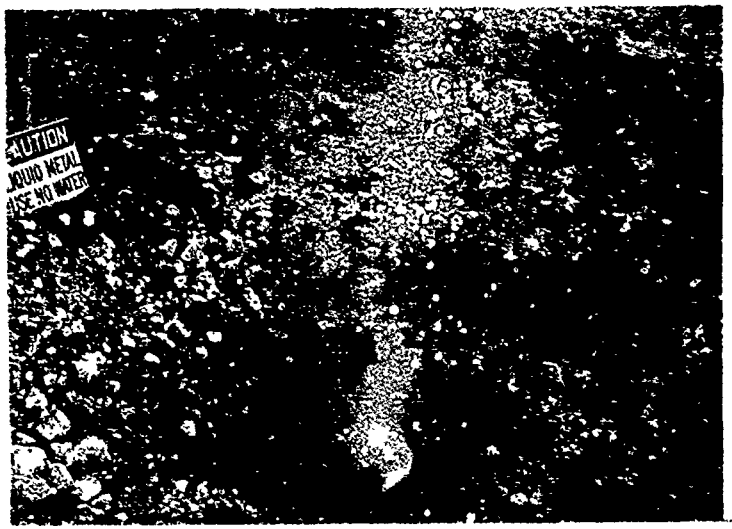

EXAMPLE OF LITHIUM COMBUSTION (INCANDESCENT SPOTS IN PAN) IN ALKALI-METAL DISPOSAL PIT

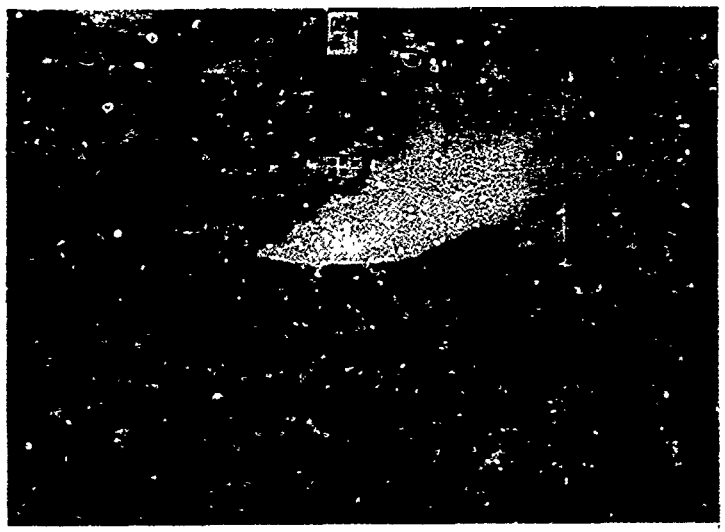

EXAMPLE OF RUBIDIUM COMBUSTION IN ALKALI-METAL DISPOSAL PIT

FIGURE 5. LIQUID-METAL EXPERIMENTAL FACILITIES

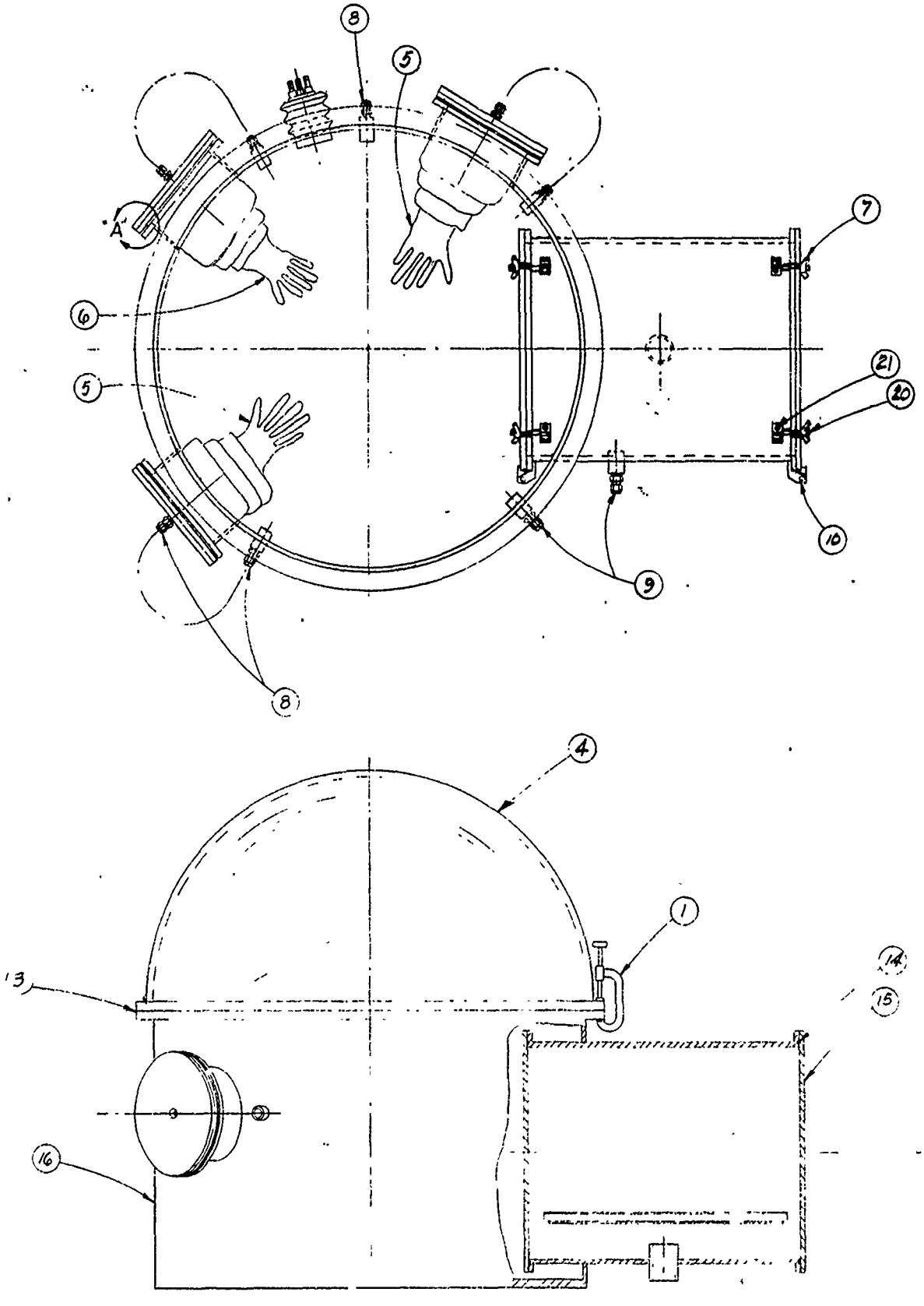

FIGURE 6. INERT-ATMOSPHERE GLOVE-BOX ASSEMBLY

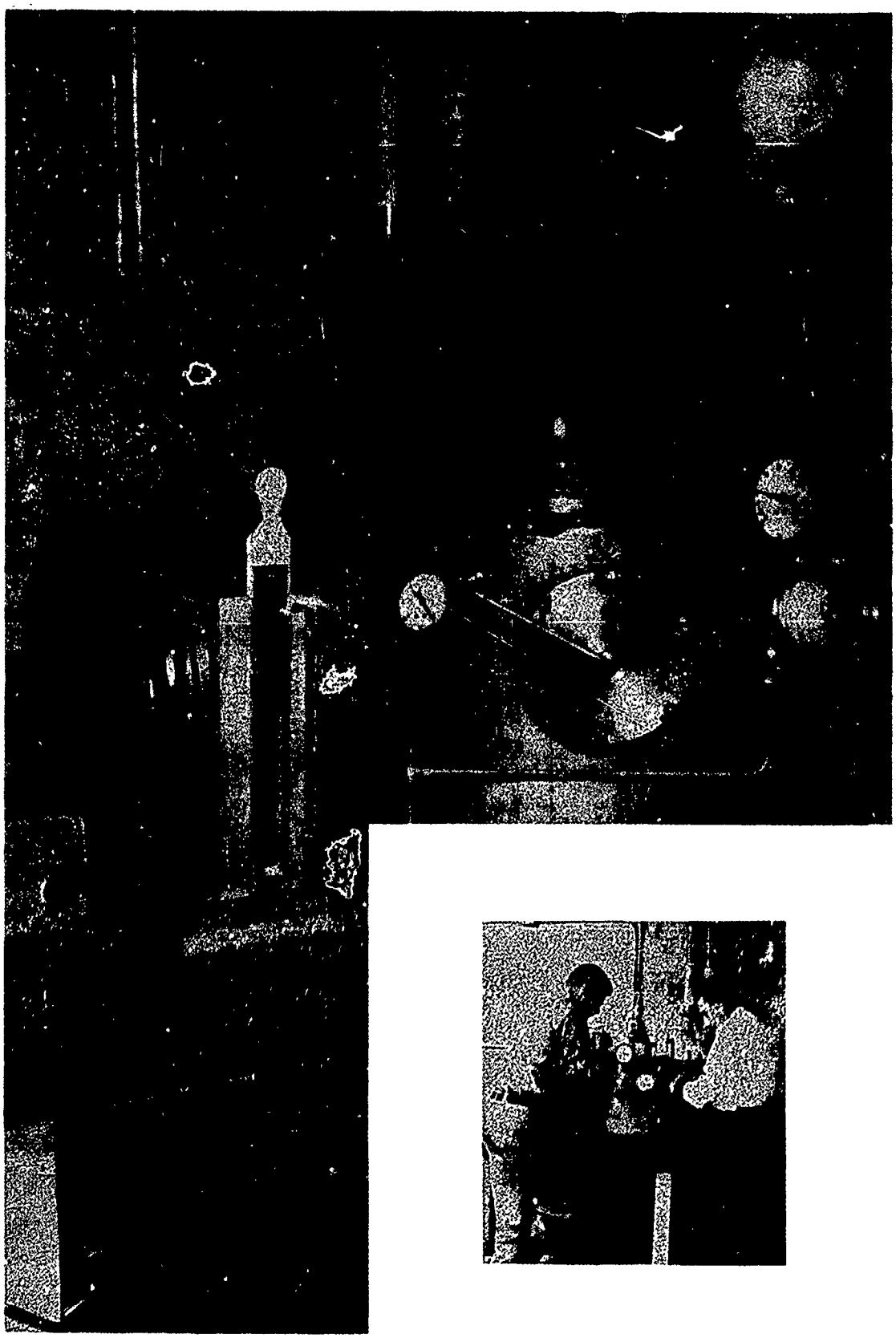

FIGURE 7. EVACUATABLE INERT-ATMOSPHERE GLOVE BOX WITH GLOVE PORTS COVERED (INSET: GLOVES IN USE).

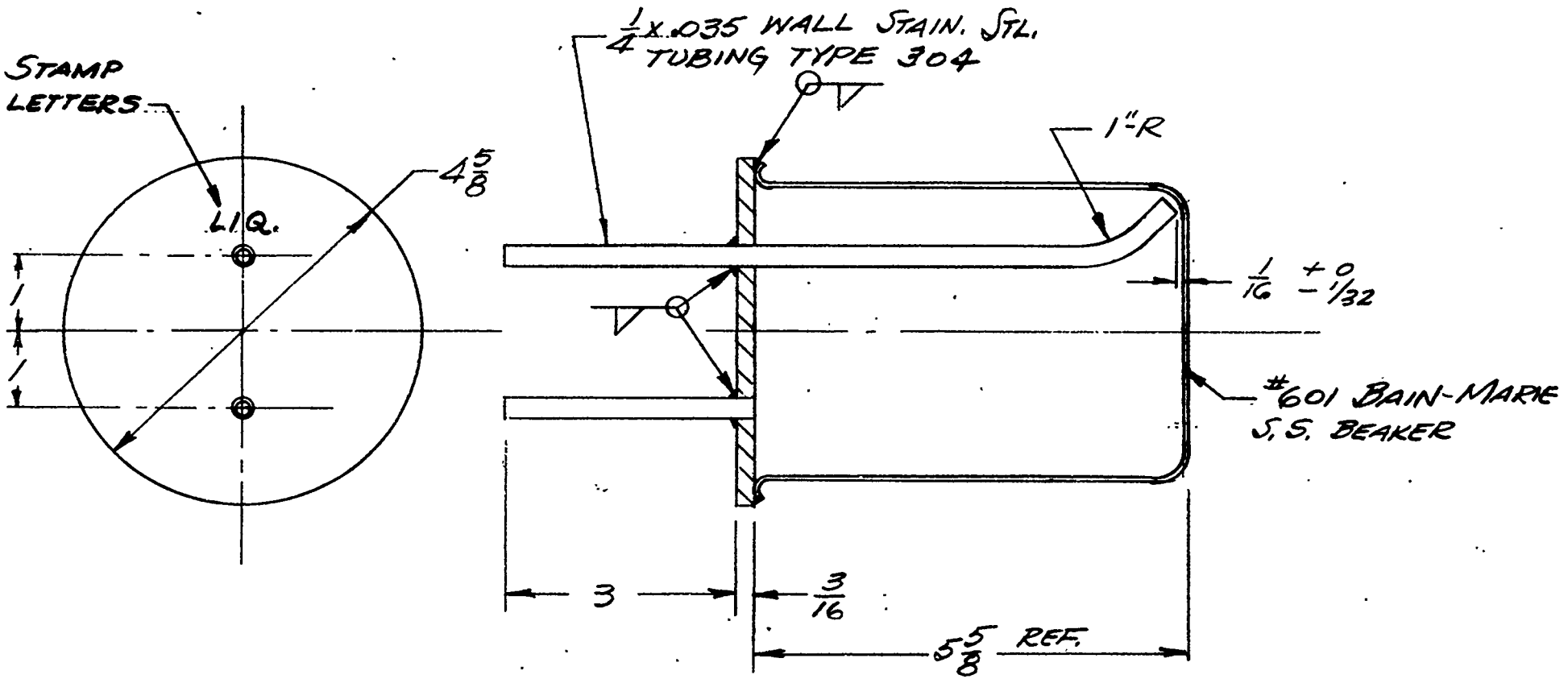

FIGURE 8. LIQUID METAL STORAGE AND TRANSFER VESSEL

lithium have been thus transferred from sealed cans into stainless steel transfer vessels, with no particular problems being encountered. Although the volume of the glove box is relatively large, the argon-vacuum system appears adequate for providing an inert atmosphere.

In many applications, it always has been general laboratory practice to perform alkali-metal transfers under kerosene or mineral oil. For certain applications, this hydrocarbon-blanket handling technique is satisfactory; however, for the purposes of this research program, it was not considered suitable for the following reasons: (1) contact of rubidium or lithium with mineral oil could lead to possible contamination with carbonaceous material, and (2) traces of moisture or constituents of air dissolved in the mineral oil could lead to the formation of oxygen-containing contaminants. The latter case is illustrated for rubidium in the lower right photograph of Figure 9. It was repeatably observed during this program that rubidium pellets developed black coatings in several hours when stored under mineral oil in screw-cap jars. This black coating, which was completely water soluble, is clearly evident in the mentioned photograph.

With the exception of wet-analysis procedures for metals, all alkali-metal handling and transfer operations have been conducted in an atmosphere of pure argon. In most cases, the 99.996 percent purity argon was bubbled through NaK(78) in the apparatus illustrated in Figure 10 in order to remove traces of oxygen and moisture. Systems to be purged were vacuum-pressure cycled with argon in order to minimize residual atmospheric contamination. For each vacuum-pressure purge cycle, the system was evacuated to less than one torr and then pressurized to about 20 psig with argon. The possible efficacy of such vacuum-pressure cycling for purging atmospheric contaminants is illustrated by the theoretical correlation presented in Figure 11.

Throughout the entire program considerable importance was given to safety of personnel and equipment, especially since relatively large quantities of alkali metal were handled. The protective clothing, consisted of hard hats with full-face shields, leather aprons, leather jackets, and leather gloves. This clothing was used whenever alkali metal was handled, and it did not hamper the operations in any respect. The main reason for this "blacksmith"-type clothing is to protect personnel against alkali metal splatter and secondary fires. Certainly, safety was inherently designed into the detailed handling techniques. (See Appendix).

In the event of alkali metal fires, two types of fire extinguishers were selected: the pressurized type and the dispensing carton type. One type of extinguishing agent, essentially powdered graphite, was selected to serve

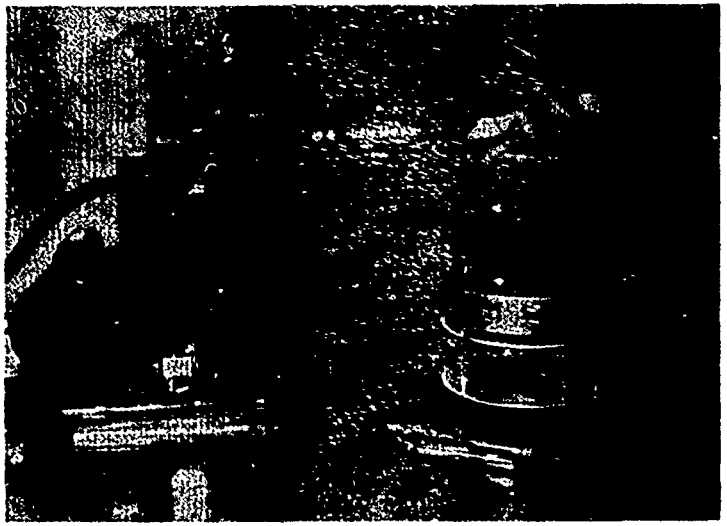

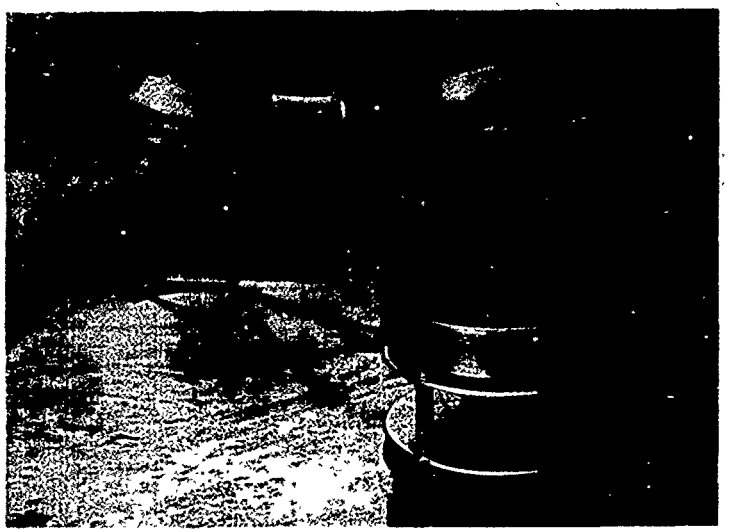

PREPARATION OF LITHIUM SAMPLE
IN POLYETHYLENE AMPOULE

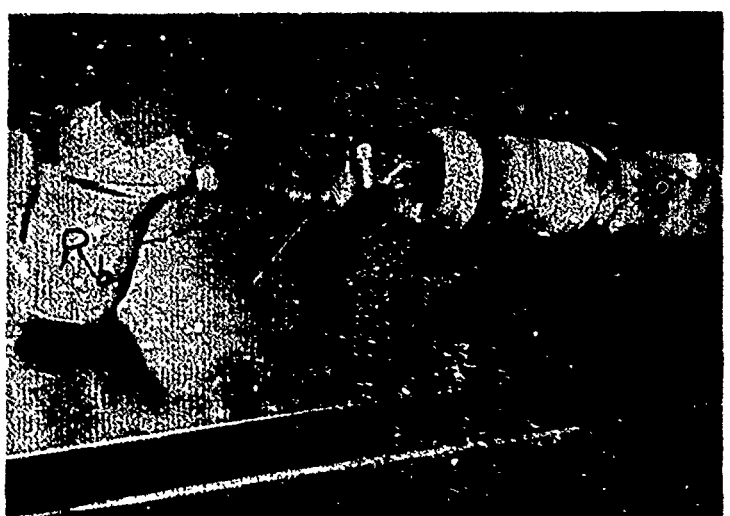

ILLUSTRATION OF FILLING OF
TRANSFER VESSEL WITH RUBIDIUM.

RUBIDIUM PELLETS UNDER
MINERAL OIL (ILLUSTRATING
BLACK WATER-SOLUBLE DEPOSIT
FORMATION)

FIGURE 9. RUBIDIUM AND LITHIUM HANDLING OPERATIONS

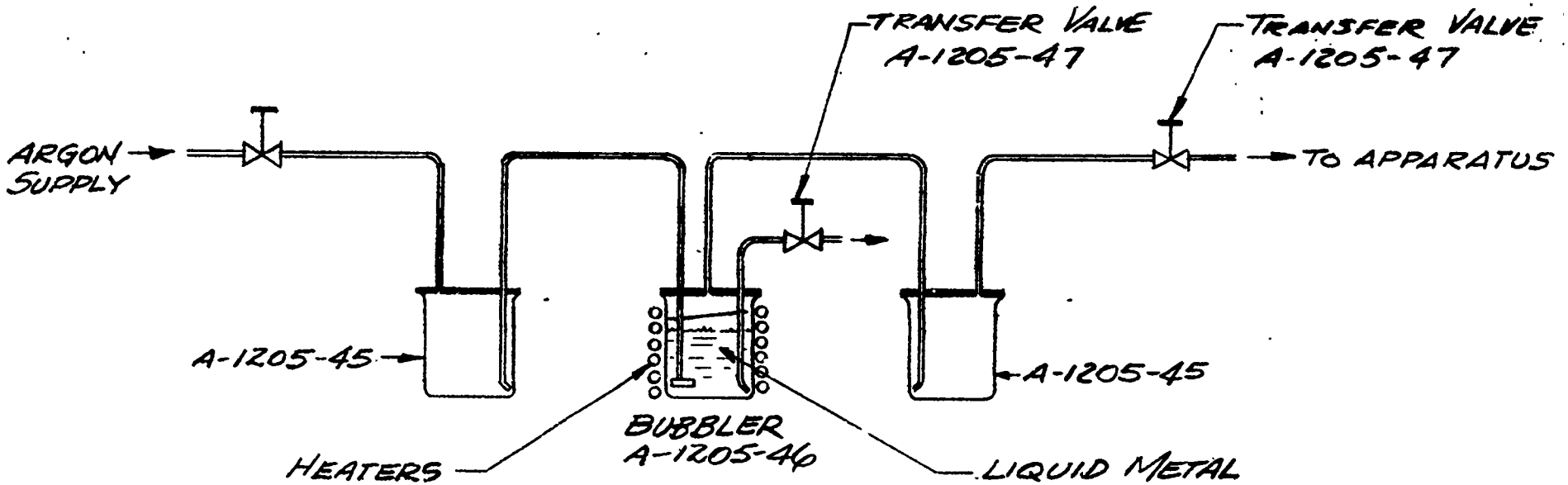

ARGON PURIFICATION SYSTEM

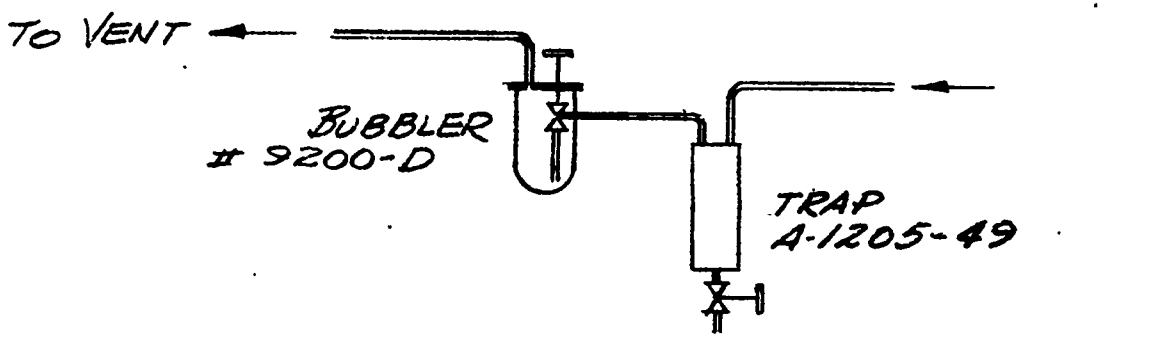

PURE ARGON BLEED SYSTEM

FIGURE 10. GAS-HANDLING FACILITIES

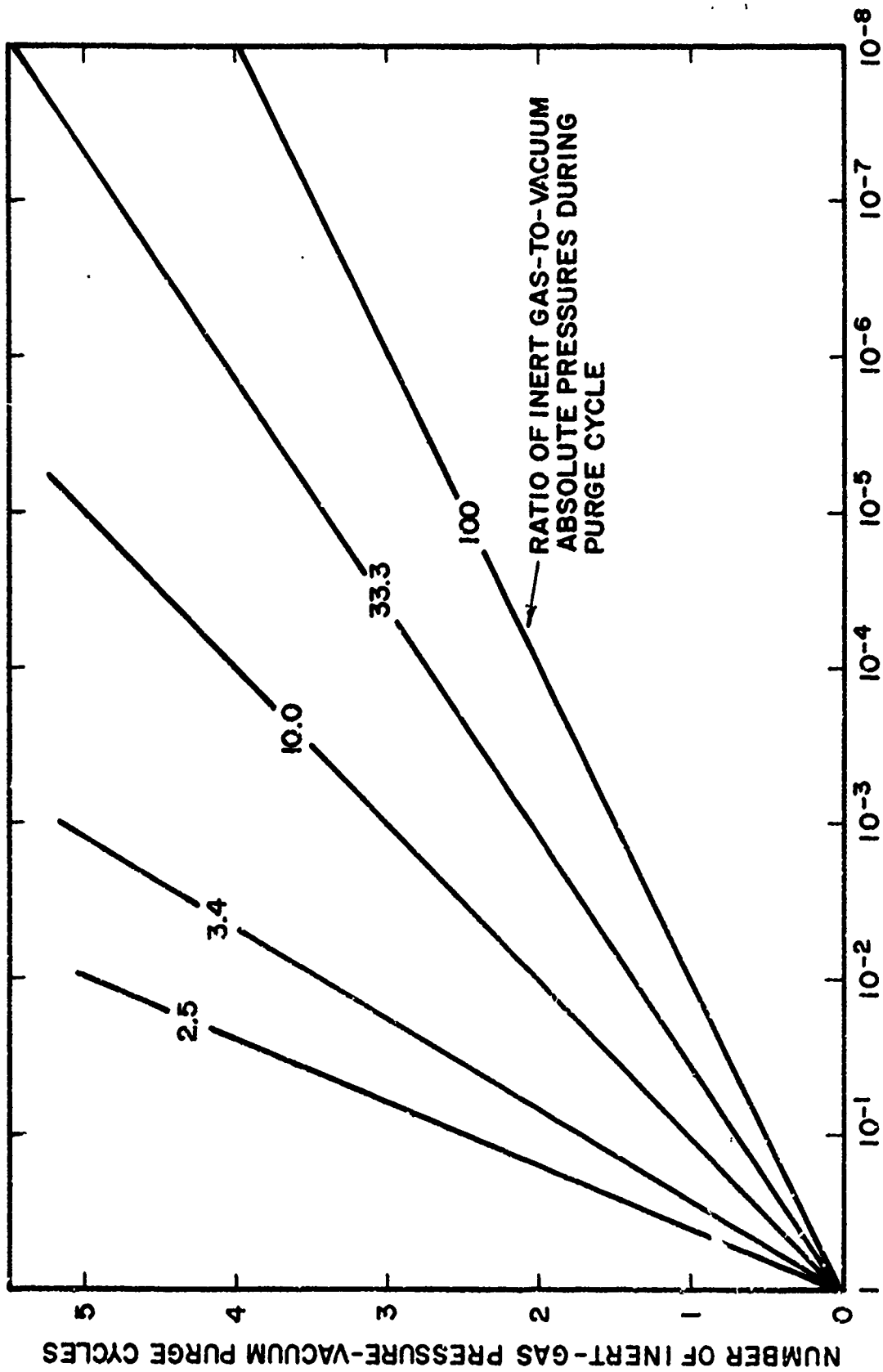

FIGURE 11. THEORETICAL PERFORMANCE OF VACUUM-PRESSURE PURGE CYCLES

NaK, Na, Rb, and Li fires. Little published information was found with regard to rubidium fires.

As the assembly of each apparatus was completed, the equipment was leak tested by pressurizing with freon gas and inspecting welded joints with an electronic halogen leak detector (capable of sensing a few parts per million of halogen in air). The systems were then cleaned with 50 percent nitric acid followed by benzene-acetone solvent, and final cleaning was accomplished with isopropyl alcohol followed by distilled water rinses. The parts, or systems, were then thoroughly dried, either in an electric oven or with built-in heating units. Once it was established that the system was leak free, clean, and dry, the handling and operating procedures detailed in the Appendix were followed.

3. Liquid Level Detection

Since contamination and temperature requirements dictated the use of a method other than a sight glass to determine the alkali-metal liquid level, an alternate method was devised. It was decided after careful investigation to use type 316 stainless steel throughout the rubidium and lithium systems. Therefore, a resistance technique was devised to measure the empty-tube resistance and to compare it to a full tube of alkali metal (Fig. 12). Since the electrical resistivity varies with temperature, a family of curves was plotted for the desired temperature range (as can be seen in Figures 13 and 14) for rubidium and lithium, respectively. By introducing a DC signal into the region of liquid-level measurement, it was possible to take the output directly from the tube to a microvoltmeter and in turn to a recorder. Figure 12 illustrates the electrical circuit used for detection of the alkali-metal level for rubidium and lithium. It was gratifying to note that the calculated and experimental measurements agreed, since some of the electrical resistivity data were extrapolated. Type 316 stainless steel wire, 1/16-in. diameter, was used for the input and output leads for both the viscometer and the loop to eliminate any thermocouple effect which would have been produced if dissimilar metals had been used.

4. Addition of Contaminants

It was felt that a standard method of adding contaminants to the systems was more effective than having individual methods for each system. Care was taken in the addition of the contaminants to prevent any foreign substances from entering the system. Techniques previously developed for handling alkali metals facilitated the development of contaminant addition. Oxygen was selected as the gaseous contaminant to be added to rubidium. As for the viscometer, it was decided to add oxygen in relatively small

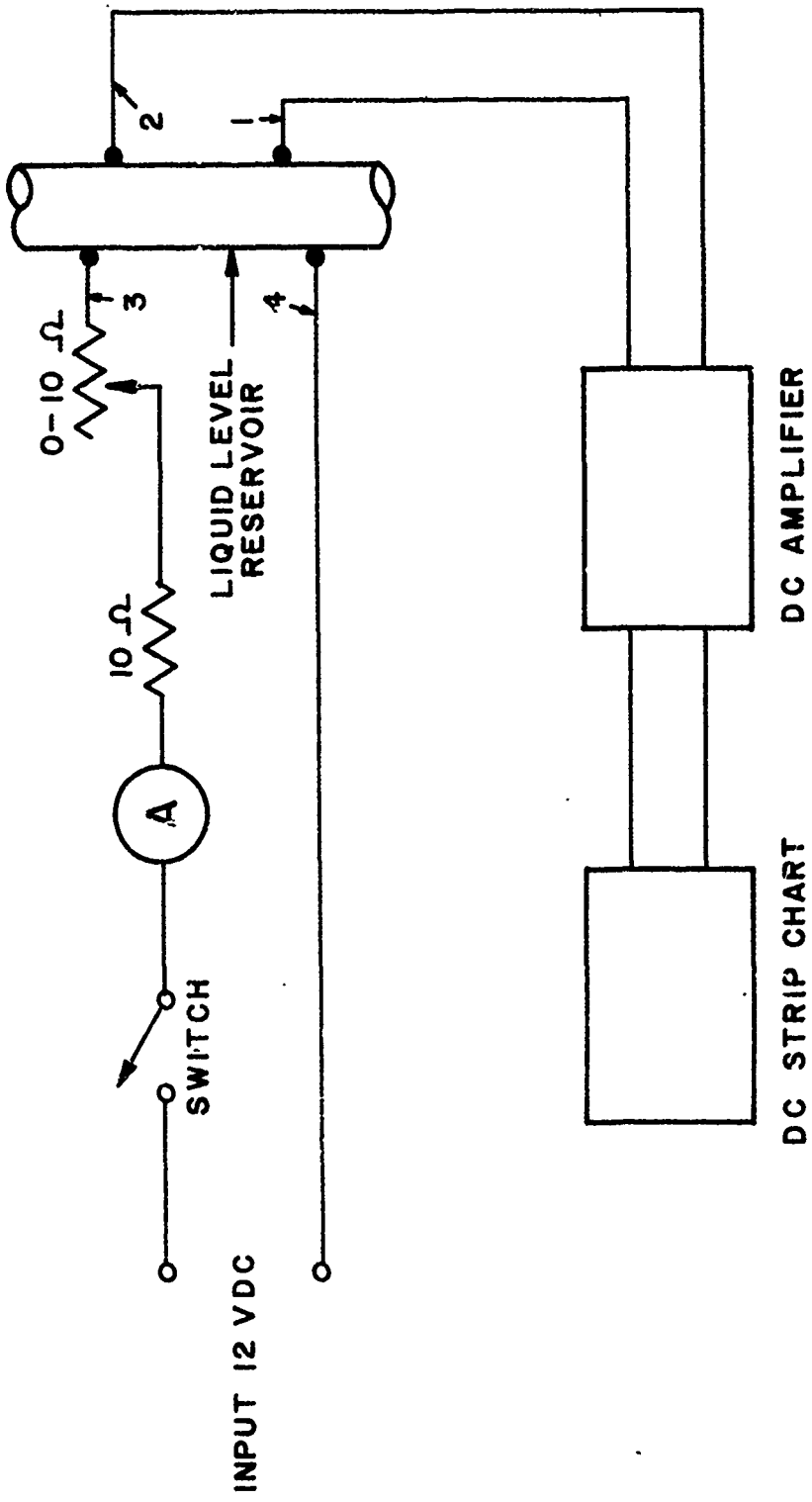

FIGURE 12. CIRCUIT DIAGRAM FOR LIQUID-LEVEL GAGE

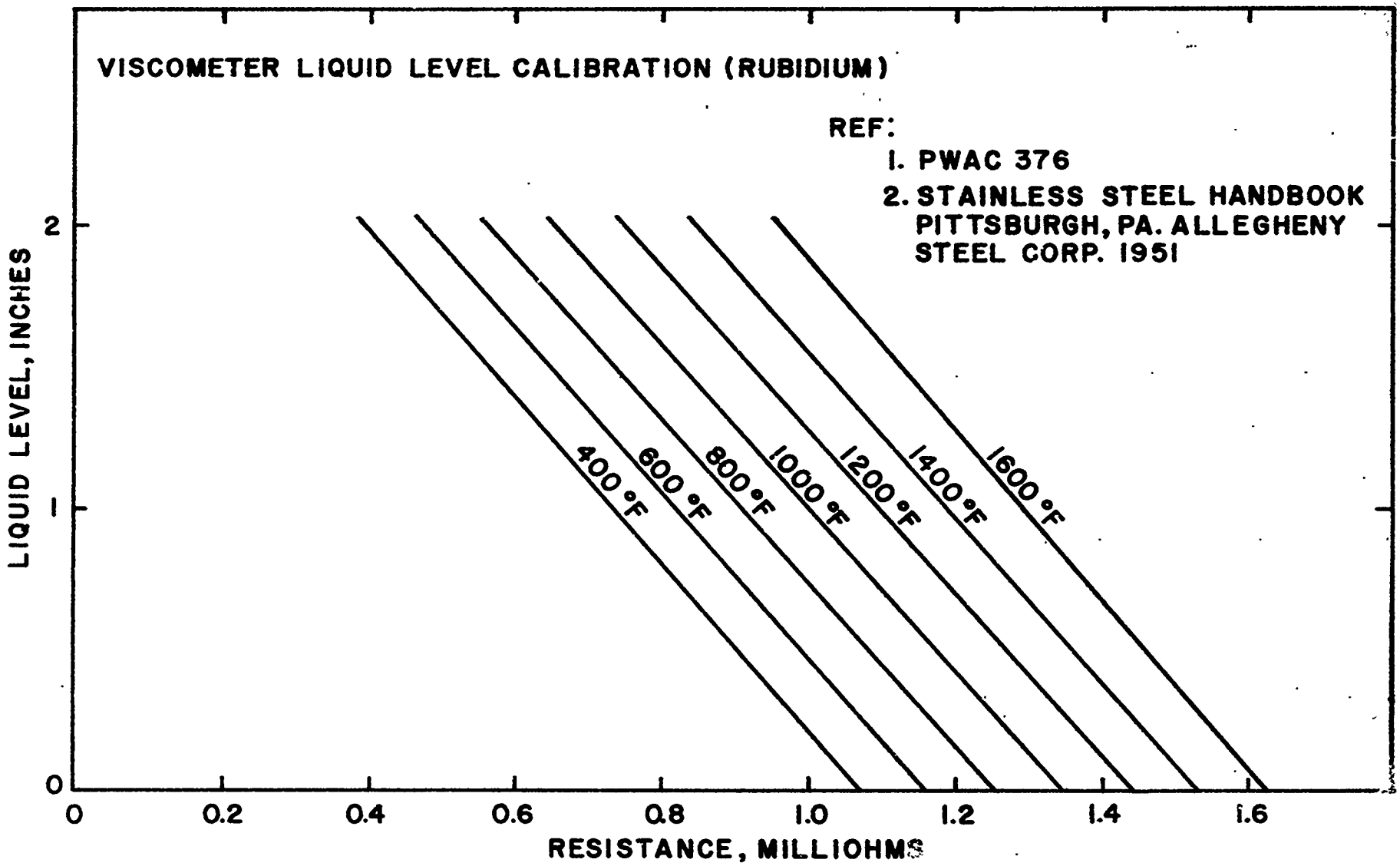

FIGURE 13. VISCOMETER-RESERVOIR LIQUID-LEVEL CALIBRATION FOR RUBIDIUM

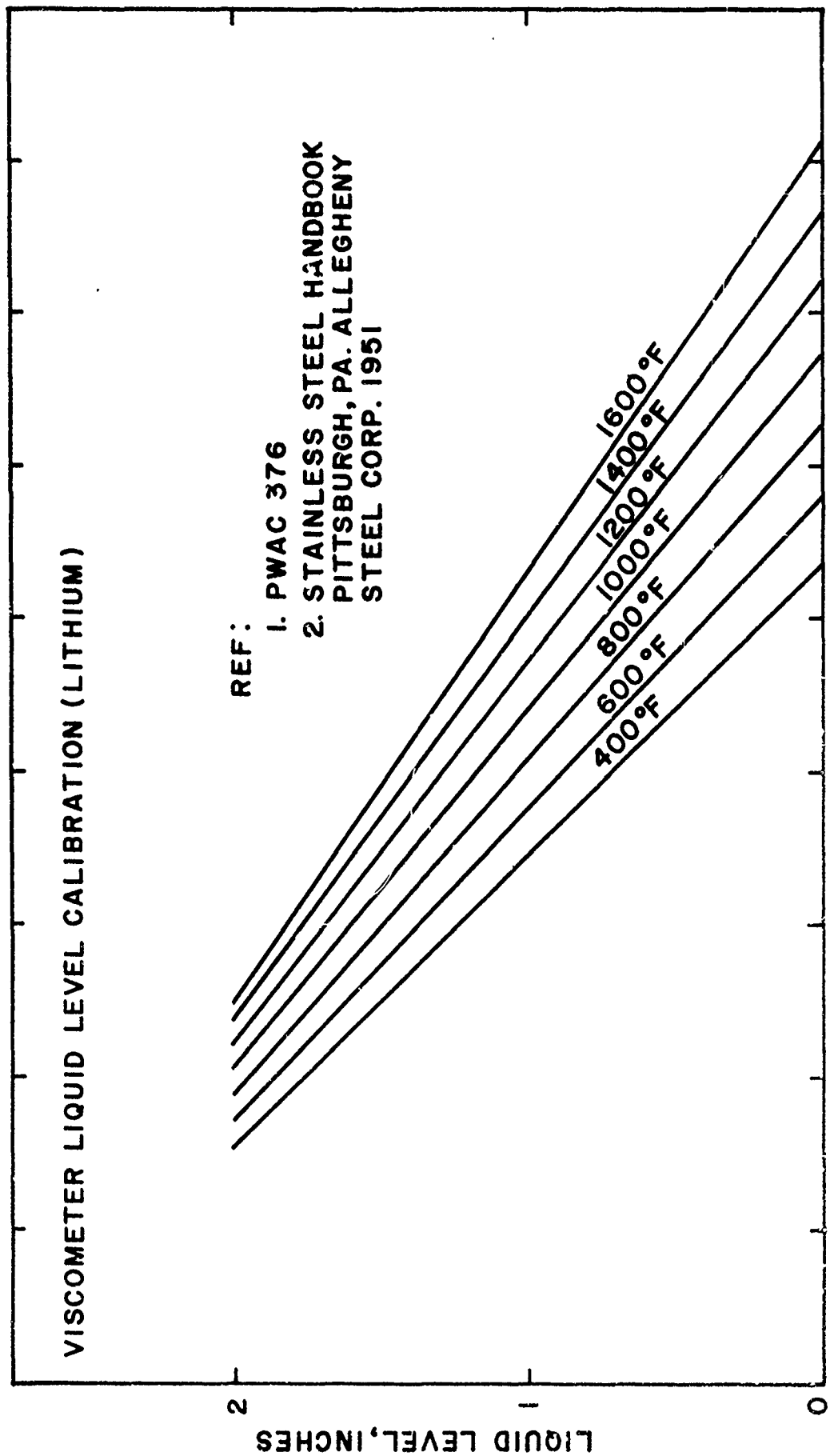

FIGURE 14. VISCOMETER-RESERVOIR LIQUID-LEVEL CALIBRATION FOR LITHIUM

increments, that is at 1000 ppm concentration increments, until appreciable changes in viscosity were noted, at which time, larger concentration increments (2000 ppm) were employed.

In order for a given quantity of oxygen to be transferred to an apparatus, a gas sample line was prepared. The gas line, valved on both ends, was attached to a tee, one side of which was attached to the apparatus, the other to the vacuum-argon supply. Once the volume between the oxygen line and the apparatus had been vacuum-argon cycled, the oxygen was ready for transfer to the apparatus. The oxygen was introduced into the previously evacuated apparatus. During the addition, the temperature of the rubidium in the apparatus was monitored. This temperature rose and finally stabilized when all of the oxygen had reacted.

In order to determine what pressure and volume of oxygen was necessary for a given contaminant concentration, the number of gram moles of contaminant was computed. The pressure volume relationship was then obtained by using the gas law. It can be seen here that since the number of gram moles had to be determined, the number of grams of alkali metal in the apparatus had to be accurately known, consequently the alkali metal fill lines and valves were precalibrated.

5. Sampling Techniques

Extreme care was exercised in order to avoid contaminating alkali metals during sampling. In the case of rubidium samples, it was desirable to collect several grams of alkali metal in a borosilicate-glass ampoule. The sample bulb was first cleaned and dried prior to its installation into a special glass-to-metal fitting. The transfer was made under vacuum to ensure a pressure difference between the apparatus and the sample bulb. The photograph of Figure 17 presented in a later section of this report illustrates the technique used in sealing the sample bulb after the desired amount of alkali metal was transferred. Once the sample bulb had been heat sealed, it could be weighed along with the fragment portion of the glass tube, from which the net weight of the sample could be determined. Multiple samples were not taken mainly because of the relatively small quantities of alkali metal present within the apparatus being sampled, as in the viscometer and the melting point-boiling point apparatus. In the case of the liquid metal loop, however, multiple samples were taken for subsequent transfer to the melting point-boiling point apparatus, and for nitrogen and oxygen determination.

This technique for sampling was effective in the sampling of rubidium: however, for the sampling of lithium, this handling technique was

impractical because of the incompatibility of glass and lithium. The samples of lithium prepared for neutron activation analysis were to be collected in polyethylene tubing. An adaptation of the glass-sampling technique to polyethylene tubing was developed for this purpose, and a detailed procedure is included in the Appendix. The photographs in Figure 9 further illustrate this technique used in lithium sampling. It should be mentioned here that temperature plays a significant role in sampling, that is, the higher the temperature required to avoid freeze-plugging, the more difficult it is to sample.

6. Storage and Disposal

Since relatively large quantities of alkali metal were to be used, a storage vault was provided to contain samples, shipping containers, and transfer containers. The storage vault (converted refrigerator) contains its own forced ventilation system whereby clean air is circulated throughout the vault to insure that no foreign gases such as hydrogen are accumulated. The vault is located externally and adjacent to the liquid-metal laboratory.

A disposal pit was provided at a location remote from the laboratory in order to allow for disposal of relatively large quantities of alkali metal. The usual procedure for disposing of large quantities of material was to place the material in the pit, covering it with earth, and allowing it to react with the traces of moisture in the ground. Care must be taken to assure that the ground is relatively dry before such disposal is attempted in order to avoid an explosion or intense fire.

As a practice-run for alkali-metal disposal techniques, a 100 gm sample of NaK(78) was collected under oil and carefully poured into the disposal pit. Smoke evolution commenced immediately because of residual moisture in the ground. Soon, a brilliant fire developed, and copious quantities of white alkali smoke were evolved. The two lower photographs of Figure 5 illustrate the incandescent burning of lithium and the near-explosive burning of rubidium. Appropriate precautions, including the use of protective gear, were taken during all transfer and disposal operations. When only small quantities of alkali metal were to be disposed of, this was done in the laboratory by the use of normal decontamination techniques which are detailed in the Appendix.

B. Melting Point-Boiling Point Studies

1. Apparatus and Procedures

The melting point-boiling point apparatus is illustrated in Figures 15 thru 17. It consists of a 1/2-in. diameter tube, closed at the bottom

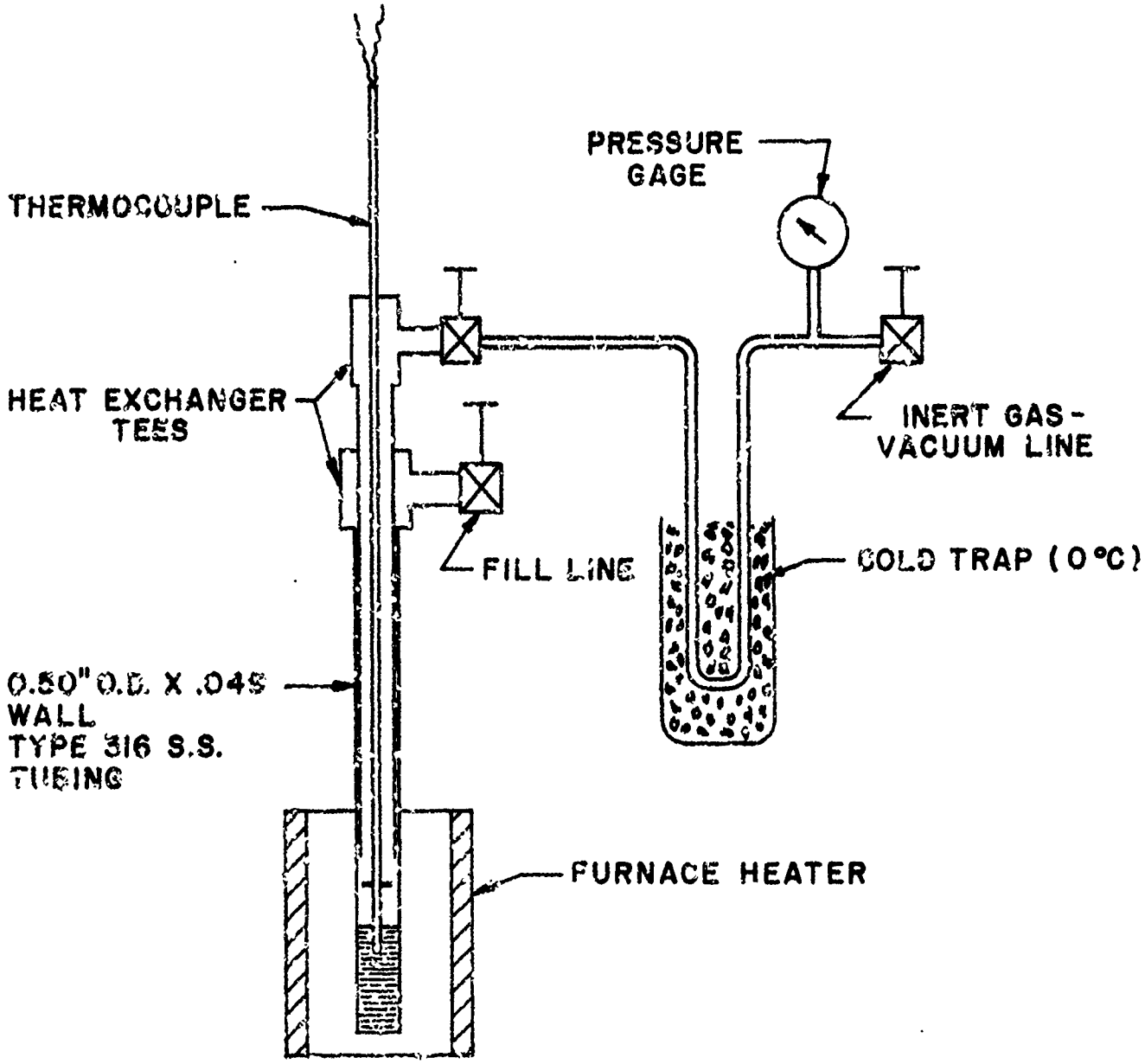

FIGURE 15. SCHEMATIC DIAGRAM OF MELTING POINT-BOILING POINT APPARATUS

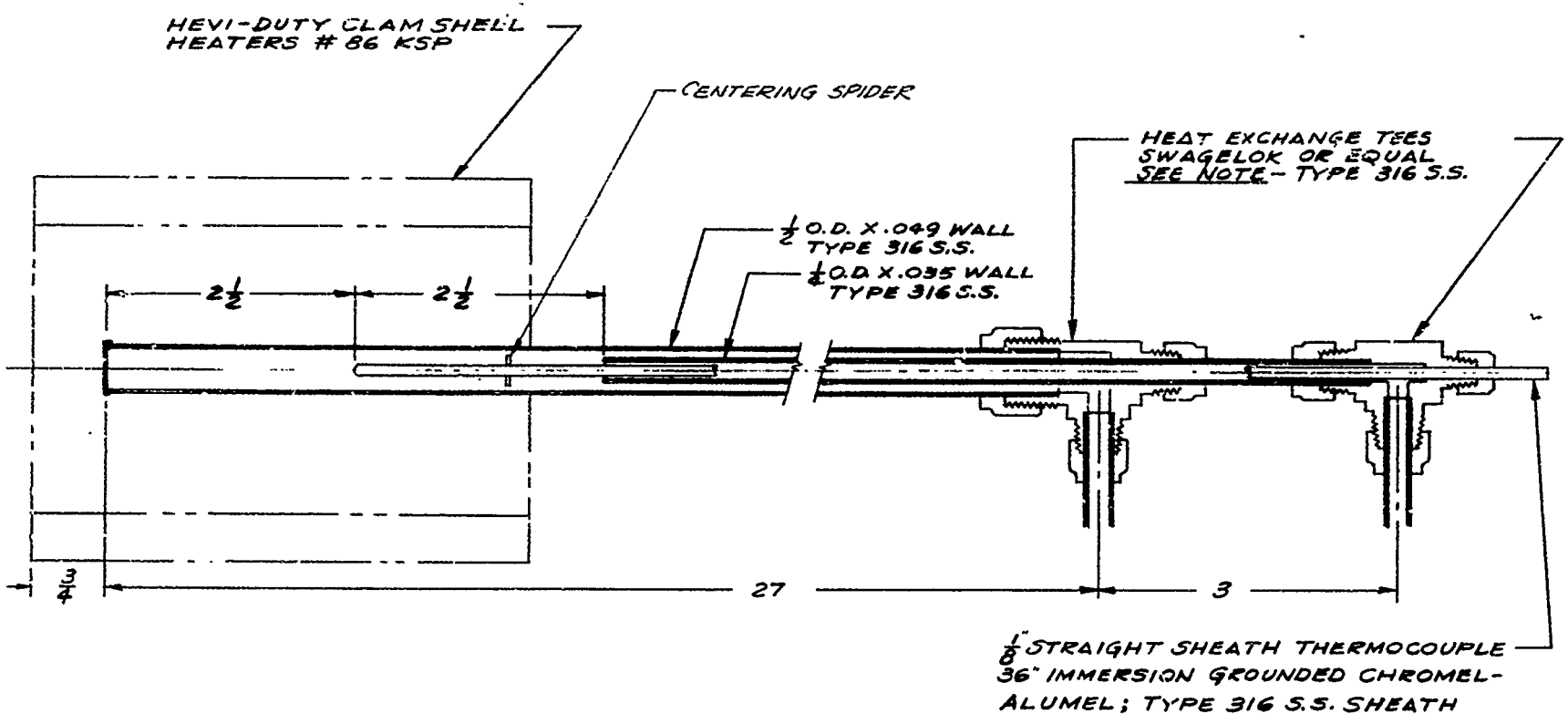

NO. REQ.D	TUBE O.D		
	JACKET	PROCESS	BRANCH
1	1/2	1/4	1/4
1	1/4	1/8	1/4

FIGURE 16. MELTING POINT-BOILING POINT APPARATUS ASSEMBLY DRAWING

and attached to a compression-fitting assembly at the top. The compression-fitting assembly comprises two heat-exchanger tees which provide for two separate connections to the apparatus. A 1/8-in. diameter sheathed thermocouple is mounted axially through the upper tee and extends to within 2-1/2 in. of the tube bottom. It is supported by a central spider 1-1/2 in. above the thermocouple tip. The thermocouple is surrounded by a 1/4-in. diameter tube which extends from the upper tee to within 1-in. of the centering spider near the thermocouple tip. The inner annulus between the thermocouple and the 1/4-in. tube provides a conduit from the side opening in the upper tee to the region near the thermocouple tip, and the outer annulus between the 1/4-in. tube and the 1/2-in. serves as a conduit from the side opening in the lower tee to the vicinity of the thermocouple tip. The inner conduit is employed for gas transfer operations, and the outer annulus is used for the introduction and removal of liquid metal. A cold trap is provided in the vapor line to the pressure gage in order to condense any vapors which might diffuse into the line. A clam-shell-heated furnace, surrounded by high-temperature insulation is provided as the temperature environment for the melting point-boiling point apparatus.

The operating principles of this apparatus are quite simple. As heat is added to the solid mass of alkali metal, the metal temperature rises until melting commences, at which time the constant-temperature melting plateau is observed. When melting is completed, the fluid temperature again begins to rise. During cooling, identical phenomena are evident as heat is lost and the metal freezes. The duration of the melting or freezing plateaus is dependent upon the rate at which heat is added or lost. The operating procedure was adjusted so that plateaus lasting at least one minute were obtained in order that several temperature readings could be taken. Boiling-point plateaus were achieved in a similar manner, with the exception that the argon pressure within the apparatus was controlled either at atmospheric or a constant higher pressure as boiling progressed.

The sheathed thermocouple and the bourdon-type pressure gage were both calibrated against precision standards in order to assure maximum accuracy in the melting-point, boiling-point, and vapor-pressure determinations. The thermocouple calibration facility employs four freezing-point standards, tin (231.8°C), zinc (419.50°C), aluminum (660.0°C), and copper (1083.3°C). These metal standards were prepared by NBS, and they are of the highest purity available. The freezing temperatures have been determined and documented by NBS. The pure metals are protected from oxidation and contamination by ultrapure graphite crucibles hermetically sealed in metallic sheaths. These freezing-point standards are instrumented with a L & N, K-3 potentiometer, standardized against an Epley reference cell. The pressure gage was calibrated against precision, dead weight standards.

FIGURE 17. LIQUID-METAL MELTING POINT-BOILING POINT APPARATUS DURING SEALING OF SAMPLE AMPOULE (INSET: APPARATUS IN OPERATING POSITION IN FURNACE).

2. Vapor Pressure of Rubidium

After several exploratory runs using NaK(78), vapor-pressure experiments were conducted using pure rubidium. After establishing the atmospheric-pressure boiling point, the system pressure was increased with argon gas in successive increments. The temperature plateaus achieved at each pressure increment were measured, and the resulting vapor pressure data are presented in Figure 18. A second series of vapor pressure measurements was then made using a second batch of pure rubidium. The results of these measurements also are presented in Figure 18 and Table 5, along with those obtained with the first batch of rubidium. Experimental vapor pressure curves reported by Bonilla, et al.[6] and Tepper, et al.[86] are also shown in this figure. The first batch gave results nearly equal to those of Bonilla, et al., whereas the second batch agreed more closely with the data of Tepper, et al.

Examination of the analyses of the two rubidium batches does not reveal any composition differences which could explain the lower vapor pressure of the second batch. However, it is known that the liquid level was below the thermocouple in the first series, whereas, the thermocouple was immersed during the second series. Therefore, the differing results are interpreted as follows: In the first series, the saturation temperatures may have been diminished somewhat by the diffusion of argon into the reflux zone where the temperature was being measured. In the second series, the immersed thermocouple could not be influenced by such vapor dilution by argon, but the saturation temperatures may have been increased somewhat by back-pressure effects resulting from the vigorous boiling in the small annular space around the thermocouple stem. Consequently, we now believe that our results tend to confirm those of Tepper, et al.

3. Melting Point of Rubidium and Rubidium with Oxygen Contaminant

a. Experiments

A melting-point study of pure rubidium and rubidium contaminated with oxygen was conducted with the melting point-boiling point apparatus, using the low-cesium (batch 2) batch of pure rubidium. The results of this study are presented in Table 6. A repeatable melting point of 102.66-102.75°F was obtained in several successive experiments. Four grams of freshly cleaned 50-50 titanium-zirconium chips were placed in the base of the melting point tube, and a fresh charge of rubidium was added. This sample was heated at 1200-1300°F for 40 hours in order to getter the oxygen content. Its melting point was then determined insitu, yielding a repeatable melting point value of 102.88°F. This value, which is the highest melting

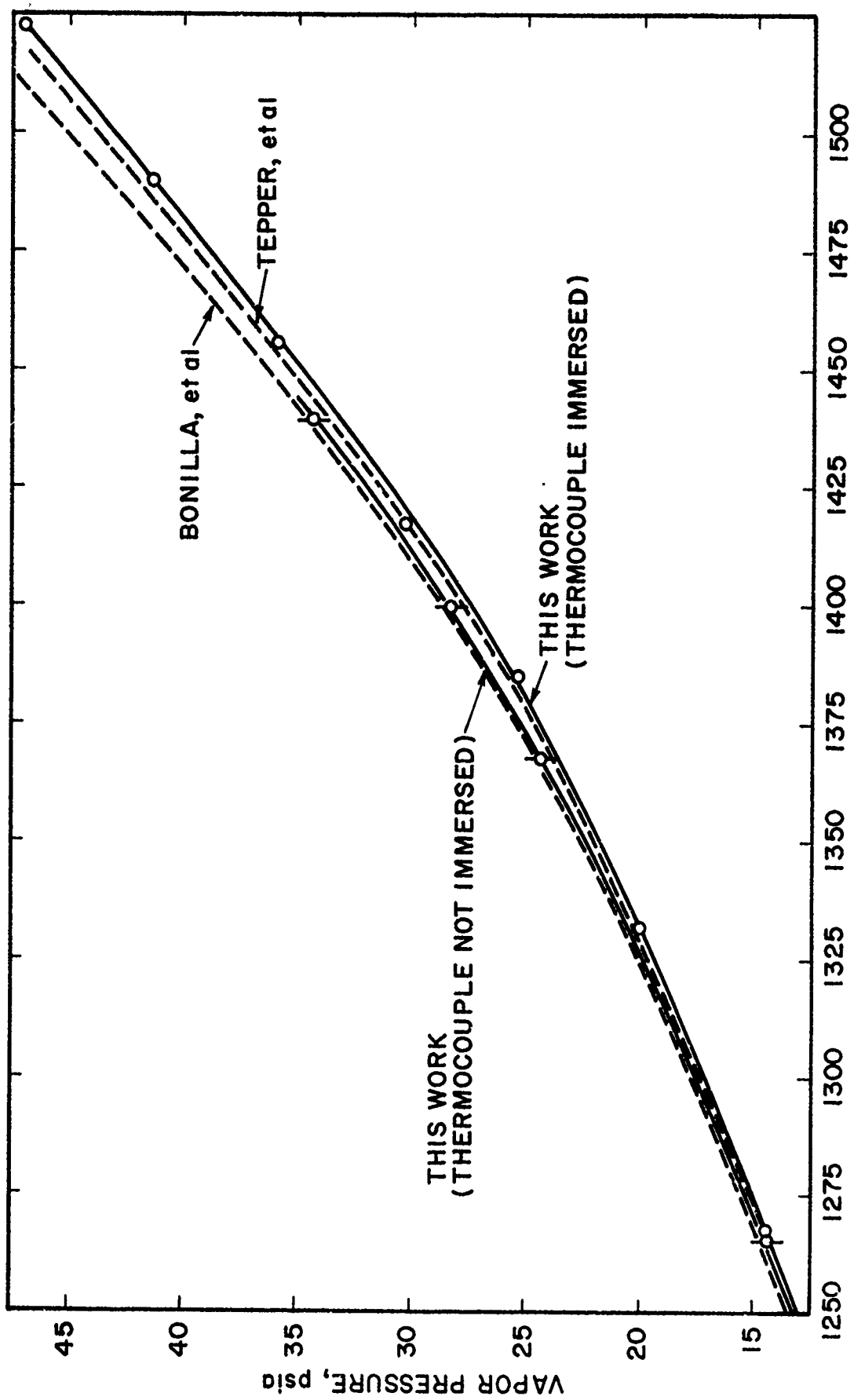

FIGURE 18. COMPARISON OF RUBIDIUM VAPOR PRESSURE DATA WITH PUBLISHED VALUES

TABLE 5. VAPOR PRESSURE DATA

Pressure, psia	Temperature, °F	Remarks
14.45	1265.3	Batch 1 Pure Rubidium
24.35	1367.9	(Thermocouple not immersed)
28.45	1399.6	
34.25	1439.6	
14.33	1267.7	Batch 2 Pure Rubidium
20.08	1332.3	(Thermcouple immersed)
26.23	1385.5	
30.33	1417.6	
36.03	1456.8	
41.23	1490.2	
47.03	1522.2	

TABLE 6. SUMMARY OF RUBIDIUM MELTING POINT DATA

O_2 Added, ppm	Melting Point, °F	Melting-Point Depression, ΔT_m, °F	O_2 Calc'd from ΔT_m, ppm
0	102.66	0.22	66
0	102.75	0.13	39
0	102.75	0.13	39
Hot Gettered	102.88	*	*
1000	100.08	2.80	840
2000	95.01	7.87	2360
7000	75-85**	18-28	5400-8400

* Rubidium assumed to contain 0.0 ppm O_2 after hot gettering with 50-50 Ti-Zr chips at 1200-1300°F for 40 hours. This melting point is the highest ever reported for rubidium, and, hence, it represents the purest sample of rubidium for which a melting point has been reported.

** Approximate visual observation.

point ever reported for rubidium, apparently represents that of the purest sample of rubidium for which a melting point has been reported.

In another series of experiments, predetermined quantities of oxygen gas were added to the rubidium in the apparatus, and the melting-point-depression was measured. The results of these studies are also included in Table 6 (The melting-point range tabulated for rubidium containing 7000 ppm O_2 is based upon visual observations made on a sample contaminated during viscosity studies which are described in a later section of this report).

b. Discussion

In most cases, only the weight (or atom) fraction concentration of contaminant can be measured, and the form of the contaminant in solution is not known. Hence, the atom fraction may be multiplied by an unknown multiplicity factor, i, with this product representing the mole (or ion) fraction concentration of contaminant molecules (or ions).

For low concentrations of nonvolatile contaminant, and assuming that the mole (or ion) fraction concentration of contaminant, (i) (x_c), is approximately equal to the natural logarithm of the mole (or ion) fraction concentration of volatile solvent, $\ell n(x_o)$, the decrease in melting point caused by dissolved contaminant may be expressed as follows.

For rubidium contaminated with oxygen, the melting-point depression is:

$$\Delta T_m,\ ^\circ F = (i)(ppm)_{O_2}/(300)$$

and the boiling-point elevation is:

$$\Delta T_b,\ ^\circ F = (i)(ppm)_{O_2}/(940)$$

For as much as 10,000 ppm oxygen dissolved in rubidium as rubidium monoxide or superoxide, the approximation of the logarithm introduces an error of less than five percent in the calculated melting point depression, and the error is even less if the oxygen is dissolved as rubidium peroxide or trioxide. If the melting point depression does not exceed five percent of the absolute melting temperature, the additional error in this calculation resulting from other mathematical simplifications is five percent or less.

The experimental melting-point-depression data for oxygen in rubidium are presented graphically in Figure 19 and curves representing various possible values of i are superposed. It appears quite evident from this

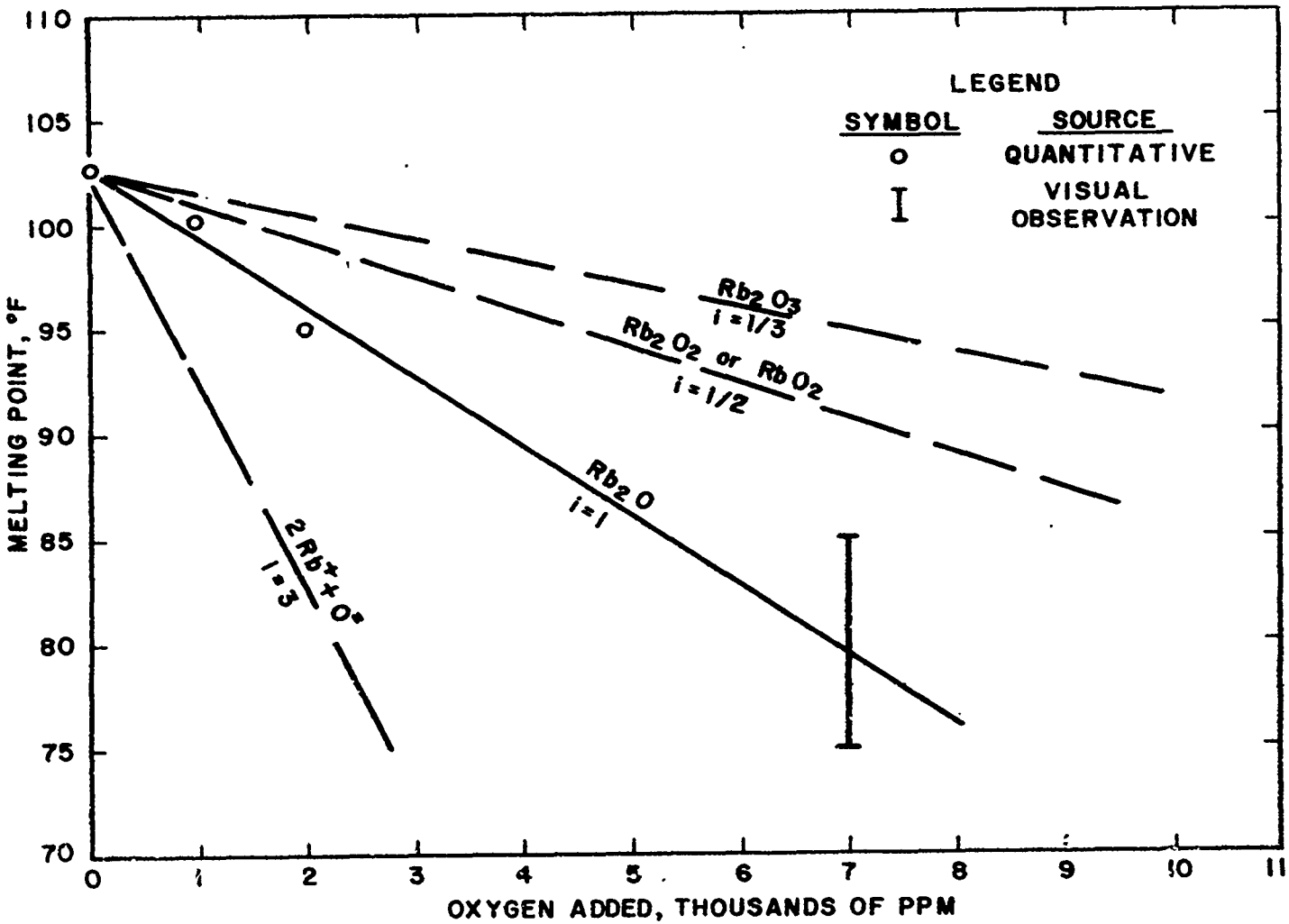

FIGURE 19. EFFECT OF OXYGEN ON MELTING POINT OF RUBIDIUM (INCLUDING COMPARISON WITH THEORETICAL PREDICTIONS)

graph that the multiplicity factor is approximately unity. Hence, for this concentration range, the oxygen contaminant must be present as rubidium monoxide, Rb_2O.

4. Melting Point of Lithium and Lithium with Nitrogen Contaminant

a. Experiments

A series of melting-point experiments was conducted on reactor grade lithium, and the results are summarized in Table 7. The melting point of the as-received lithium was found to be repeatable at 359.2°F. The melting-point sample was then contaminated by adding nitrogen gas, equilibrating at a fixed preabsorption temperature. Following equilibration, the apparatus was removed from its furnace and allowed to cool rapidly while the sample temperature was monitored by the immersed thermocouple. The temperature of the freezing-point plateau was measured with a precision potentiometer, and the sample was reheated while the temperature of the melting-point plateau was measured. Consecutive melting points were thereby determined from the alternate heating and cooling curves while the sample experienced an overall temperature oscillation of about ±50°F. After the addition of nitrogen, a repeatable melting point depression of 0.4°F was observed while the sample experienced the alternate heating and cooling. The temperature of the sample was then increased to about 670°F for about two hours, and the sample was then cooled to the freezing point in 3-5 minutes. The initial freezing curve yielded a distinct plateau for a melting-point depression of 4.0°F. Successive alternate plateaus then demonstrated a steadily decreasing melting-point depression. Following a subsequent preabsorption period at about 610°F, the initial freezing curve revealed a melting-point depression of 0.3°F, with all subsequent values being 0.1°F. Repetition of the latter procedure demonstrated that the initial melting-point depression of 0.3°F was repeatable.

Additional nitrogen was added to the apparatus, and the system was again heated for about two hours at about 610°F. The subsequent melting-point data again displayed a depression of about 4°F which decreased steadily with time. As in the previous experiments, a subsequent equilibration at a preabsorption temperature of 650°F yielded the repeatable melting-point depression of 0.3°F corresponding to the absence of residual nitrogen gas above the lithium sample.

b. Discussion

The results of these lithium melting-point studies have revealed several interesting features of the role of nitrogen contamination in

TABLE 7. SUMMARY OF LITHIUM MELTING-POINT DATA

N_2 Preabsorption Temperature, °F	Average Melting Point, °F	Melting Point Depression, ΔT_m, °F	Dissolved Li_3N in Liquid Lithium, ppm N_2 (Calc'd from ΔT_m)	Time at Melting Point*, min
(No N_2 added)	359.2	0	--	--
400 (Residual N_2 gas)	358.8	0.4	80	0 - >60
670 (Residual N_2 gas)	355 2	4.0	790	0
	356.2	3.0	590	4
	357.5	1.7	340	10
	358.0	1.2	240	15
610 (No residual N_2 gas)	358.9	0.3	60	0 - 1
	359.1	0.1	20	3
	359.1	0.1	20	6
	359.1	0.1	20	8
610 (No residual N_2 gas)	358.9	0.3	60	0 - 1
610 (Residual N_2 gas)	355.5	3.7	730	0
	356.5	2.7	530	2
	356.3	2.9	570	4.5
	357.2	2.0	400	4.5
	357.8	1.4	280	14.5
650 (No residual N_2 gas)	358.9	0.3	60	0 - 1

* Melting Point ± ~50°F during alternate freezing point-melting point plateau determinations.

lithium. In order to place these data in clearer focus, the following relationship has been derived in a manner similar to that previously discussed for rubidium:

$$\Delta T_m, \ ^\circ F = [(ppm)_{N_2} + (0.88)(ppm)_{O_2}] / (198)$$

Using this relationship, the dissolved lithium nitride content (as ppm N_2) corresponding to each measured melting-point depression has been computed, and these results are also presented in Table 7.

The most obvious conclusion dictated by these melting-point studies is that the equilibrium solubility of lithium nitride in lithium at its melting point is quite low. The repeatable initial value of about 60 ppm N_2 obtained in the absence of residual nitrogen gas appears to represent the equilibrium solubility of lithium nitride in liquid lithium, whereas the ultimate value of 20 ppm N_2 appears to represent the equilibrium solubility of lithium nitride in solid lithium.

In the presence of residual nitrogen gas, a different dynamic equilibrium was apparently established at the preabsorption conditions. Because of the simultaneous diffusion of nitrogen gas into the lithium while precipitation of lithium nitride occurs, higher apparent solubilities are evident. In this case, the rate of change of dissolved lithium nitride content was sufficiently slow to allow measurement of the precipitation rate when the system was cooled to the vicinity of the melting point. The resulting rate data which are presented in Figure 20, yield a first-order rate constant of 1.2×10^{-3} ppm/ppm/sec.

C. Capillary Viscometer Experiments

1. Apparatus and Procedures

The capillary viscometer, shown in Figures 21 through 24, consists of a 0.027-in. diameter capillary tube which is coiled in the form of a helix. A reservoir and a receiver are located above and below the capillary, respectively. A pressure equalizing line which is connected to the top of the receiver is attached to a coiled tube leading to a three-valve manifold. A similar coiled tube is connected to the top of the reservoir. The coiled tubes were incorporated to minimize thermal gradients within the viscometer proper. Type 316 stainless steel bellows valves with stellite seats were used on the manifold. Chromel-alumel thermocouples were welded to the reservoir and receiver to monitor the alkali metal temperature during runs. Electrical leads for the liquid level gauge were welded to the reservoir as shown schematically in Figure 21. Ceramic insulators were used to electrically insulate the liquid-level-gage lead wires as well as the thermocouple lead wires. All wires were brought out on the manifold side to a terminal board.

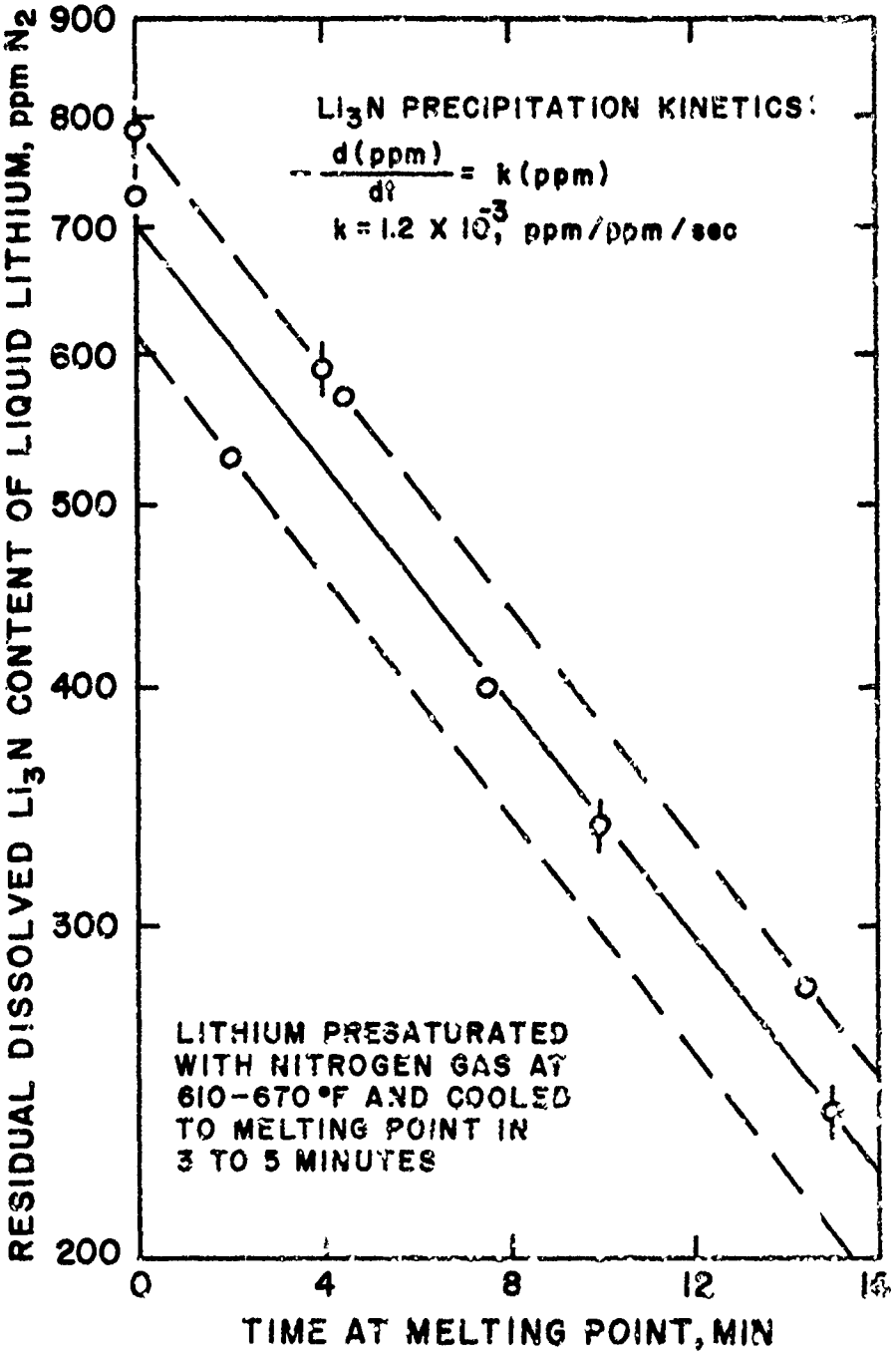

FIGURE 20. GRAPHICAL DETERMINATION OF RATE CONSTANT FOR LITHIUM NITRIDE PRECIPITATION FROM SUPERSATURATED LITHIUM

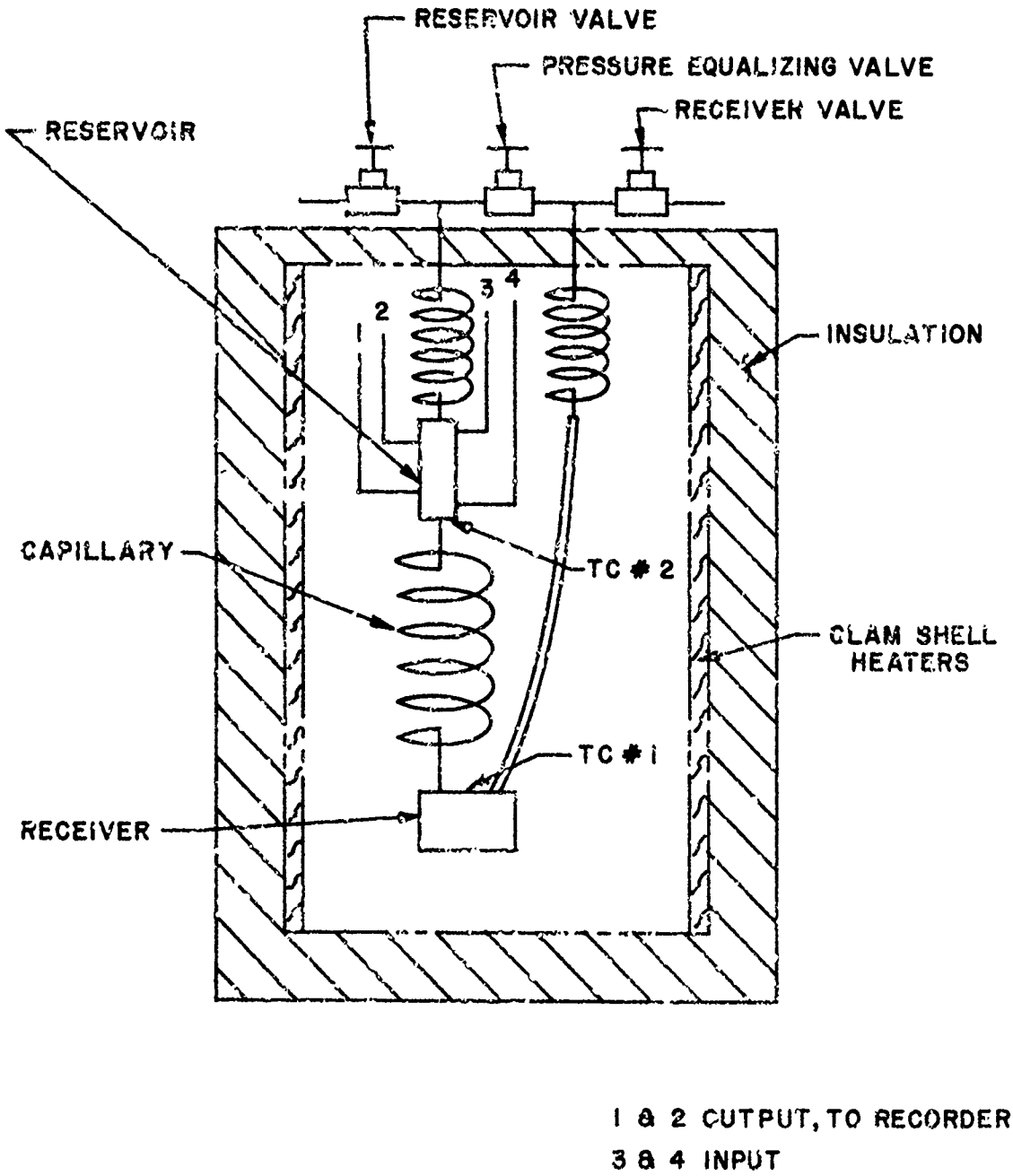

FIGURE 21. SCHEMATIC DIAGRAM OF VISCOMETER APPARATUS

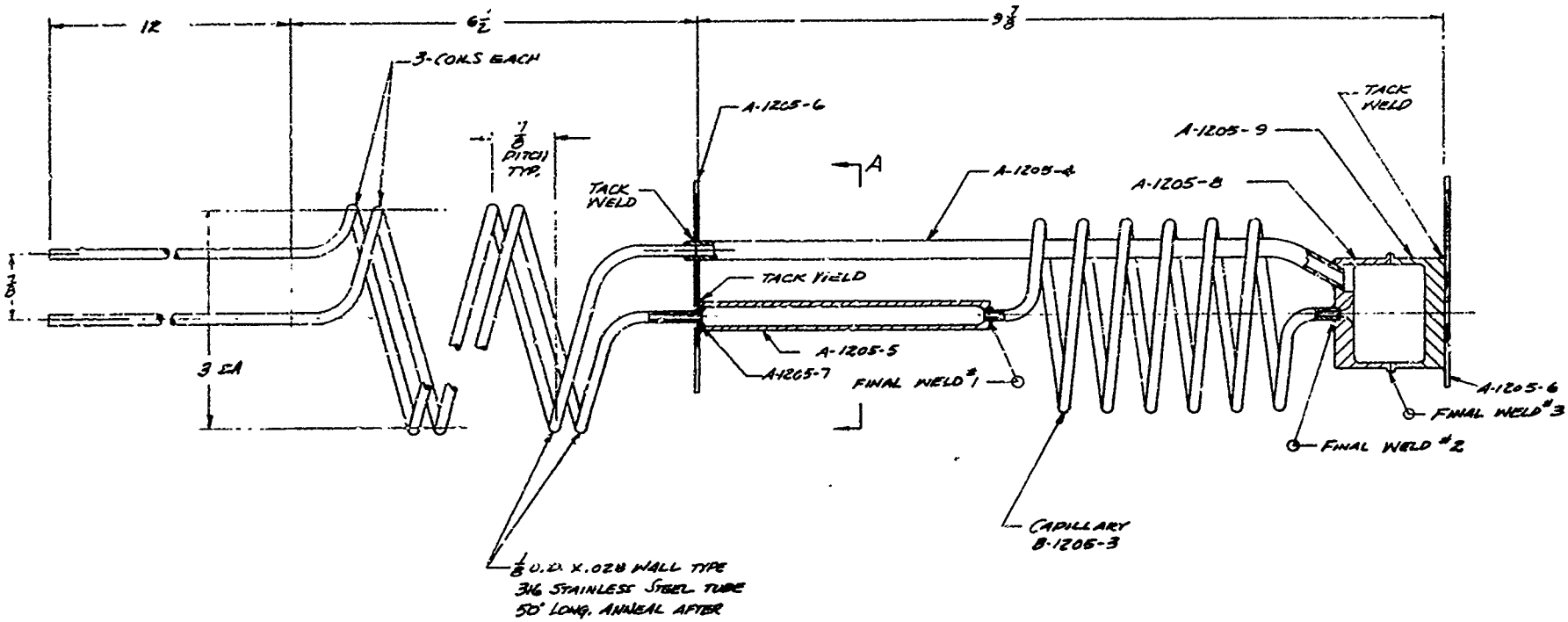

FIGURE 22. DETAIL DRAWING OF CAPILLARY VISCOMETER

FIGURE 23. LIQUID-METAL CAPILLARY VISCOMETER IN OPERATION (INSET: SAMPLE BEING SEALED IN GLASS AMPOULE).

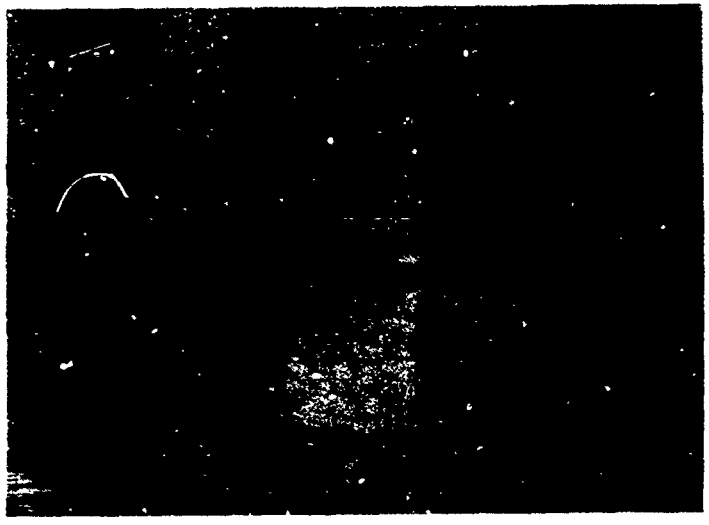

CAPILLARY VISCOMETER
(VALVE-MANIFOLD ATTACHED)

VISCOMETER APPARATUS
(SAMPLE-COLLECTION AMPOULE ATTACHED)

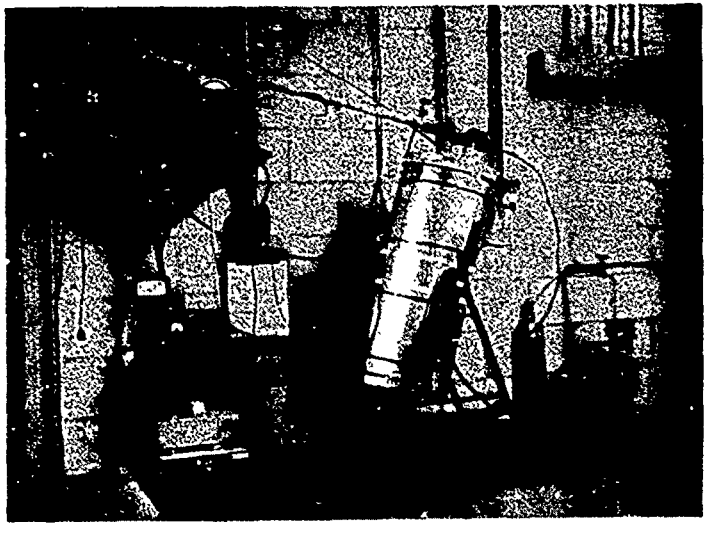

VISCOMETER APPARATUS
(FILLING-TUBE ATTACHED)

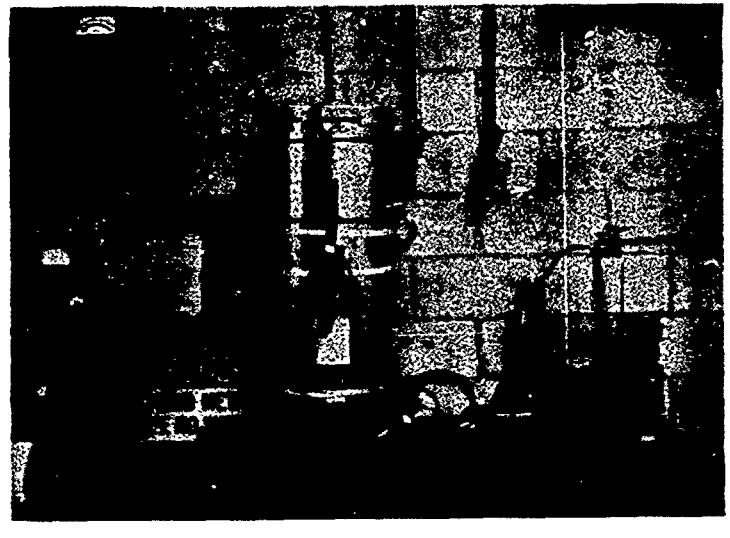

VISCOMETER APPARATUS
(INVERTED FOR EMPTYING)

FIGURE 24. VISCOMETER APPARATUS DURING VARIOUS STAGES OF OPERATION

The viscometer was heated by a pair of clam-shell heaters around which semi-rigid insulation, capable of withstanding 1900°F, was used. This assembly in turn was mounted on an "A" frame to permit 360° rotation of the apparatus for experimental runs and subsequent decontamination procedures.

The manifold was wrapped with glass-fiber heating tape, thereby assuring that all portions of the assembly would be above the melting point of the alkali metal. Additional thermocouples were attached to the valves to allow monitoring of valve temperatures.

In order for the viscometer to operate properly, about 18 cm^3 of alkali metal was needed in the receiver. By rotating the viscometer counter clockwise to a predetermined angle, the liquid metal could be pressurized up through the capillary and into the reservoir. The location of the liquid level could be monitored by the liquid level gage. Once the alkali metal was in the reservoir, the viscometer was rotated clockwise to a vertical position and the pressure equalizing valve was opened, allowing the liquid metal to flow through the capillary under the influence of gravity. A recording potentiometer provides a visual record of the rate at which the alkali metal level traveled from the full to the empty position in the reservoir. All viscosity runs were performed at a slight positive pressure of argon (about 5 psig) to ensure that no foreign gas could be admitted, in the event that minute leak existed.

2. Development of Viscometric Method

This capillary viscometer has certain features which affect the method of calculating the viscosity results. The most important feature is the use of a coiled capillary, which requires the use of a semi-empirical correction factor developed by White[93] and refined by Mencik[57]. This correction factor, which is presented in Figure 25, has been largely ignored in many viscometric studies. It can be neglected without appreciable error at very low Reynolds numbers, but it becomes significant even at moderate Reynolds numbers. For example, with a curvature ratio (coil radius: tube radius) of 100.1, which is approximately the ratio for the present viscometer, the correction factor that must be applied is approximately 1.03 for Re = 170, 1.19 for Re = 400, and 1.50 for Re = 1000. Since the viscometer designed for this program was required to cover a wide range of temperatures and fluid viscosities, it was inherently necessary to operate with a wide range of Reynolds numbers.

Prior to assembling the viscometer, tests were run on the stainless steel capillary tube to calibrate its bore and to determine its flow characteristics. The inside diameter, as determined by the mercury weight method, assuming a uniform round cross-section, was very close to the nominal 0.027" and was not affected appreciably by the coiling operation:

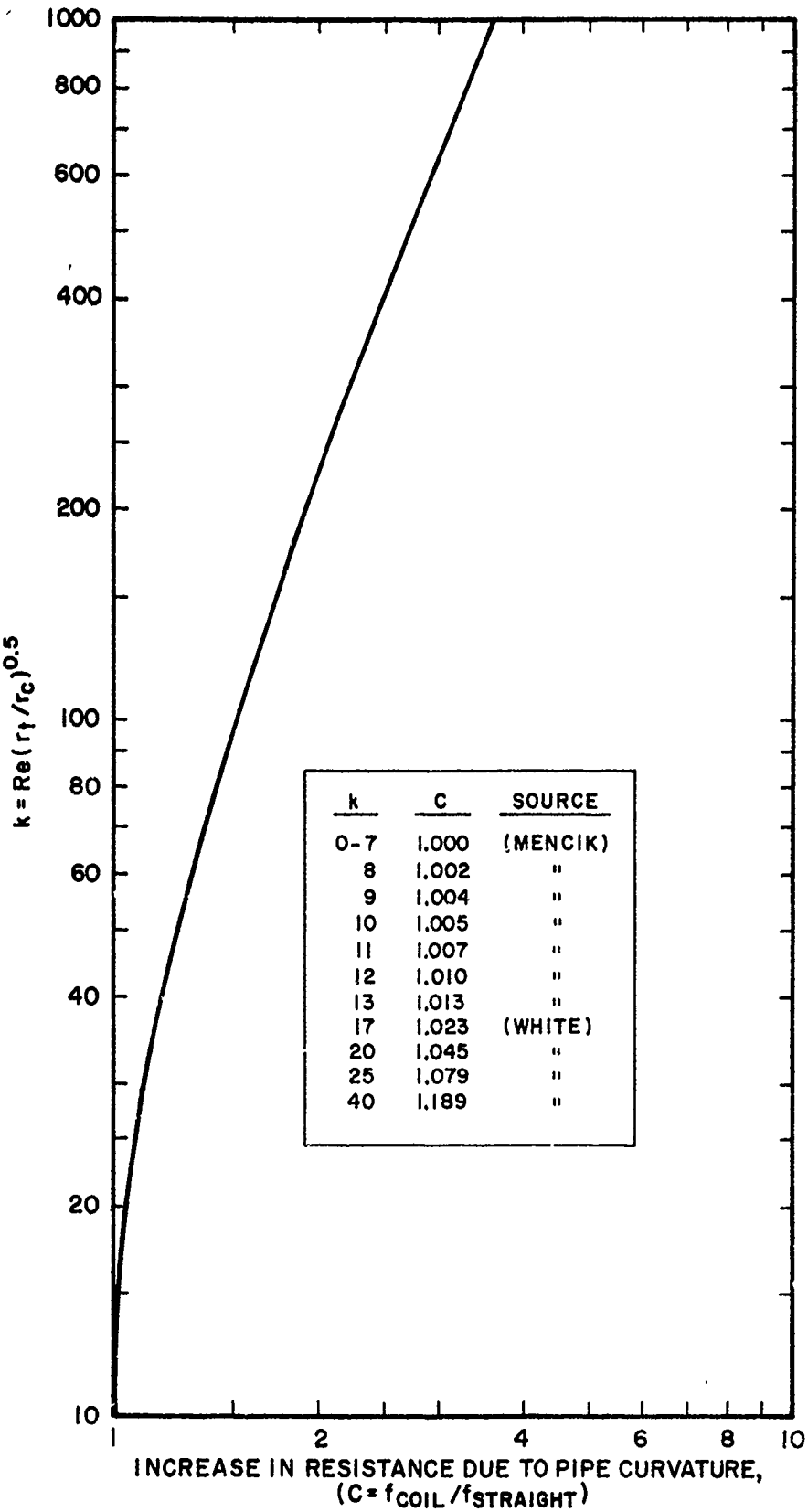

FIGURE 25. EFFECT OF CONDUIT CURVATURE ON FLOW RESISTANCE

Before coiling	0.02674"
After coiling	0.02671"

A flow check on the capillary before coiling, using mercury under 8" of head at a Reynolds number of 1050, gave a viscosity approximately 4.7% higher than the handbook value. This type of deviation is ordinarily accounted for in viscometric practice by lumping it into a viscometer constant. However, as will be evident from the subsequent discussion, the presence of considerably larger corrections under some conditions ruled out this approach.

Tests were conducted after the tube was coiled, using various heads of mercury or water to evaluate the viscometric behavior over a wide range of Reynolds numbers. The following data were obtained:

	Mercury			Water			
Head,h, cm	40.64	20.32	10.16	5.08	304.8	121.9	60.96
Reynolds number	1477	847	477	242	326	167	86
Viscosity, cp							
Apparent	2.66	2.28	2.06	2.03	0.925	0.774	0.746
Handbook value	1.46	1.48	1.46	1.46	0.773	0.722	0.722

The major discrepancies noted at high Reynolds numbers were peculiar to the coiled tube; i.e., they had not been observed when the tube was straight. These data indicated that the "coil effect" would definitely have to be taken into account in setting up the viscometer calibration. A further consideration was the "belling" of the lower end of the capillary in its final assembled form, which presumably creates a suspended level similar to that in the Ubbelohde viscometer and thus eliminates surface tension corrections of the capillary outlet as well as any question of the lower level placement. In view of the magnitude of the coil effect and the necessary reservoir-level surface-tension correction, it was believed that a separate analysis of these effects would give a much more reliable viscometer correlation than does the usual method of lumping everything into viscometer constants.

The preceding data were then refined by introducing the Hagenbach kinetic e: , correction and a surface tension correction*. The Hagenbach

---

* The Couette correction (for length of tube required to develop true Poiseuille flow) is insignificant, owing to the extremely high L/D ratio of our capillary-approximately 1820:1.

correction is rather minor over the range studied here, amounting to about 1.5% at most. The surface tension correction is very significant at low heads, but difficult to assign, since the dropwise flow problem has thus far not received an exact mathematical solution. For the case of mercury issuing from the lower, square-cut end of a capillary tube (as in our case during this calibration of the capillary tube before assembly) an analysis of the problem showed that the back pressure due to mercury surface tension should vary between approximately 0 to 2.2 cm head, as each drop is formed and breaks away. By means of some rather arbitrary averaging, we assigned a value of 1.0 cm Hg for the time-average effective back pressure due to surface tension. Applying this correction and the Hagenbach correction to the preceding data, we obtain values agreeing almost exactly with the previously-mentioned curvature-effect correlation of White and Mencik (Fig. 25).

In most viscometric work, the instrument is calibrated on a standard fluid and the calibration is reduced to "viscometer constants," usually two in number, which express the dimensions of the apparatus and the kinetic energy correction. This approach was not considered suitable for present purposes, for two reasons. First, the "White function" cannot be adapted readily to incorporation as a "viscometer constant." Second, there is no well-standardized fluid that can be used as a reference point for calibrating this instrument. Data on the viscosity of alkali metals are rather scarce, particularly at high temperatures, and in some cases are contradictory. Unfortunately, mercury cannot be used for calibration (the liquid level gage will not function properly with mercury, which does not wet the reservoir walls), and nonmetallic fluids are unusable because of their insufficient electrical conductivity.

There was a further reason for preferring to avoid the use of a calibration fluid. Many of the high-temperature data on liquid alkali metals have been obtained with viscometric methods that involve principles other than tube flow - e.g., damped torsional oscillations. So far as we know, no high-temperature viscosity data on alkali metals have ever been obtained with a capillary viscometer, except the data of Ewing, et al.[19], which included temperatures up to 708°C (1306°F) on Na-K alloys. Some of the noncapillary viscometric methods may involve assumptions that are unjustified or incompletely substantiated. Further, the purity of the alkali metal was not established in all cases. As an incidental point of interest, it may be noted that the paper of Ewing, et al. did not state whether or not a coiled capillary was used. However, the capillary was 520 cm (17 ft) long, so it is reasonable to assume that it was coiled. No attempt was made in their article to correct for capillary curvature, although Reynolds numbers were on the order of 500-2500.

The development of reliable methods of calculating viscosities from capillary flow data without the use of a "standard fluid" was contingent

on including all pertinent parameters in the calculation. If this could be done, it was felt that data obtained with our instrument would be sufficiently reliable to serve as a check on the validity of literature data. As will be shown subsequently, all factors can be accounted for quite well.

In the sections that follow, equations are developed for direct calculation in viscosities from viscometric data, and a plan of numerical calculation is set forth.

a. Nomenclature

C = "White function," empirical
E = linear thermal expansion factor for stainless steel (length at test temperature relative to length at room temperature)
g = acceleration of gravity, cm/sec^2
h = head, instantaneous (from liquid level to suspended level), cm
h_1 = head with level at top tap, cm
h_2 = head with level at bottom tap, cm
h_m = log mean head, cm
h_e = kinetic energy correction, cm
h_γ = surface tension correction, cm
H = corrected head, cm
k = "White parameter," $= Re(r/r_c)^{0.5}$
L = capillary length, cm
m = factor in kinetic energy correction, = 1.12
q = liquid volume, cm^3
q_f = efflux volume between taps, cm^3
r = capillary radius, cm
r_c = radius of curvature of coil, cm
Re = radius of upper reservoir, cm
R = Reynolds number in capillary
ρ = density, g/cm^3
t = time, sec
t_f = efflux time between taps, sec
v = liquid velocity in capillary, cm/sec
γ = surface tension, dynes/cm
μ = viscosity, centipoises

b. Basic Equations

Starting from the Poiseuille equation

$$\mu/\rho = \frac{\pi g r^4 h}{8L(-dq/dt)} \tag{1}$$

and noting that $(-dq/dt) = \pi R^2(-dh/dt)$, we obtain

$$\frac{dh}{h} = \frac{-A dt}{\pi R^2(\mu/\rho)} \tag{2}$$

where $A = \frac{\pi g r^4}{8L}$

Integrating between limits 1 and 2, rearranging, and noting that $t_f = t_2 - t_1$, we obtain

$$\mu/\rho = \frac{A\, t_f}{\pi R^2 \ell n(h_1/h_2)} \tag{3}$$

and, noting that $q_f = \pi R^2(h_1 - h_2)$ and that $h_m = \frac{h_1 - h_2}{\ell n(h_1/h_2)}$,

Equation (3) assumes the form

$$\mu/\rho = \frac{\pi g r^4 h_m t_f}{8 L q_f} \tag{4}$$

It will be noted that all of the quantities in the right-hand side of Equation (4), with the exception of t_f, are dimensions of the apparatus.

We will next consider the change in apparatus dimensions due to thermal expansion (see Fig. 26). The convention will be adopted that the symbols r, h_m, L, and q_f (the latter including R and $h_1 - h_2$) will refer to the room temperature dimensions. Then, if E is the linear expansion factor for type 316 stainless steel (length at test temperature relative to length at room temperature), it is seen from Equation (4) that E enters the numerator to the fifth power and the denominator to the fourth power; i. e., a first-power thermal expansion factor must be applied.

$$\mu/\rho = \frac{\pi g r^4 h_m E t_f}{8 L q_f} \tag{5}$$

Now it is necessary to introduce the Hagenbach kinetic energy correction. This is commonly handled as a head term, $h_e = mv^2/g$, in which m is a factor depending on the viscometer geometry; here it should

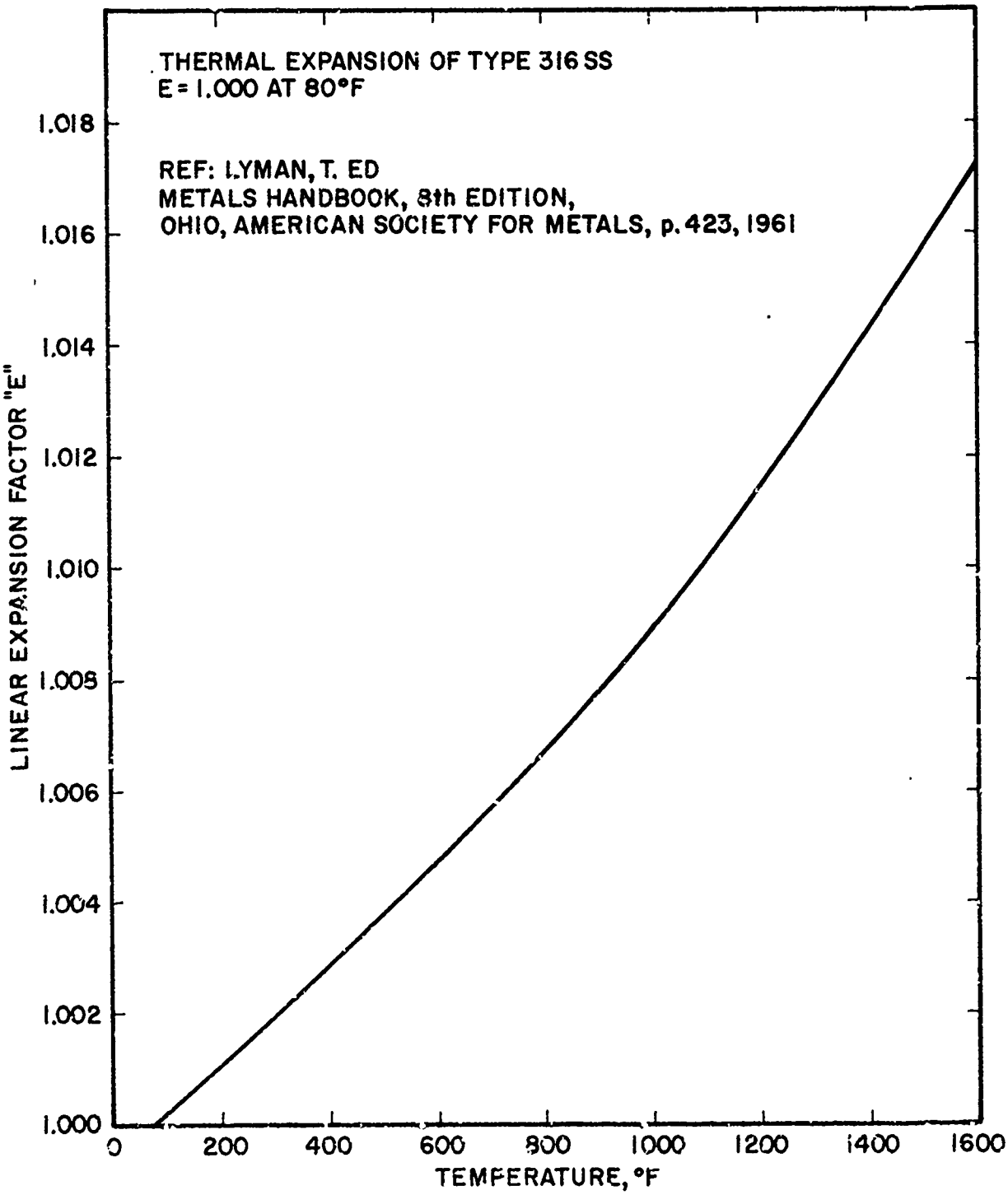

FIGURE 26. LINEAR THERMAL EXPANSION OF TYPE 316 STAINLESS STEEL

be approximately 1.12. Close definition of the value of m will not be necessary in our case, as shown below.

In our calculations, the kinetic energy correction h_e will be subtracted from the log-mean head at operating temperature (h_mE). This procedure is not entirely rigorous, as the kinetic energy correction should theoretically be applied to the initial and final heads (h_1 and h_2) prior to calculating the log mean head h_m. However, this rigorous procedure is not justified here, as calculations have shown that for our case the simplified procedure can be used without significant error. For example, with h_1 = 19.40 cm, h_2 = 14.32 cm, and h_e = 1.0 cm, we find that h_m = 16.73 cm and $h_m - h_e$ = 15.73 cm; the rigorously calculated value of the corrected h_m is 15.72 cm. Actually, h_e should never become as great as 1.0 cm. At our maximum-flow design conditions (Rb, 1600°F, Re = 1000), the calculated kinetic energy correction is only 0.36 cm. Therefore, the simplified method of applying the kinetic energy correction is sufficiently precise. Further, assuming m = 1.12 is also sufficiently precise.

Since

$$v = \frac{q_f}{t_f \pi r^2} = \frac{R^2(h_1 - h_2)}{t_f r^2} \tag{6}$$

then

$$h_e = \frac{mv}{g} = \frac{mR^4(h_1 - h_2)^2}{t_f^2 r^4} \tag{7}$$

It can be seen that the thermal expansion coefficient E will appear in Equation (7) to the second power; therefore,

$$h_e = \frac{mv^2}{g} = \frac{mR^4(h_1 - h_2)^2E^2}{t_f^2 r^4} \tag{8}$$

Equation (5) now becomes

$$\mu/\rho = \frac{\pi g r^4 H t_f}{8LQ_f} \tag{9}$$

where H, the corrected head, is defined as

$$H = h_m E - h_e = E\left[h_m - \frac{mR^4(h_1 - h_2)^2 E}{t_f^2 r^4}\right] \tag{10}$$

Another correction that must be considered in viscometry is the Couette "end correction" that allows for nonstreamline flow at the ends of the capillary. It has been determined that this correction is negligible for our viscometer under any conditions, owing to the extremely large L/r ratio.

The following method of handling the surface tension correction has been selected. It appears safe to assume that there will be no bottom-end surface tension correction, since the shape of the bottom opening of the capillary will tend to create a suspended level. In the upper reservoir, however, there will be a significant effect due to surface tension. This will appear as a "negative" head, opposing flow. Assuming complete wetting (zero contact angle), the head correction will have the form

$$h\gamma = \frac{2\gamma}{g\rho R} \tag{11}$$

Recommended surface tension values for the alkali metals are presented in Figure 27. With the exception of potassium, these data agree with experimental values from published literature[84, 88, 92]. The values for potassium represent recommended best estimates based upon a correlation presented in reference 90.

c. Effect of Capillary Curvature

The White correlation for the effect of capillary curvature is a semi-empirical method. The choice of the correlating parameter, $k = Re(r/r_c)^{0.5}$, is based on theory, but the actual correlation of the "correction factor" C against k is empirical. In application to our apparatus, the usual definition of Reynolds number in the capillary ($Re = 2rv\rho/\mu$), on substituting the value of v from Equation (6), becomes

$$R_e = \frac{2R^2(h_1 - h_2)}{t_f r(\mu/\rho)} \tag{12}$$

or with the necessary thermal expansion factor,

$$R_e = \frac{2R^2(h_1 - h_2)E^2}{t_f r(\mu/\rho)} \tag{13}$$

and, by definition,

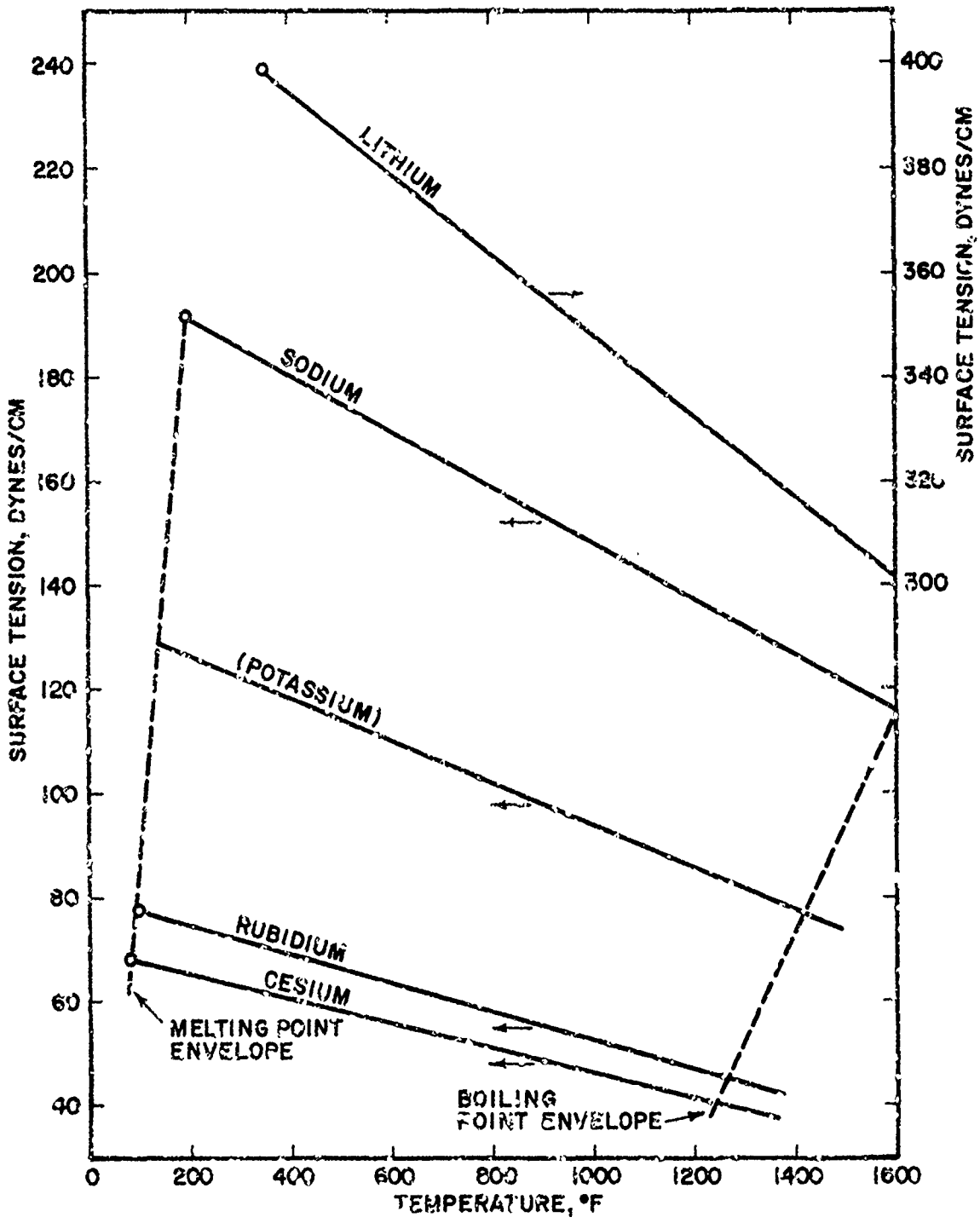

FIGURE 27. RECOMMENDED BEST VALUES OF ALKALI-METAL SURFACE TENSION

$$k = Re(r/r_c)^{0.5} \tag{14}$$

The relation of C to k was found empirically (by White) to be

$$C^{-1} = 1 - \left[1 - (11.6/k)^{0.45}\right]^{2.22} \tag{15}$$

which is said by White to be valid down to k = 11 (at which C = 1). With k less than 11.6, according to White, C remains at 1.0; i.e., there is no correction for capillary curvature.

The values of C in the lower range of values of k were modified slightly by Mencik. Combining Mencik's values with those of White for k > 13, the following are tabulated:

k:	0-7	8	9	10	11	12	13	17	20	25
C:	1.000	1.002	1.004	1.005	1.007	1.010	1.013	1.02_3	1.04_5	1.07_9
k:	40	60	100	200	400	600	1000	2000		
C:	1.18_9	1.30_9	1.50_3	1.89_7	2.48	2.85	3.61	4.93		

The factor C must be applied to the calculated viscosity in order to correct for capillary curvature. It will be observed that the function of C vs k is not adaptable to direct incorporation in the viscosity calculation equations, as it includes Re which in turn includes μ. This implies that a trial solution is necessary. This is accomplished by first determining μ/ρ through Equations (9) and (10), then using this μ/ρ to calculate k and thus find C from White's curve or from the tabulated values. If this C (which we will designate as C_1) differs appreciably from unity, a new value $k_2 = k_1 C_1$ is determined, and from this, a new value C_2 is found. This process is repeated until the solution converges; no more than four trials should be required in any case of interest to us. The final value of C is used as a correction factor:

$$\mu = \mu_1 / C \text{ final} \tag{16}$$

where μ_1 is the viscosity calculated from Equations (9) and (10).

d. Numerical Calculations

The following dimensions of the present viscometer are used in the calculations (all dimensions in cm):

$r = 0.033937$* $\qquad r^4 = 1.3265 \times 10^{-6}$
$L = 124.62$
$r_c = 3.175$

---

* Value of r was determined by mercury weight method.

$R = 0.3175$
$h_1 = 20.12$
$h_2 = 15.04$

The log mean head (at room temperature) based on these dimensions is 17.5 cm.

Substituting these dimensions into Equation (9), we obtain

$$\mu/\rho = 2.543 \times 10^{-6} Ht_f \tag{17}$$

and Equation (10) becomes

$$H = E\left[17.5 - \frac{225.9\,E}{t_f^2}\right] \tag{18}$$

Note that Equation (18) does not include any correction for surface tension, which must be further subtracted to obtain the true effective head.

The expression for Reynolds number, Equation (13), becomes

$$Re = 30.18\left[\frac{E^2}{t_f(\mu/\rho)}\right] \tag{19}$$

and k is given by

$$k = 0.1029\,Re = 3.106\left[\frac{E^2}{t_f(\mu/\rho)}\right] \tag{20}$$

We will now outline the application of these equations to the computation of viscosity from efflux-time data:

1. Obtain the value of E for the test temperature.
2. Determine H from Equation (18), applying a surface tension correction.
3. Determine μ/ρ from Equation (17). Assuming that the density of the fluid at the test temperature is known, this gives the first approximation of viscosity.
4. Using the value of μ/ρ obtained in step 3, calculate k_1 by Equation (20).
5. Using this value k_1, determine C_1 from White chart (Fig. 2b) or tables.
6. If C_1 is greater than 1.01, find $k_2 = k_1 C_1$, find the new C_2, and repeat until the solution converges.

7. Using the final value of C, calculate $\mu = \mu_1 / C_{final}$, where μ_1 is the value viscosity determined in step 3.

It will be noted that this sequence can be applied equally well for computing kinematic viscosity (μ/ρ) in case the density is unknown.

3. Viscosity of NaK(78) and Sodium

Preliminary experimental viscosity measurements were made on NaK(78) and C. P. Sodium in order to accumulate experience with the handling and operation of the viscometer apparatus. The experimental viscosity data obtained during these preliminary experiments are presented in Table 8. The NaK(78) was filtered through a five-micron sintered stainless steel filter at room temperature prior to being transferred into the viscometer.

The recording potentiometer trace obtained in one of the NaK runs is reproduced in Figure 28 to illustrate the type of information directly produced during each viscosity run. It can be seen in this figure that a smooth transition in electrical resistance occurs as the liquid level moves between the full position (corresponding to about 340 microhms resistance) and the empty position (corresponding to about 940 microhms resistance). For the purposes of this illustration, a logarithmic curve was penciled in over the recorder trace in the transition region. This was done in order to demonstrate the extrapolation procedure used for obtaining the full and empty intercepts. The chart distance, along the time axis, between the full and empty intercepts is measured with an optical micrometer, and the efflux time is thereby obtained since the chart speed is known. Knowing the temperature and efflux time, the previously derived calculation procedures are then employed to convert these measurements into viscosity data.

Some difficulty was encountered during early runs because of the wide spread in temperature between the reservoir and receiver. However, this difficulty was alleviated somewhat in later runs by better sealing of the viscometer furnace ends and by conducting temperature equilibration with the apparatus in a horizontal position.

The results of the NaK viscosity measurements are compared with published data [18, 19, 44] in Figure 29. The agreement of these data with the published data is considered gratifying in view of the facts that only two points were measured and that the viscosity data were computed from efflux times without the necessity of prior calibration with a reference fluid.

Viscosity data were also obtained on C. P. Sodium, which was transferred in the inert-atmosphere glove box to a valved container and then charged to the viscometer. All transfers from this sodium container were made at temperatures well above the melting point of sodium in order to assure effective transfer. The sodium was cold filtered through a 5 micron sintered stainless steel filter. Four viscosity runs were performed at about 600°F. In this particular series of experiments, the temperature gradient between the reservoir and receiver was somewhat excessive, hence, the actual capillary

TABLE 8. SUMMARY OF EXPERIMENTAL VISCOSITY DATA FOR NaK(78) AND SODIUM

Reservoir Temp, °F	Receiver Temp, °F	Mean Temp, °F	Viscosity		No. of Runs Averaged
			Kinematic centistokes	Absolute centipoises	
			NaK		
79	77	78	0.925	0.800	2
975	928	928	0.218	0,164	3
			Na		
640	580	609	0.335	0.293	4

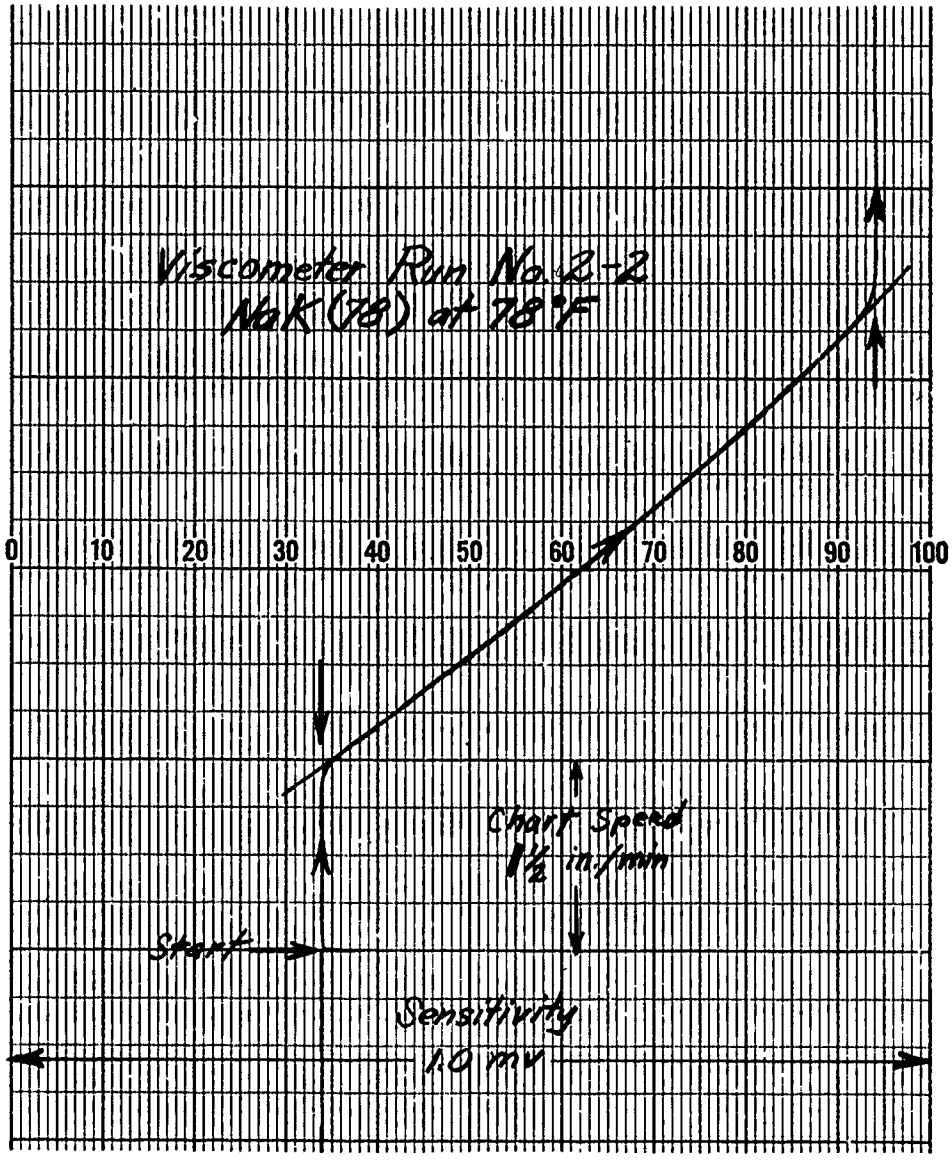

FIGURE 28. SAMPLE TIME-OF-EFFLUX CHART FOR CAPILLARY VISCOMETER

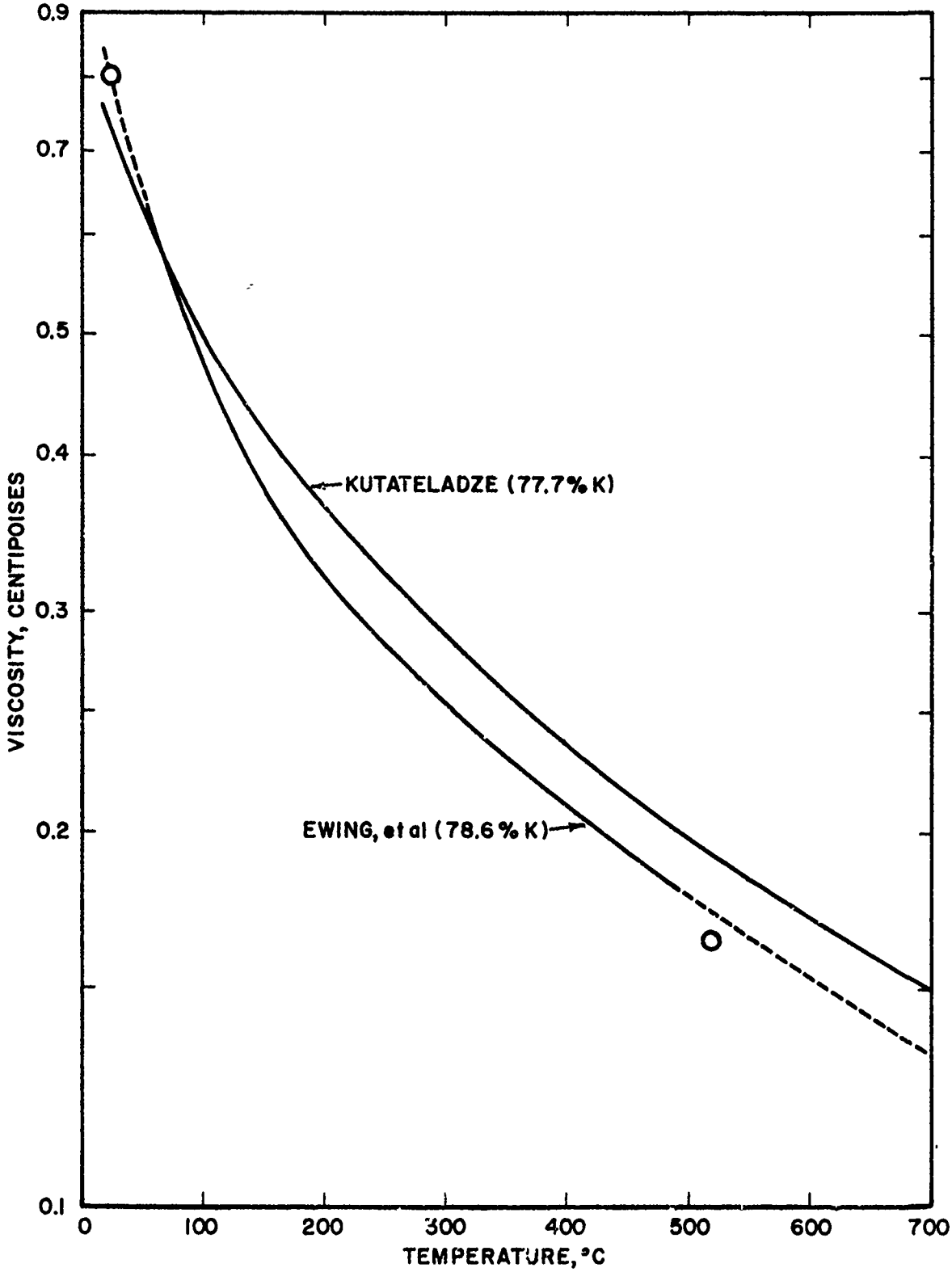

FIGURE 29. COMPARISON OF NaK (78) VISCOSITY VALUES WITH PUBLISHED DATA

temperature was somewhere between 580 and 640°F. The experimental viscosity data reported by Kutateladze vary from 0.333 to 0.297 centipoises for this temperature range (Fig. 30). Therefore, our experimentally measured average value of 0.293 centiposes may be considered realistic.

4. Viscosity of Rubidium and Rubidium with Oxygen Contaminant

By this time, considerable confidence had been gained in the operation of the viscometer. Therefore, a series of experiments was undertaken to obtain viscosity data on rubidium with and without oxygen contaminant. The results of these experiments are summarized in Table 9. Typical standard deviations are presented in Table 10.

About 100 viscosity points were measured with the first batch of pure rubidium, with good experimental repeatability. Fourteen series of runs were performed at various temperature levels from 200 - 1200°F. About 80 additional viscosity measurements were then made at temperatures from 150-800°F on the second batch of pure rubidium. These values were in agreement with those previously obtained.

All of these data for pure rubidium are presented in Figures 31 and 32 along with prior experimental values[48]. These results which appear quite reasonable, represent the first experimental rubidium viscosity measurements reported for temperatures greater than 500°F. They are quite gratifying in view of the complexities involved, both in the viscometer design and data interpretation. Density values used in data reduction calculations were those of Tepper, et al.[86].

Following these measurements, oxygen contaminant was added in steps of 1000, 1000, 1000, 2000, and 2000 ppm (to a total of 7000 ppm), and viscosities were measured at temperatures from about 100-550°F for each step. The results of these measurements are shown for each contamination level in Figures 33 through 37. As in the case of pure rubidium, the logarithm of the kinematic viscosity for each contaminant level appears to vary linearly with the reciprocal absolute temperature. Therefore, linear correlations were derived from the data of pure rubidium and those of each contaminant level, and the resulting family of curves is presented in Figure 38. Using these derived linear relationships, the data were cross plotted, yielding the correlation in Figure 39. This correlation illustrates the influence of added oxygen on kinematic viscosity at various temperature levels.

The low-melting sample of oxygen-contaminated rubidium (7000 ppm) removed from the viscometer after these runs, was analyzed for heavy metals. The following metal contents were found. <3ppm Cr, 11 ppm Ni, and 804 ppm Fe. These results strongly indicate that iron is selectively extracted from type 316 stainless steel by oxygen-contaminated rubidium under the conditions of these experiments.

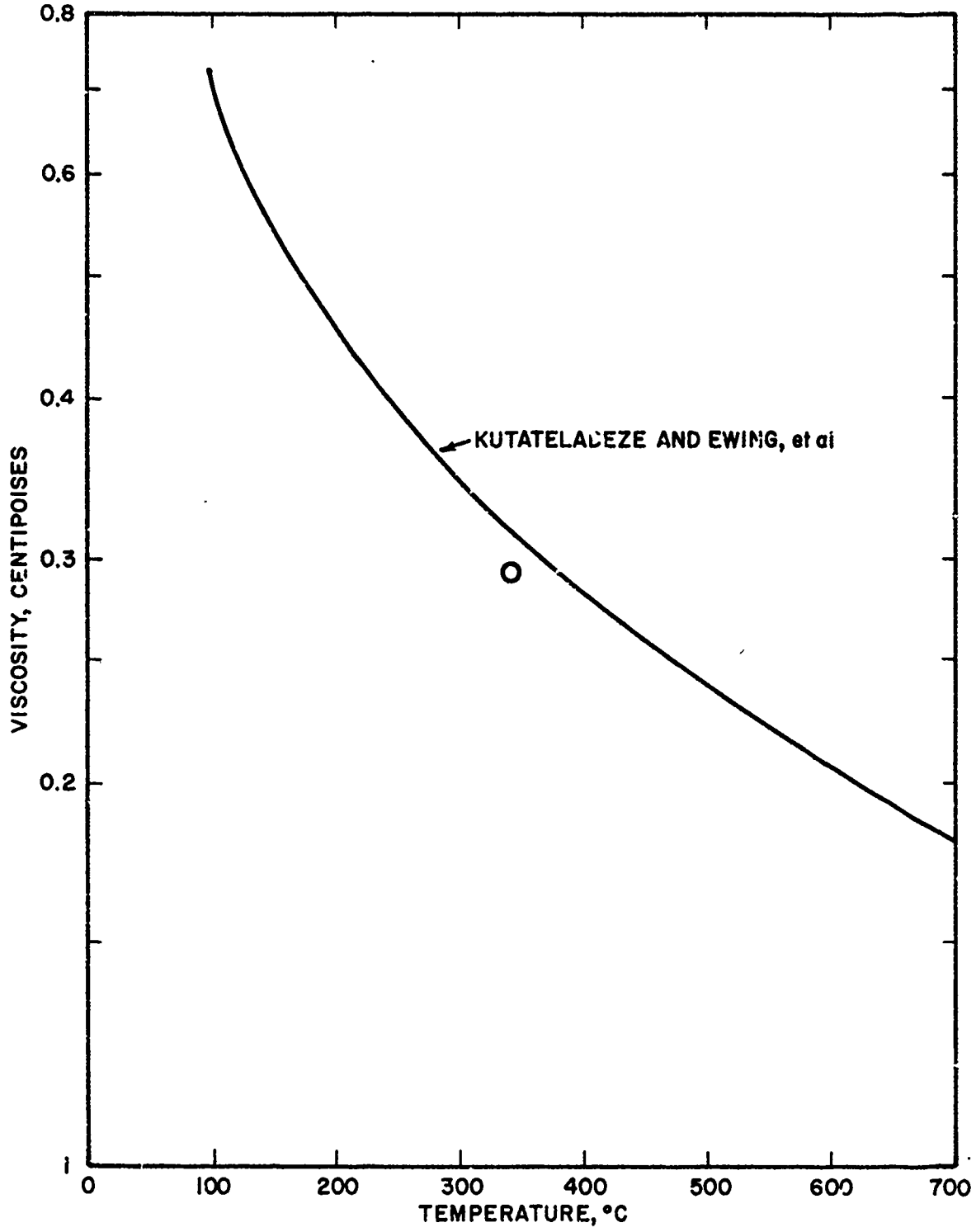

FIGURE 30. COMPARISON OF SODIUM VISCOSITY VALUES WITH PUBLISHED DATA

TABLE 9. SUMMARY OF EXPERIMENTAL VISCOSITY DATA FOR RUBIDIUM

Reservoir Temp, °F	Receiver Temp, °F	Mean Temp, °F	Viscosity Kinematic centistokes	Viscosity Absolute centipoises	No. of Runs Averaged	Remarks
551.8	517.8	534.8	0.203	0.284	9	Batch No. 1
1100.2	1064.0	1082.1	0.134	0.169	4	
359.0	338.0	348.5	0.281	0.406	3	
344.6	332.6	338.6	0.275	0.392	5	
342.6	326.7	334.7	0.271	0.383	13	
559.6	532.3	546.0	0.199	0.277	12	
1007 8	979.2	993.5	0.143	0.182	5	
1004.7	975.0	989.9	0.146	0.187	3	
567.2	536.5	551.9	0 193	0.269	6	
769.0	736 2	752.6	0.164	0.220	12	
221.6	206.0	213.8	0.325	0.481	3	
217.3	203.6	210.5	0.323	0.478	3	
1241.3	1214.0	1227.6	0.127	0.156	3	
1234.5	1207.4	1220.9	0.133	0.163	7	
339.0	314.5	326.8	0.277	0.402	12	Batch No. 2
824.6	802.1	813.4	0.161	0.214	12	
204.0	193.0	198.5	0.339	0.503	12	
651.4	628.6	640.0	0.160	0.247	11	
461.4	444.2	452.8	0.227	0.321	12	
152.3	145.5	149.2	0 384	0.574	4	
207.7	199.3	203.5	0.336	0.498	4	
273.8	261.3	267.6	0.291	0.426	4	
314.0	295.3	304.7	0.266	0.387	4	
362.3	338.3	350.3	0 249	0.360	4	
386.5	405.0	395.8	0.233	0.334	4	
415.0	397.3	406.2	0 233	0.334	4	1000 ppm O_2 added
153.5	143.3	147.9	0.382	0.571	4	
214.7	195.7	205.2	0.320	0.474	3	
261.8	243.3	252.6	0.296	0.435	4	
300.8	285.8	293.5	0.280	0.435	4	
351.8	336.0	343.9	0.245	0.368	4	
407.3	389.0	398.2	0.232	0.332	4	
462.3	442.0	451.1	0.216	0.307	4	
511.5	490.5	501.0	0.207	0.291	4	
167.3	160.3	163.8	0.370	0.564	4	2000 ppm O_2 added
205.0	192.0	198.5	0.343	0.509	4	
263.8	240.3	252.1	0.301	0.442	4	
300.3	284.3	292.3	0.283	0.413	4	
154.0	150.0	152.0	0.400	0.598	4	3000 ppm O_2 added
203.0	191.0	197.0	0.348	0.515	4	
258 0	240.3	249.2	0.308	0.452	4	
301.3	293.0	297.2	0.286	0.417	4	
355.0	344.3	349.7	0.261	0.377	4	
412.3	391.5	401.9	0.238	0.340	4	
459.5	438.0	448.5	0.229	0.325	4	
512.8	492.5	502.7	0 214	0.301	4	
553.5	533.0	542.8	0.205	0.286	4	
207.0	194.8	200.9	0.364	0.540	4	5000 ppm O_2 added
263.0	242.5	252.8	0.323	0.475	4	
106.5	96.3	101.4	0.491	0.740	4	
514.0	498.8	506.4	0.214	0.300	5	
356.8	342.6	349.8	0.273	0.395	4	
112.8	108.6	110.7	0.463	0.697	5	
206.2	199 0	202.5	0.364	0.540	5	
255.8	239.0	247.4	0.320	0.470	4	
303.0	295.0	299.0	0.288	0.420	4	
356.9	344.5	350.7	0.263	0.381	4	
114.8	104.8	109.8	0.499	0.752	4	7000 ppm O_2 added
351.0	337.5	344.3	0.271	0.391	4	
304.3	290.5	297.4	0.303	0.441	4	
252.8	238.8	245.8	0.335	0.493	4	
200.0	190.5	195.3	0.386	0.572	4	
99.9	96.9	98.4	0.521	0.787	12	
211.5	197.0	204.3	0.373	0.553	4	
328.3	301.0	314.7	0.301	0.437	4	
354.0	334.0	344.0	0.273	0.395	4	

TABLE 10. EXAMPLE STANDARD DEVIATIONS IN RUBIDIUM VISCOSITY MEASUREMENT

Temperature, °F			No. of Points	Mean Viscosity, centistokes	Standard Deviation, %	Remarks
Max	Min	Avg				
769.0	736.2	752.6	12	0.164	0.93	Pure Rb (Batch 1)
461.4	444.2	452.8	12	0.227	0.88	Pure Rb (Batch 2)
99.9	96.9	98.4	12	0.521	1.08	7000 ppm O_2 in Rb

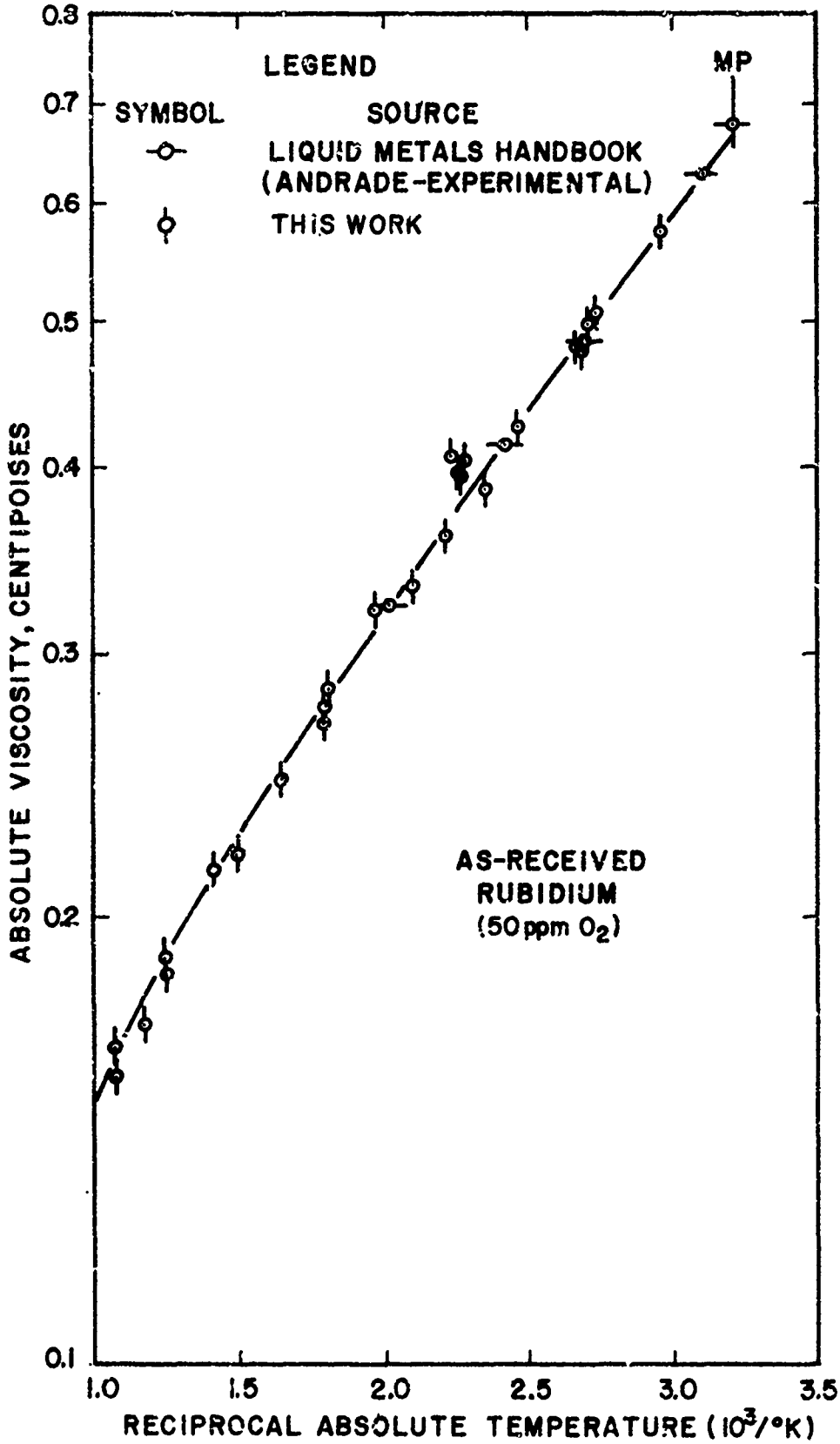

FIGURE 31. EXPERIMENTAL ABSOLUTE VISCOSITY DATA FOR AS-RECEIVED RUBIDIUM

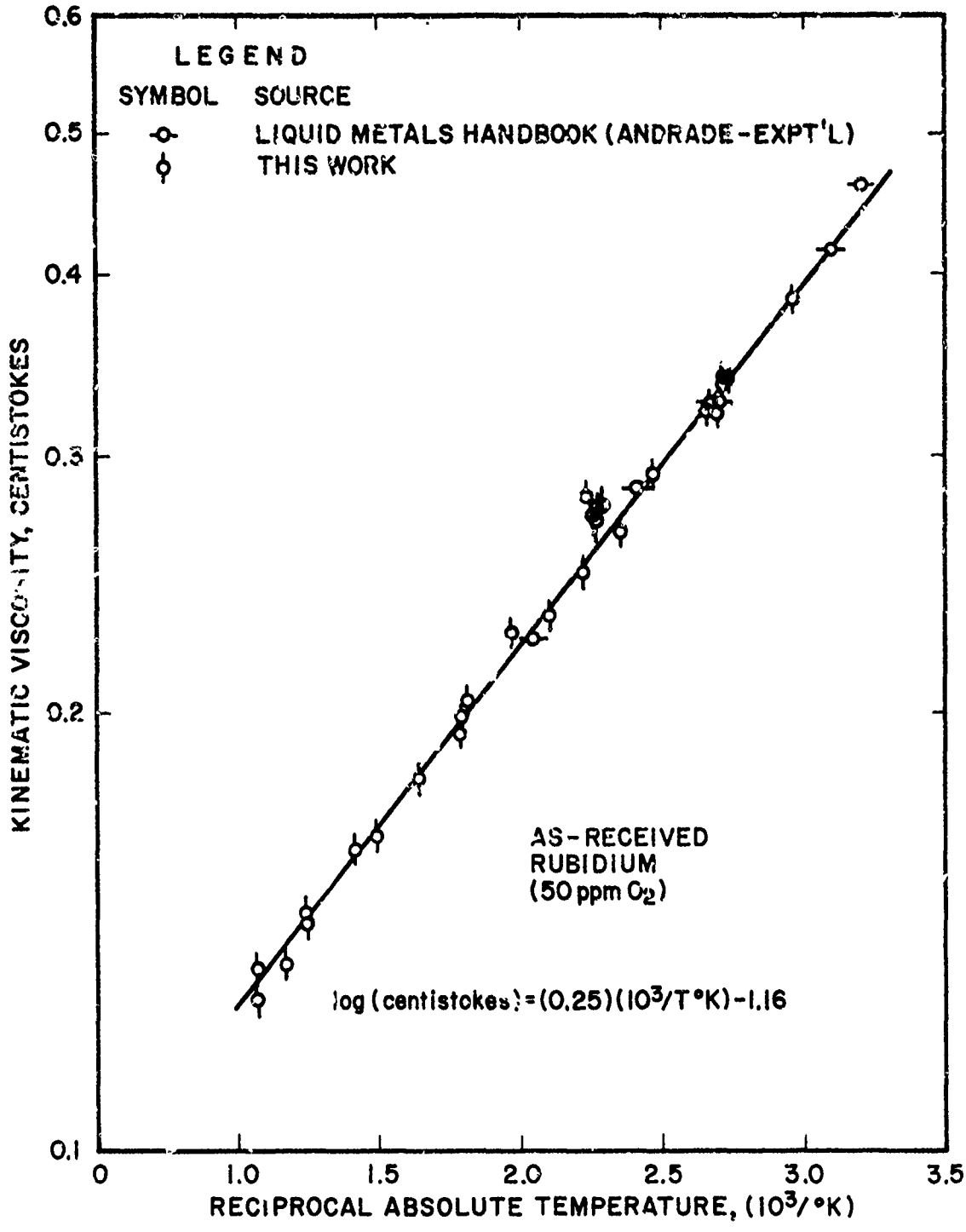

FIGURE 32. EXPERIMENTAL KINEMATIC VISCOSITY DATA FOR AS-RECEIVED RUBIDIUM

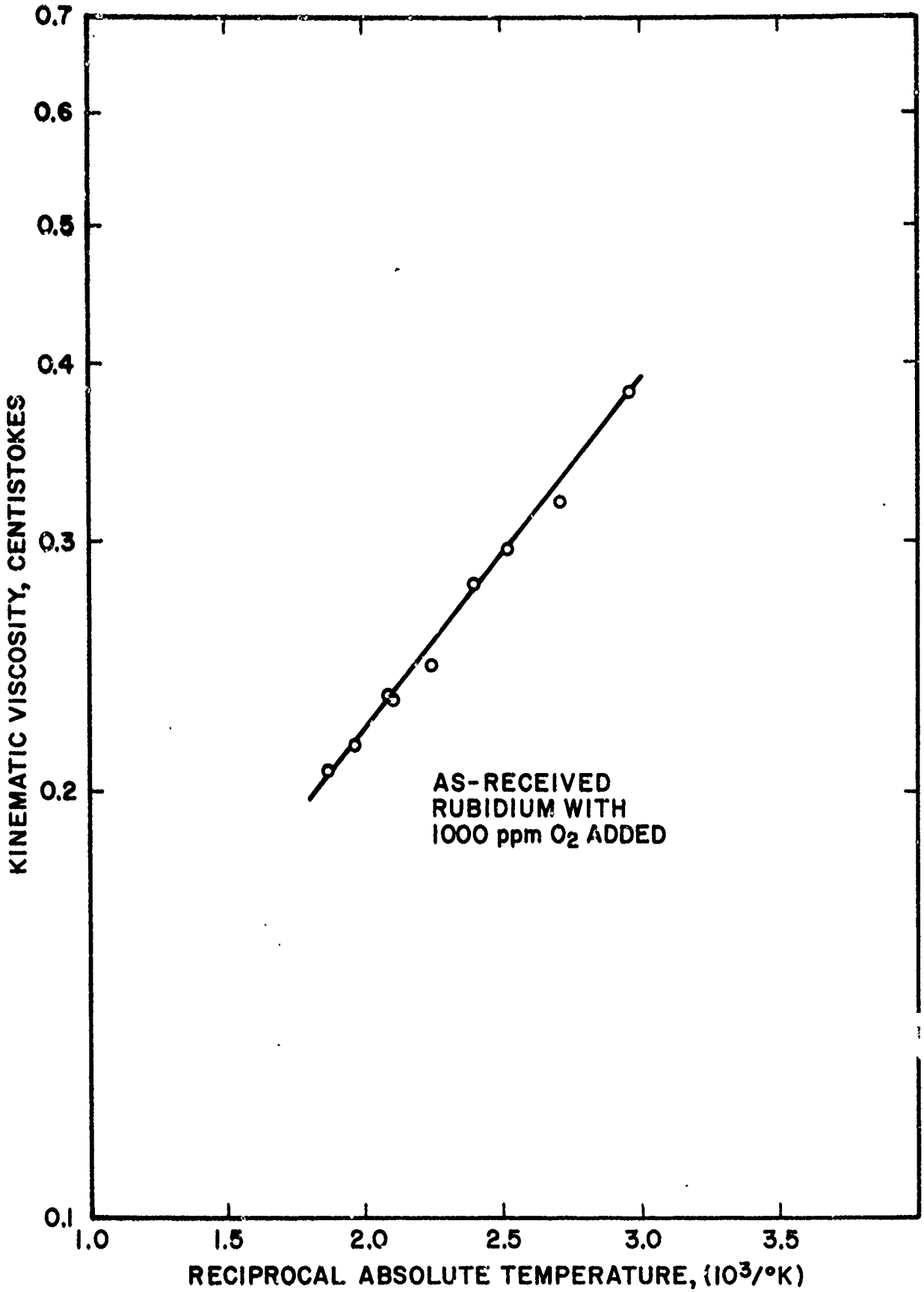

FIGURE 33. EXPERIMENTAL KINEMATIC VISCOSITY DATA FOR CONTAMINATED RUBIDIUM

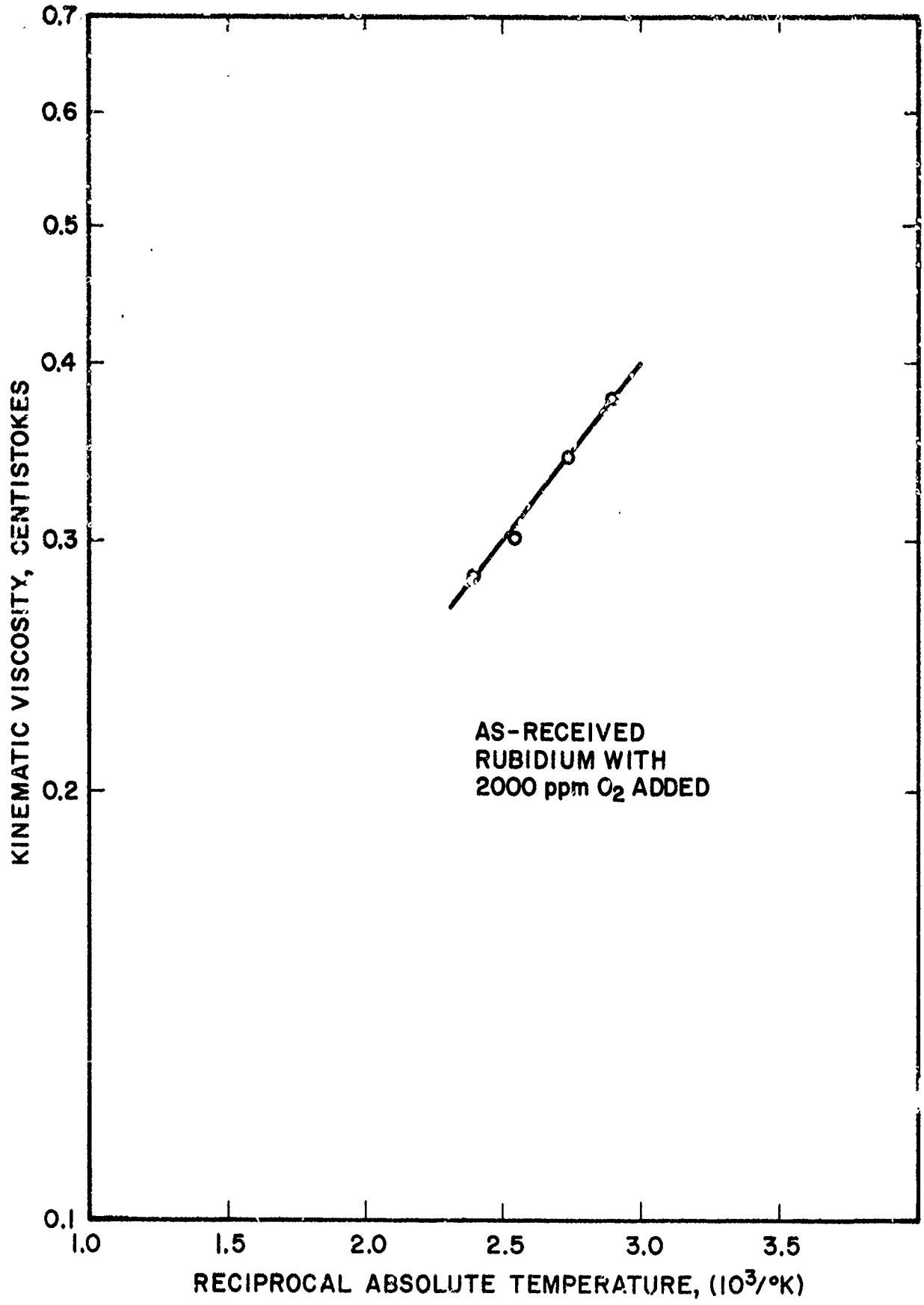

FIGURE 34. EXPERIMENTAL KINEMATIC VISCOSITY DATA FOR CONTAMINATED RUBIDIUM

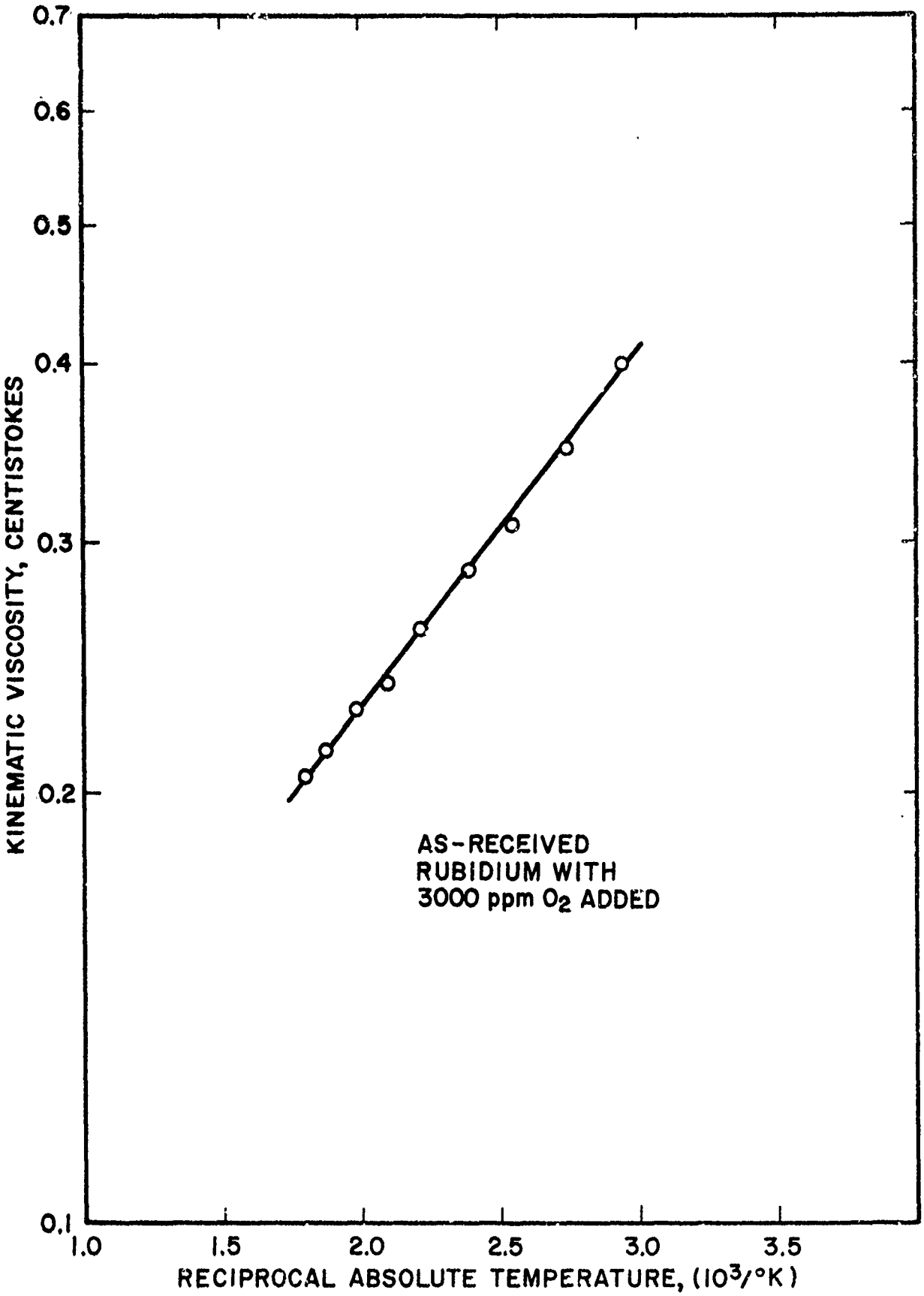

FIGURE 35. EXPERIMENTAL KINEMATIC VISCOSITY DATA FOR CONTAMINATED RUBIDIUM

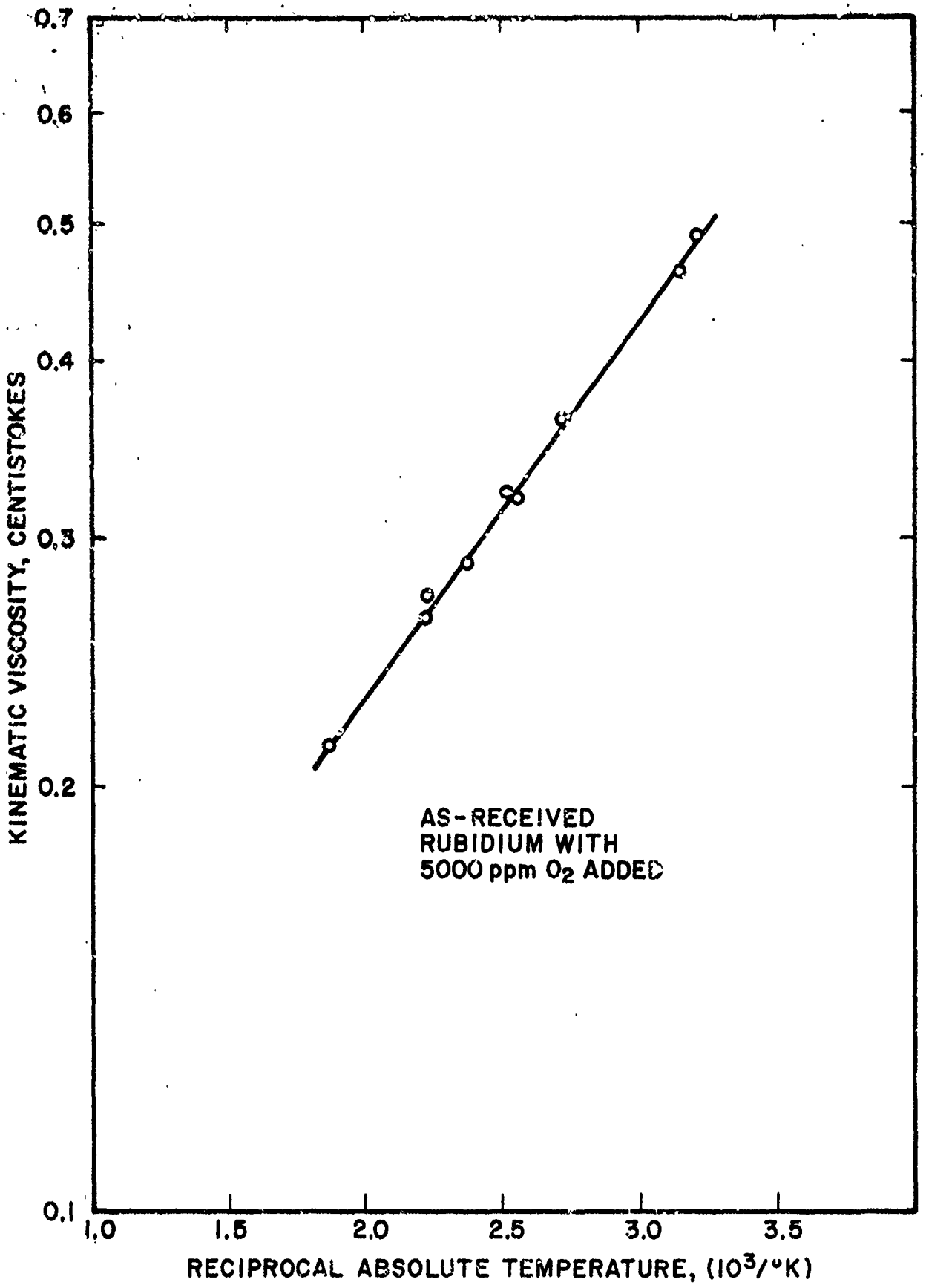

FIGURE 36. EXPERIMENTAL KINEMATIC VISCOSITY DATA FOR CONTAMINATED RUBIDIUM

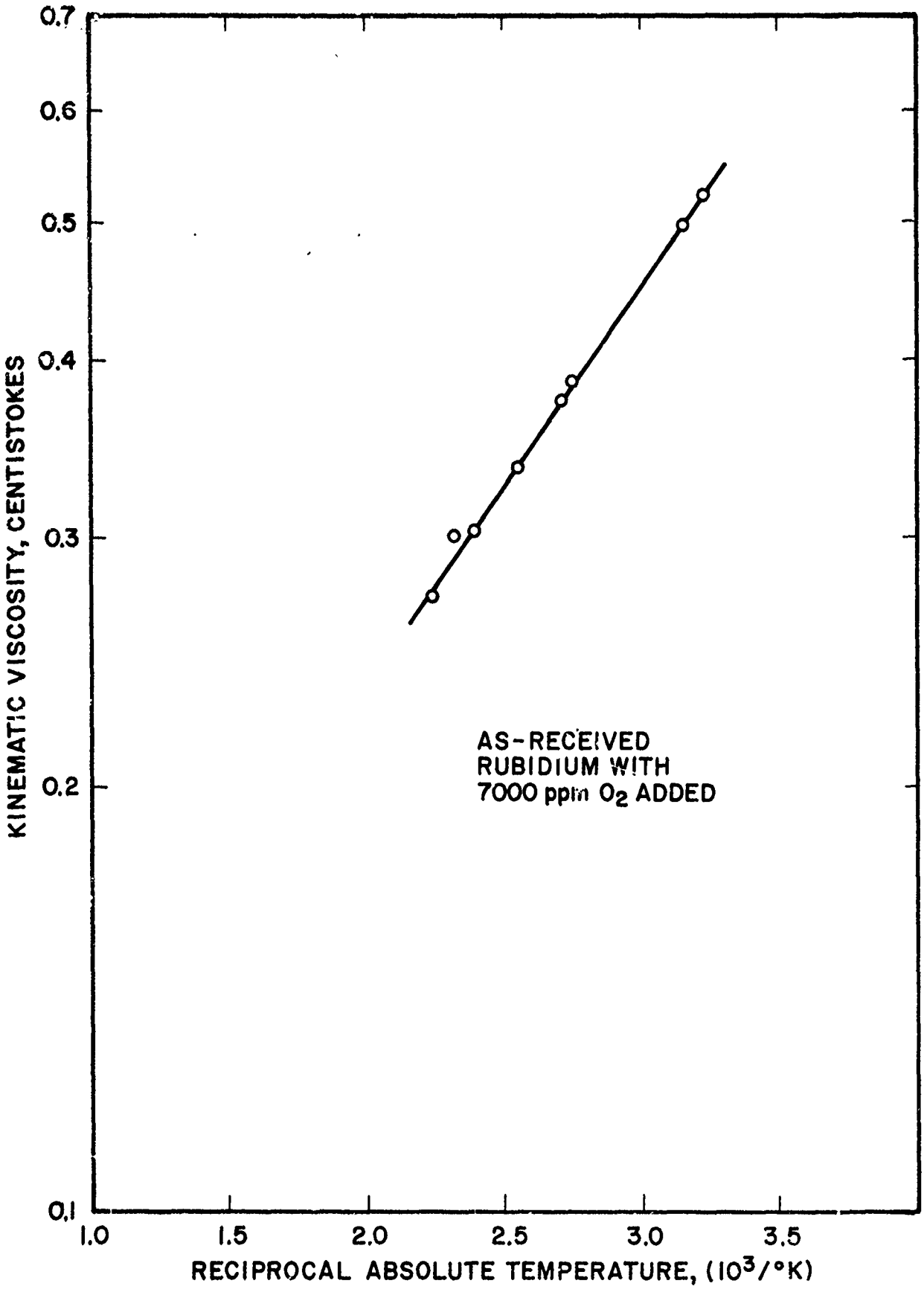

FIGURE 37. EXPERIMENTAL KINEMATIC VISCOSITY DATA FOR CONTAMINATED RUBIDIUM

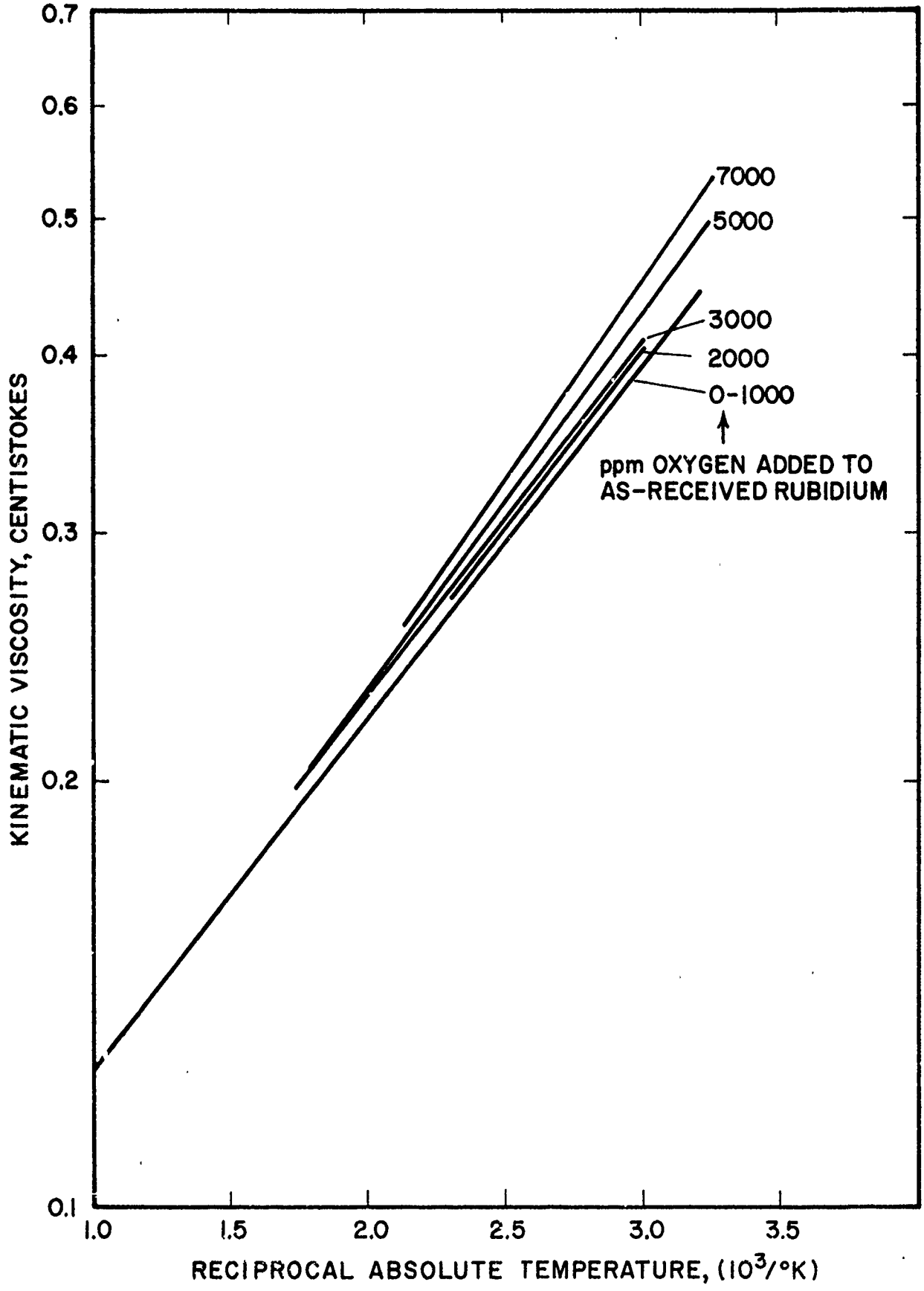

FIGURE 38. CORRELATION OF EXPERIMENTAL RUBIDIUM VISCOSITY DATA

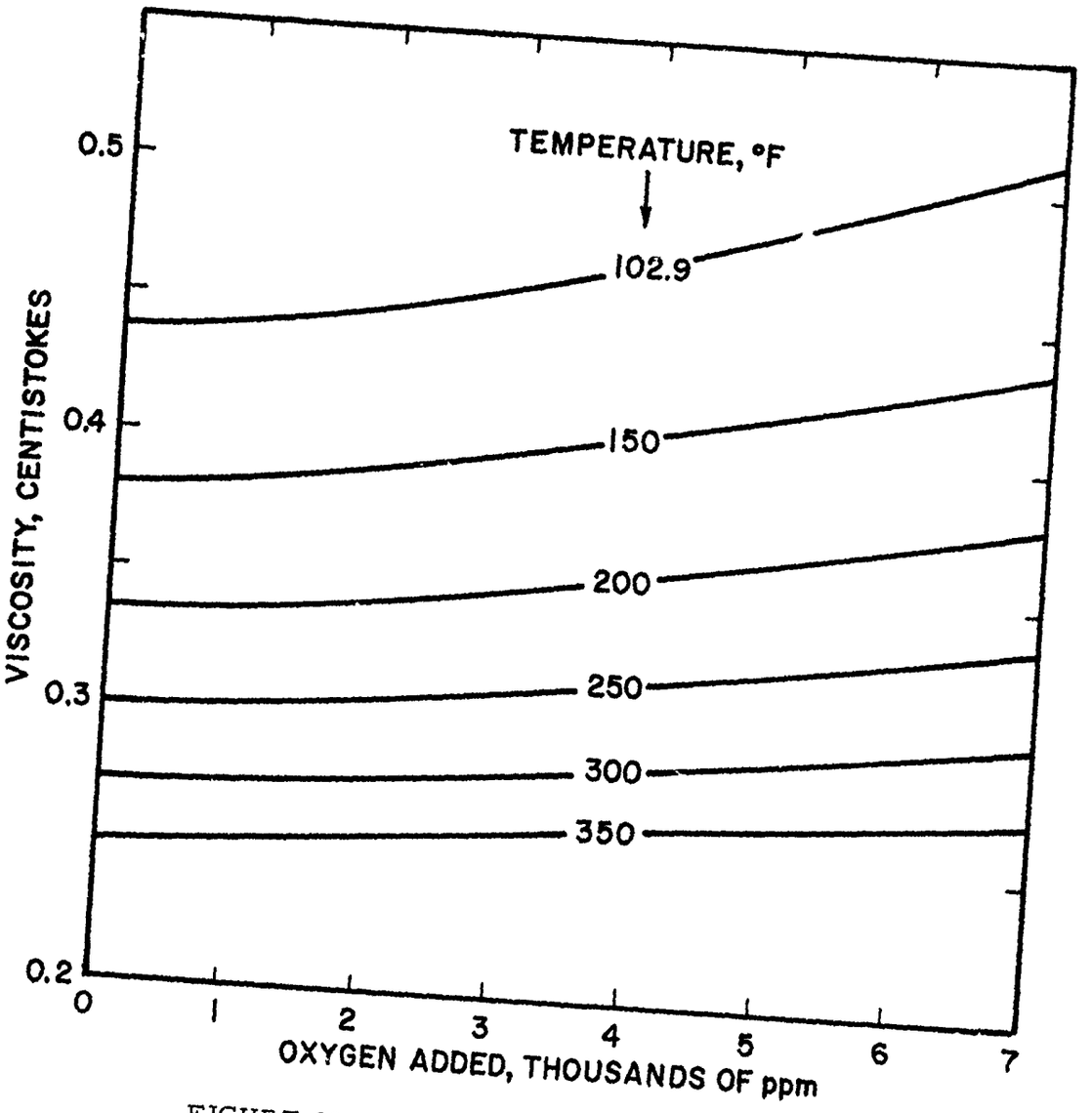

FIGURE 39. CORRELATED EFFECT OF OXYGEN CONTAMINANT ON RUBIDIUM VISCOSITY

5. Viscosity of Lithium

The viscometer was charged with reactor-grade lithium, and viscosity measurements were undertaken. Because of the extremely high surface tension and low density of lithium, extreme operating difficulties were encountered. In fact, no single run was completely successful in the sense that the reservoir drained completely during the run. On the other hand, in three runs, it was possible to compute the lithium viscosity, from the initial slope of the transition in the liquid-level resistance trace. The results of these data-reduction calculations are presented in Table 11.

In order to compute the viscosity from this initial slope, the previously-derived equations were modified to utilize the full-reservoir fluid head rather than the log-mean fluid head as was done in all prior experiments. The results of these calculations are compared with published data[48] in Figure 40, and the agreement is considered satisfactory in view of the previously-mentioned operating difficulties.

Parallel experiments on the effect of nitrogen contamination on the melting point of lithium clearly demonstrated that no useful purpose could be served by adding nitrogen contaminant to the lithium in the viscometer. The results of this previously-described melting-point study indicated that precipitation, and hence plugging, would occur upon such contamination. Therefore, the lithium viscosity experiments were terminated.

When the viscometer was drained and cleaning was begun, extreme plugging difficulties were encountered because of the formation of nitride and hydroxide. As in the case of rubidium, the system was heated to above the melting point of these reaction products, but the apparent formation of high-melting oxides from the hydroxide rendered this technique useless. Repeated treatments alternately with acetic acid and hydrochloric acid at about 200° F and subsequent heating to 1600° F while pressuring one side of the viscometer with argon removed the obstructions, and final cleaning was achieved by flooding with 50-50 acetic acid followed by 50-50 nitric acid and then distilled water. Because of the limited solubility of lithium compounds in water, these final cleaning steps had to be repeated successively at a temperature of about 200° F in order to flush the reaction products from the system.

D. Pumped Isothermal Loop Performance

1. Apparatus and Procedures

In order to investigate the pumping characteristics of liquid rubidium and liquid lithium, an isothermal loop was designed and constructed of type 316 stainless steel. The isothermal design was selected for this study

TABLE 11. SUMMARY OF EXPERIMENTAL VISCOSITY DATA FOR LITHIUM

Reservoir Temp, °F	Receiver Temp, °F	Mean Temp, °F	Viscosity		No. of Runs Averaged
			Kinematic centistokes	Absolute centipoises	
636	618	627	0.93	0.47	1
655	635	645	0.74	0.37	1
680	713	697	0.89	0.44	1

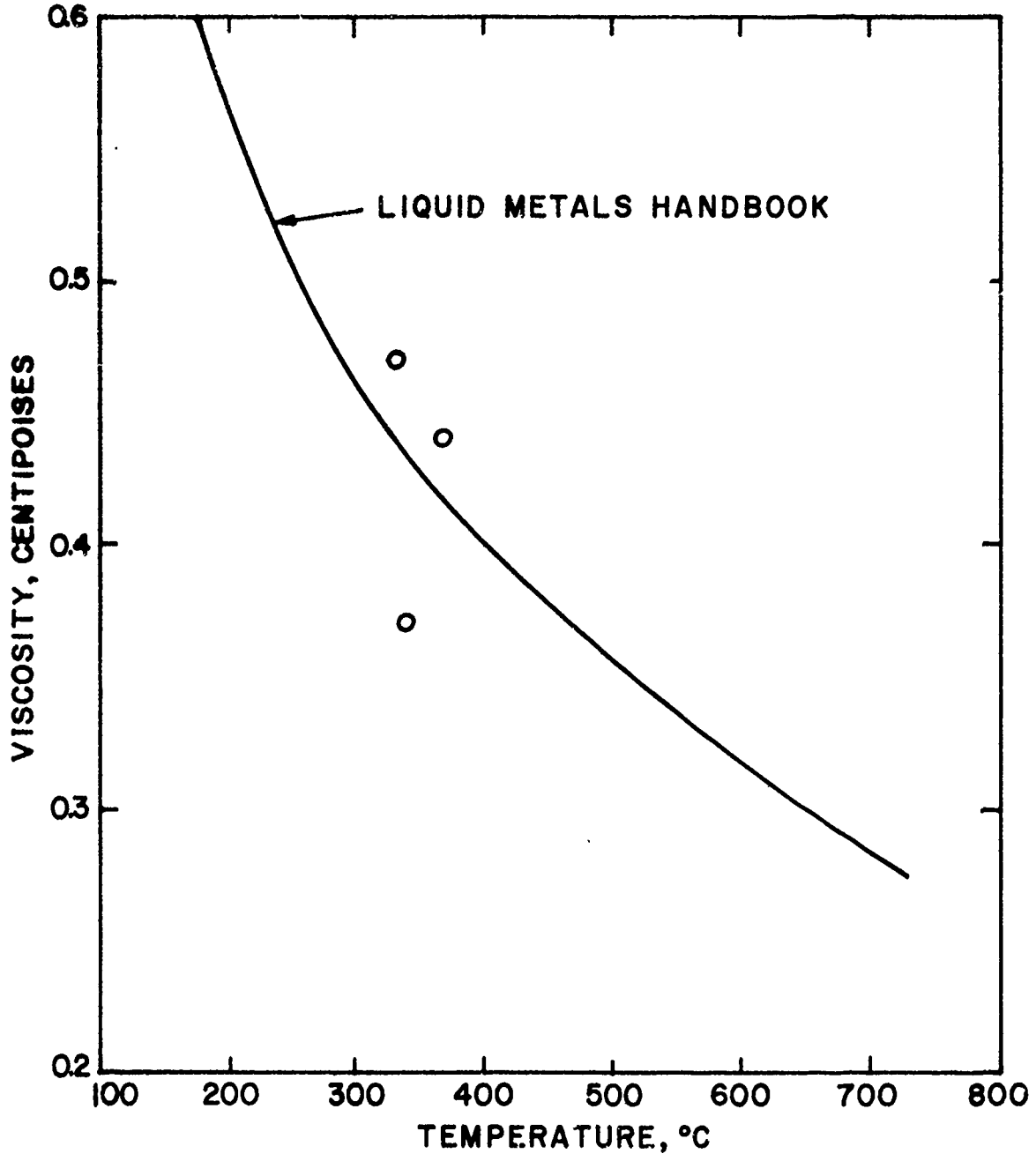

FIGURE 40. COMPARISON OF LITHIUM VISCOSITY VALUES WITH PUBLISHED DATA

because of several inherent advantages offered by the absence of significant thermal gradients. These anticipated advantages include the following:

(1) Minimum thermal-gradient mass transfer.

(2) More stable operation.

(3) No drastic localized heat-input or heat-dissipation loads.

(4) No burnout problems in the event of flow stoppage.

The loop shown in Figures 41 through 43 consists of five major components, an electromagnetic pump, a flowmeter, a liquid-level test section, a filter section, and two balanced-pressure detectors. The commercially available electromagnetic pump is controlled by a 240v variable transformer. Flow is monitored with a commercially available electromagnetic flowmeter (calibrated for rubidium and lithium by the manufacturer). As the alkali metal passes through the flowmeter, it goes to the test section, which is composed of an impingement zone and an annular region. Above this annular zone is located the liquid level reservoir. From the test section the liquid metal flows to the filter section, which consists of two parallel filter units. The alkali metal then flows from the filters to the suction side of the electromagnetic pump. It can be seen from the drawing of Figure 41 that all of the horizontal lines have been canted 5° to facilitate and ensure complete drainage.

The entire system was fabricated from Type 316 Stainless Steel in order to minimize corrosion by alkali metals at elevated temperatures, up to 1500°F. Pairs of tubular heating elements were used to trace the entire loop tubing. These elements were installed between each of the major components which were provided with their own independent heating elements, as in the cases of the pump and the flowmeter. Clam-shell heaters were utilized for heating the liquid-level test section, filters, and the balanced pressure detectors. The entire loop was mounted within a steel frame under which was placed a large steel pan, capable of containing all of the alkali metal in the loop in the event of a spill. Chromel-alumel thermocouples were carefully heliarc welded onto all of the major components and at various locations along the loop. Additional thermocouples were attached to the tubular heating elements themselves, in order to monitor heater-element temperatures to prevent burnouts. Pilot lights were provided in each heater circuit to ensure immediate notification in the event of a heater burnout. Each heater was provided with an independent power supply.

The dynamic loop is located within an enclosed cell which has been described previously. The main control panel is located adjacent to this enclosure. It contains the heater and pump power supplies, the remote accessories for the balanced-pressure detectors, and the inert gas

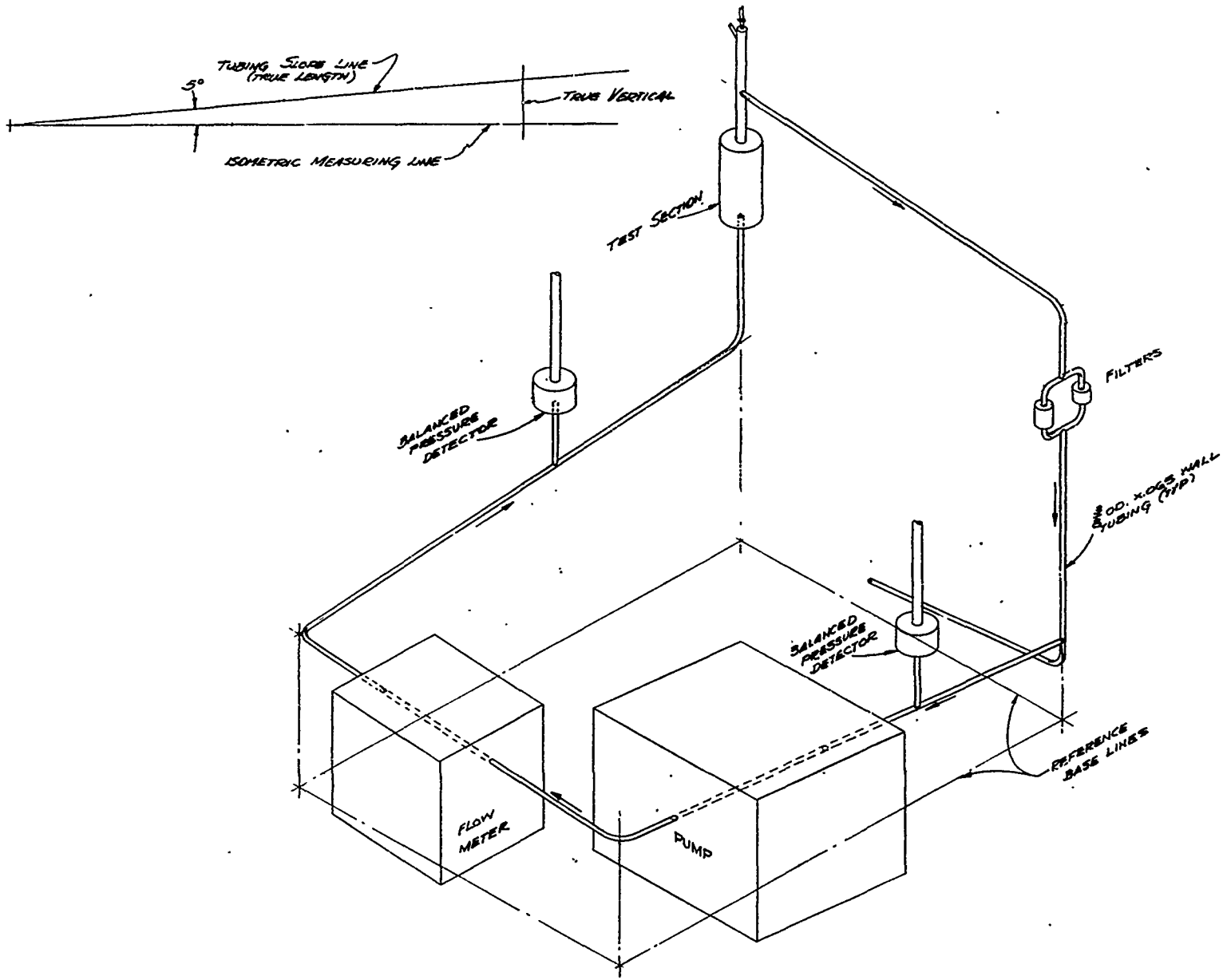

FIGURE 41. ISOMETRIC ASSEMBLY DRAWING OF LIQUID-METAL LOOP

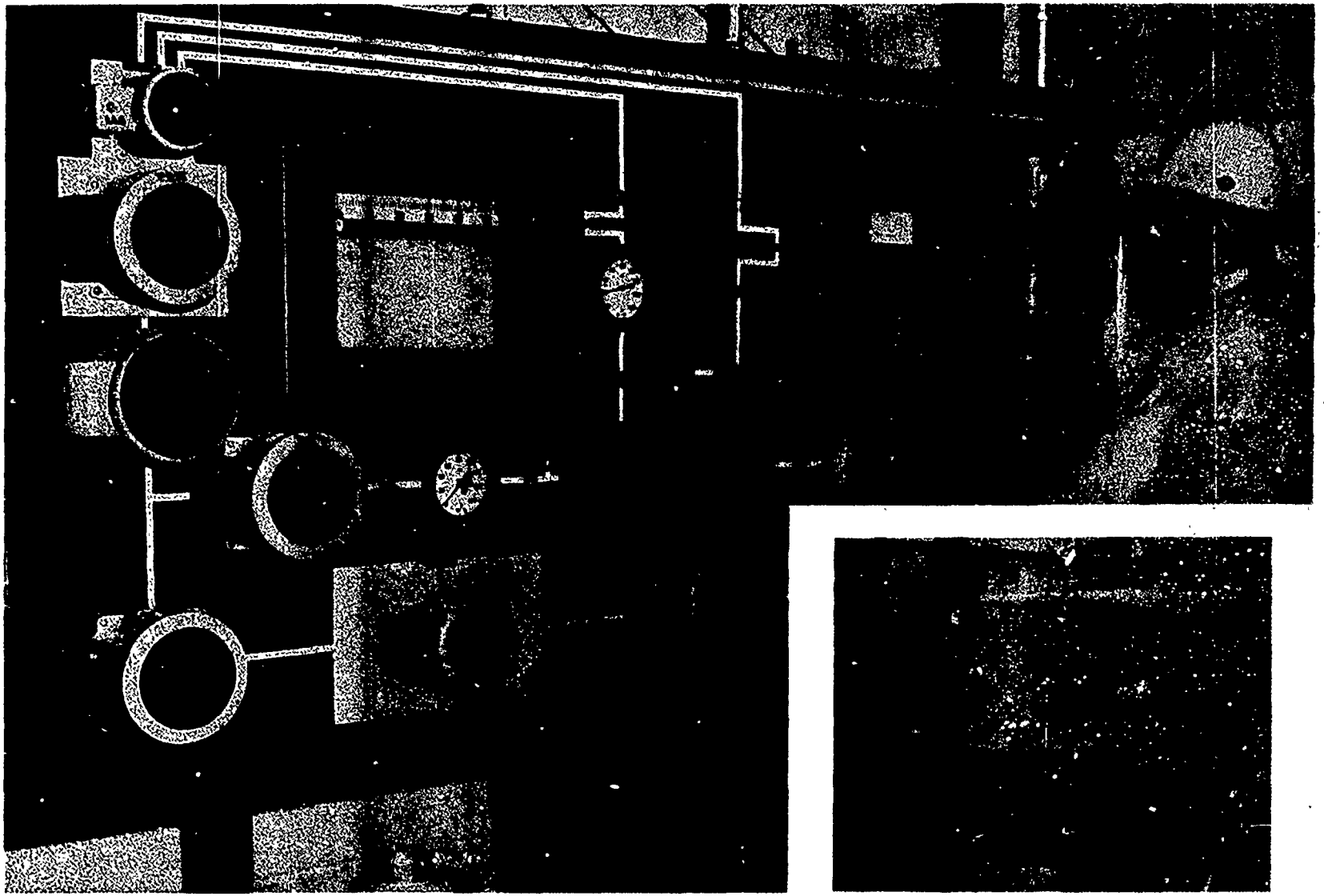

FIGURE 42. LIQUID-METAL LOOP CONTROL PANEL
(INSET: VIEW OF LOOP IN OPERATION).

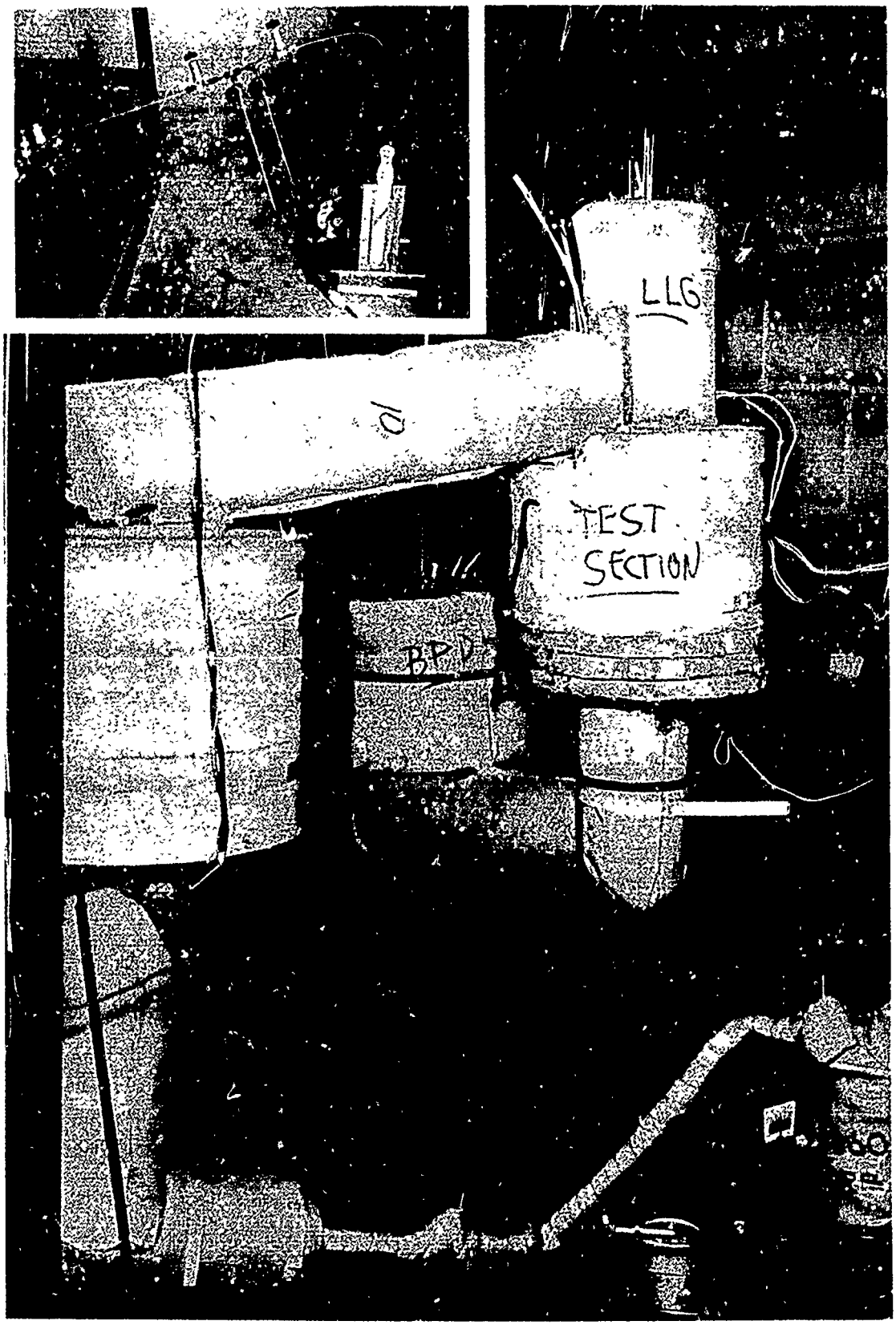

FIGURE 43. LIQUID-METAL LOOP WITH HEATED, FLEXIBLE FILL LINE AND HEATED, TARED TRANSFER VESSEL (INSET LOOP SAMPLING AMPOULES BEFORE INSTALLATION OF SAMPLE-LINE HEATERS).

supply. In order to facilitate operation of the loop, a flow diagram of the alkali metal and gas lines was superimposed on the control panel. One 24-point temperature recorder was used for temperature observation at the main points of interest in the loop. The adjacent temperature indicator was incorporated to serve other less-important temperature readings. The liquid-level gage and the flow meter were monitored by a microvoltmeter and a recording potentiometer. The argon pressure was introduced into the loop at the top of the liquid-level section, with an argon return line being provided a few inches below the supply line. In order to ensure leak-tight connections throughout the loop, all loop connections were heliarc welded. The entire loop was designed for isothermal operation with the exception of the fill line to which was attached a stainless steel bellows valve capable of a maximum temperature of 600° F. The entire loop was covered with split insulation (capable of withstanding 1900° F) which was readily removable for inspection and maintenance.

Once the temperatures of the various components of the loop were near the desired value, pumping was begun, and the various temperatures rapidly equilibrated to a near-isothermal condition because of the excellent heat-transfer characteristics of the liquid metals. In order to measure pressure-drop data, the pump discharge and suction pressures were monitored with the balanced-pressure detectors illustrated in Figure 44.

In each of these detectors, nitrogen pressure was applied to the upper surface of a diaphragm to balance the liquid-metal pressure beneath the diaphragm. Accessory nitrogen pressure gages and electrical circuits were provided for detection of this balancing pressure. To calibrate these detectors, liquid-metal flow was stopped momentarily while pressure measurements were made, and these readings were correlated with the pressure above the liquid level as illustrated for one run in Figure 45. For dynamic conditions, these correlations were employed as calibration curves and to correct the indicated balancing pressures to the same basis (no-hydrostatic-head conditions). During pumping operations the liquid level gage and flowmeter were monitored regularly, and appropriate temperatures were recorded. A typical data sheet for one pumping performance run is illustrated in Table 12.

2. Pumping Characteristics of Rubidium and Rubidium with Oxygen Contaminant

The loop was filled (under vacuum) with pure rubidium, and several consecutive runs were made (under argon) in which pressure drop was monitored. It was noted that relatively good repeatability was obtained from day to day as shown in Figure 46, and that the flow rate was not very sensitive to liquid temperature. Once the operating characteristics were established, about 5000 ppm of oxygen (based on total rubidium inventory in loop) were added to the liquid-level chamber while the system was under vacuum and not being pumped.

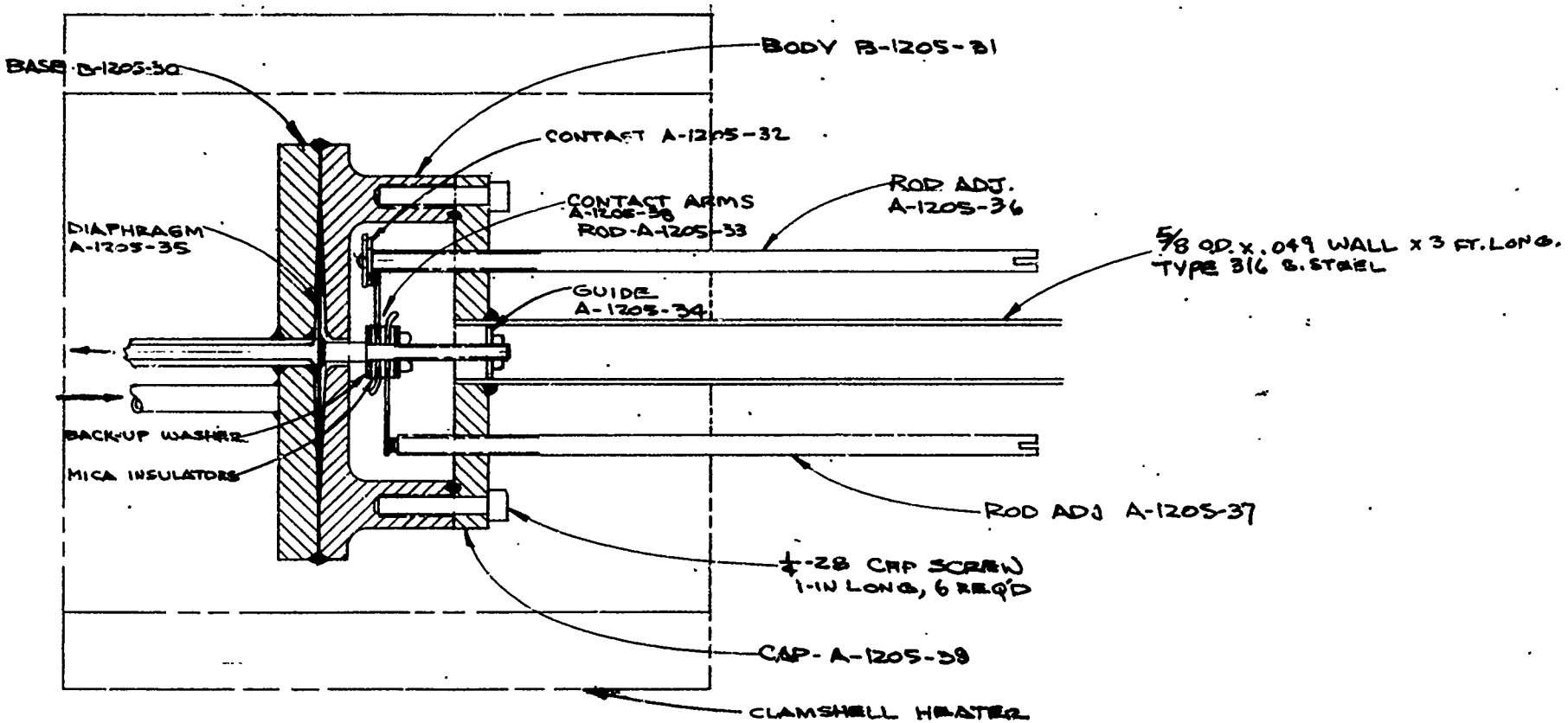

FIGURE 44. BALANCED-PRESSURE DETECTOR ASSEMBLY DRAWING

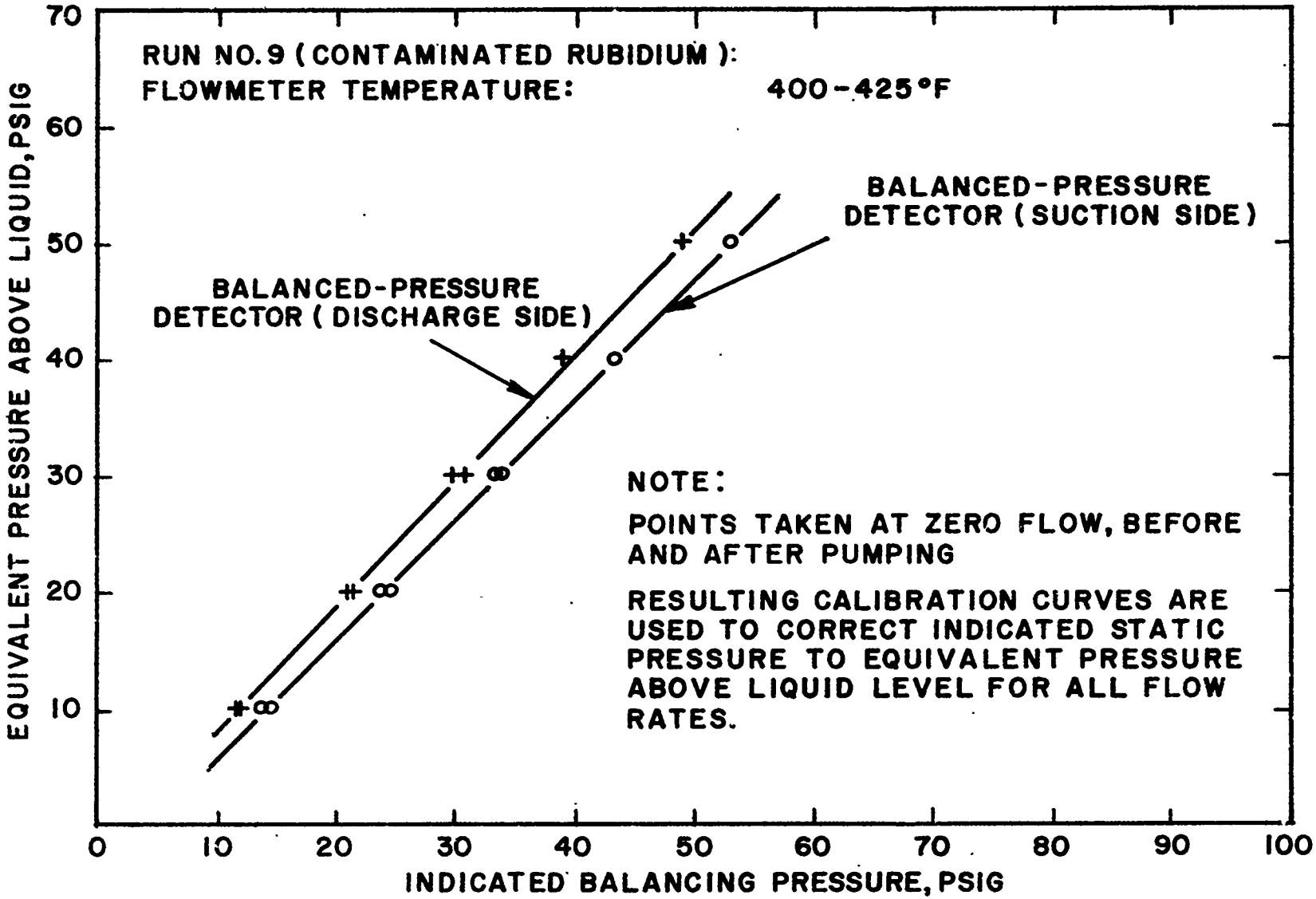

FIGURE 45. TYPICAL CALIBRATION CURVE FOR BALANCED-PRESSURE DETECTORS

TABLE 12. SAMPLE LIQUID-METAL-LOOP OPERATION DATA

Pump Voltage, % of 240	Flowmeter Temp, °F	Flow, gpm	Suction, psig	Discharge, psig	Reservoir Pressure, psig	Pump Pressure Rise, psi
20	417	.169	9.5	10.2	10	0.7
20	417	.169	29.5	30.5	30	1.0
20	417	.169	49.0	50.0	50	1.0
			Average			0.9
30	403	.266	9.5	10.2	10	0.7
30	403	.266	29.5	30.5	30	1.0
30	403	.266	49.5	50.0	30	1.0
			Average			0.9
40	400	.369	9.5	10.2	10	0.7
40	400	.369	29.0	30.5	30	1.5
40	400	.369	48.7	50.2	50	1.5
			Average			1.23
50	403	.471	8.5	10.0	10	1.5
50	403	.471	28.7	31.5	30	2.8
50	403	.271	47.7	50.7	50	3.0
			Average			2.4

Date 3/20/63 Run No. Rb-7

Remarks:

Operating data immediately following addition of oxygen contaminant to liquid-level reservoir (before drastic flow attenuation occurred).

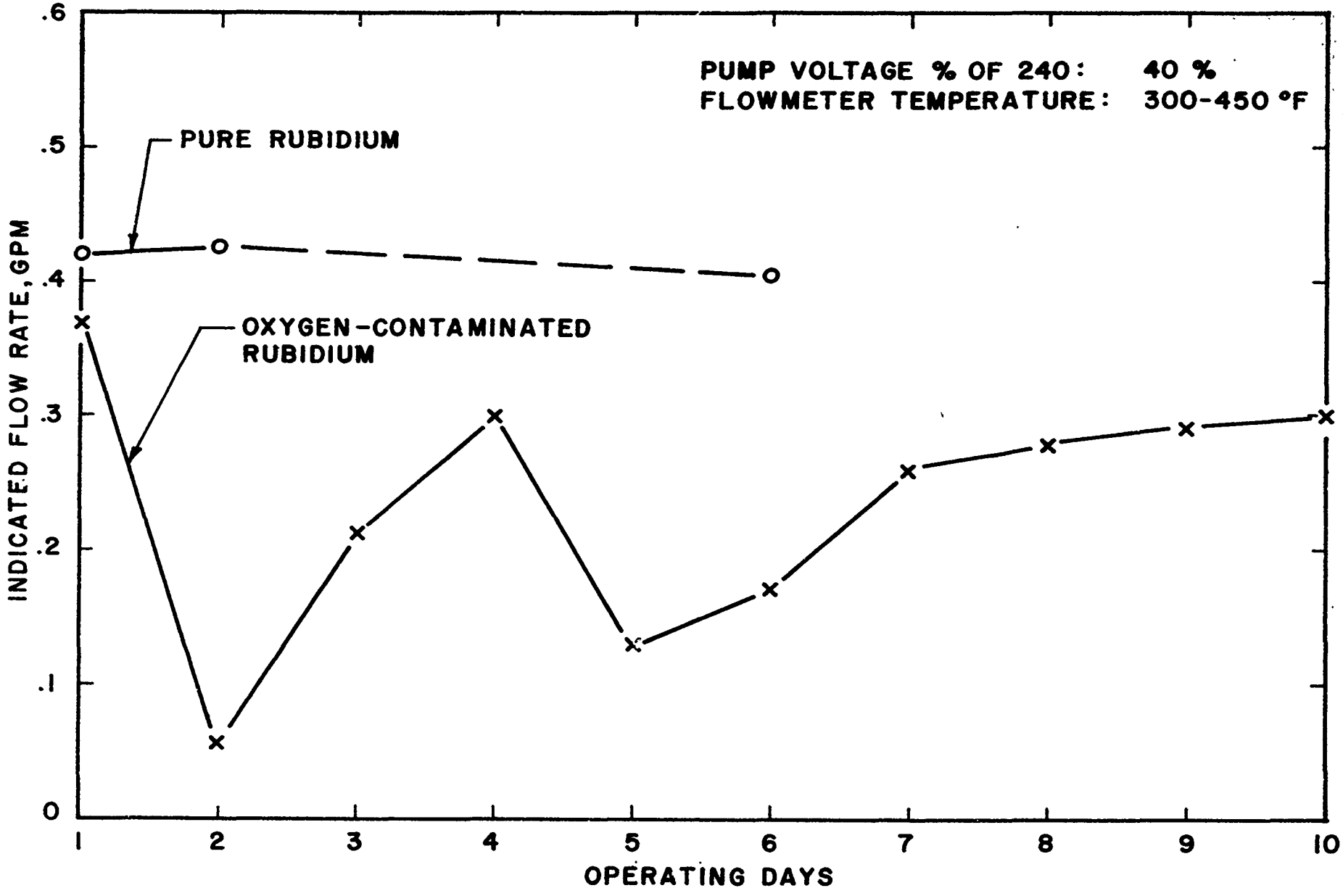

FIGURE 46. GRAPHICAL SUMMARY OF LOOP PERFORMANCE WITH PURE AND CONTAMINATED RUBIDIUM

The pumping performance did not change immediately, but as shown in Figure 46 the performance deteriorated rapidly, with the indicated flow rate decreasing sharply and then rising and falling from day to day in an erratic manner.

It is apparent that the presence of oxygen contaminant seriously affected the pumping characteristics, and it is now believed that the erratic behavior stemmed from changes in the distribution of dissolved oxygen throughout the system during overnight shutdowns.

When the pump pressure rise is correlated against the indicated flow rate as shown in Figure 47, certain phenomena become apparent. In general, the pump pressure rise decreases (although the pump voltage is constant) as the indicated flow rate decreases, approaching zero at the lower flow rates. However, the set of points for the lowest flow-rate run (which occurred on the morning following the initial oxygen addition) demonstrated higher pressure-rise values, corresponding to the dashed extensions of the curves in Figure 47. The decreasing pump pressure rise with decreasing indicated flow rate illustrated in this figure cannot be explained in terms of viscosity increase since the data of Figure 39 indicate a viscosity increase of only about 10% caused by 5000 ppm of oxygen contamination. Hence, it appears that the oxygen content may have altered the electromagnetic properties of rubidium significantly; however, further work would be required to confirm this effect.

With the exception of the set of points for the lowest flow rate, the impaired performance could not have been caused by plugging of the filters or test section. Such flow-throttling would have increased, rather than decreased, the pump pressure rise as the flow rate was decreased. On the other hand, the data for the lowest flow rate do indicate that some plugging may have occurred during the first overnight shutdown after addition of the oxygen. The data trend indicated in Figure 47 appears to be real, and similar trends are indicated for operation at other temperature levels as shown in Figure 48. Based on the smoothed data of Figure 47, the correlation of Figure 49 was developed to demonstrate the pumping characteristics of uncontaminated pure rubidium. This correlation illustrates the anticipated increasing pump pressure rise with increasing flow rate as the pump voltage is increased.

At the conclusion of the contaminated-rubidium pumping studies, samples of the used rubidium were withdrawn, and the heavy metals content was found to be. 7 ppm Cr, 21 ppm Ni, and 423 ppm Fe. The analyses strengthen the previously discussed evidence obtained with the viscometer that oxygen-contaminated rubidium tends to leach iron selectively from type 316 stainless steel under the conditions of these experiments. A melting point of 101.63° F was measured on this contaminated rubidium sample with the melting point-boiling point apparatus. This melting point corresponds to a computed

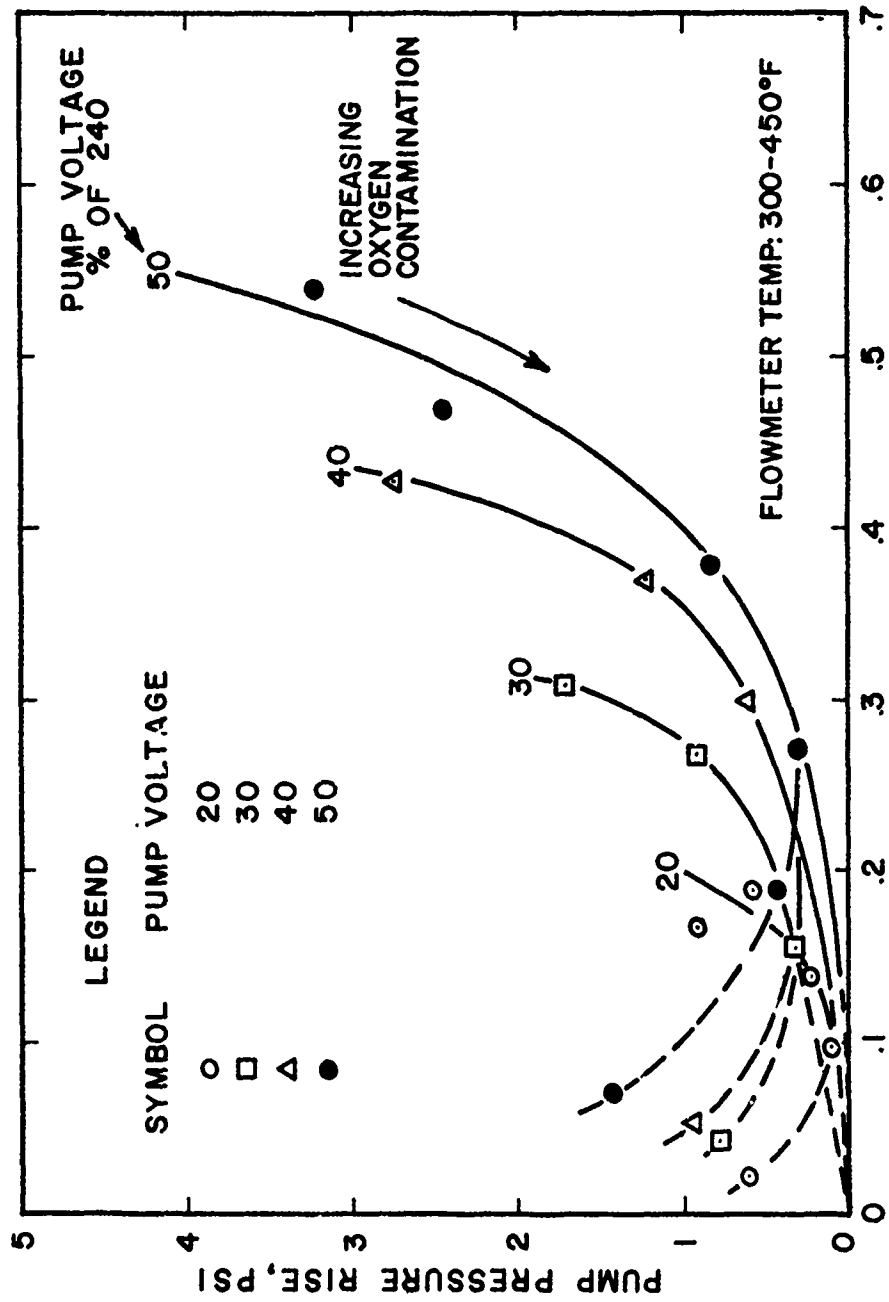

FIGURE 47. CORRELATION OF PUMPING PERFORMANCE OF RUBIDIUM CONTAMINATED WITH OXYGEN

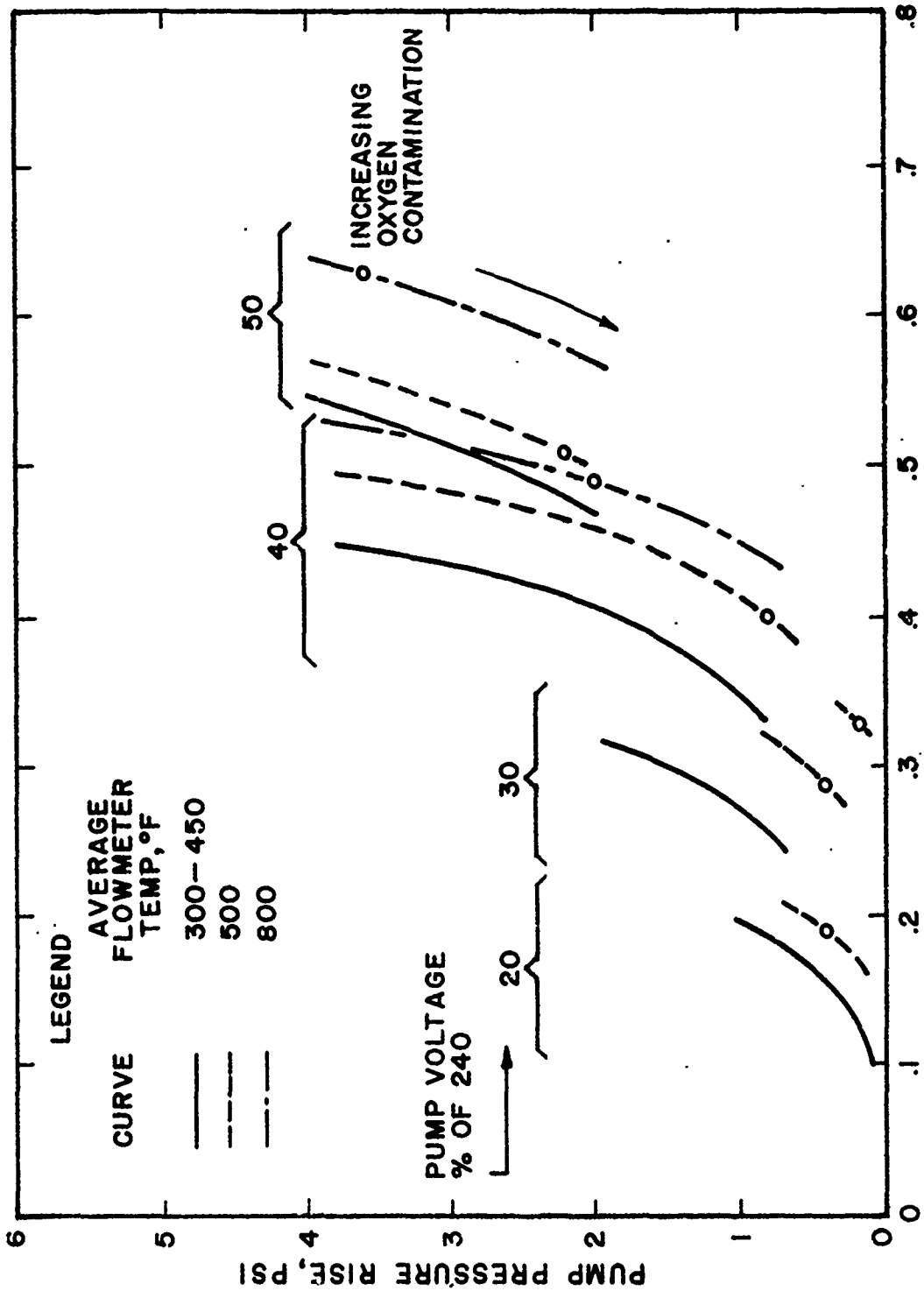

FIGURE 48. EFFECT OF TEMPERATURE ON PUMPING CHARACTERISTICS OF OXYGEN-CONTAMINATED RUBIDIUM

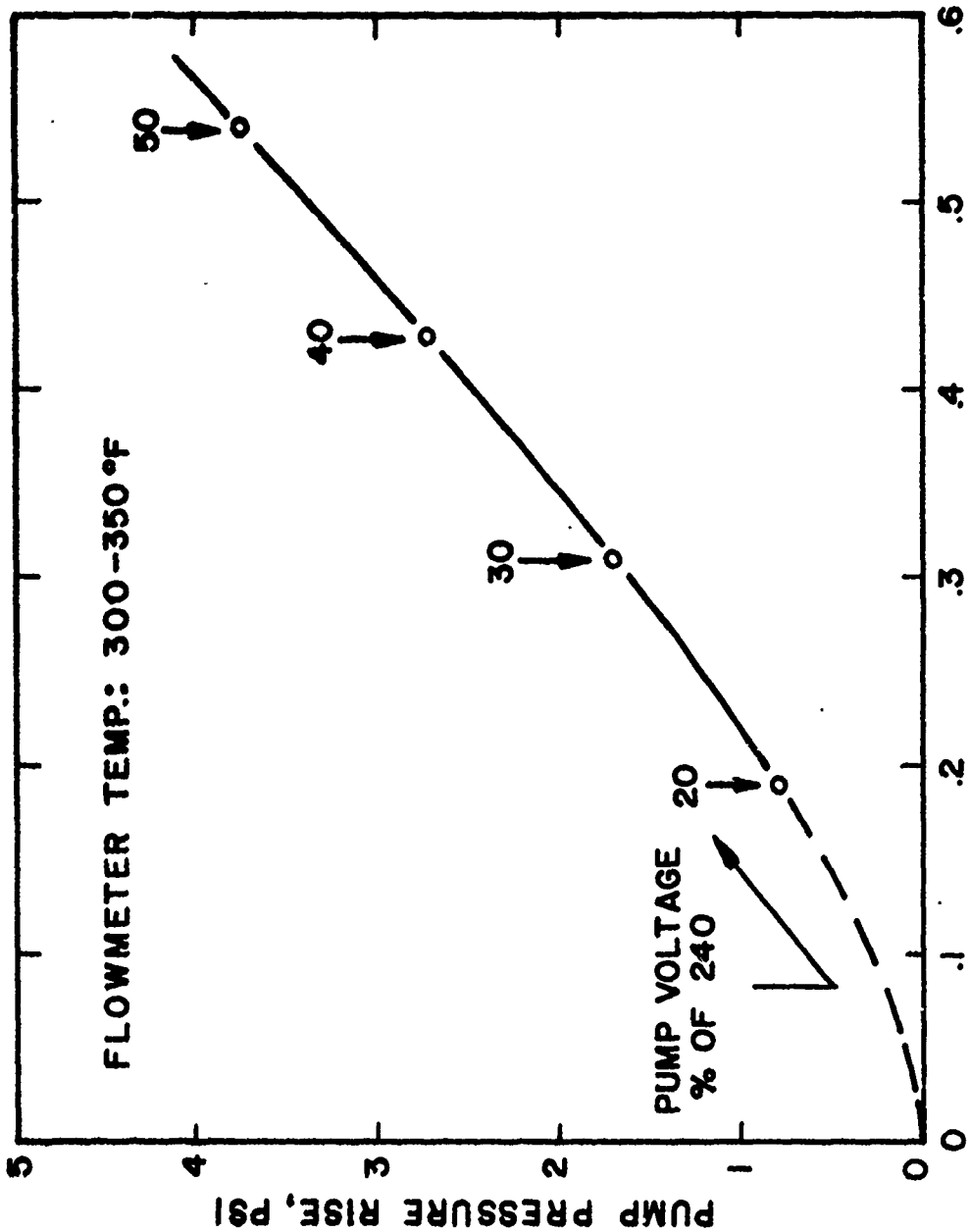

FIGURE 49. ELECTROMAGNETIC PUMPING PERFORMANCE OF PURE RUBIDIUM

oxygen content of 375 ppm, and this result is considered as further evidence of the previously-suggested nonuniform distribution of oxide contaminant throughout the loop.

3. Pumping Characteristics of Lithium

Following the rubidium experiments, the loop was filled (under vacuum) with reactor-grade lithium, and several runs were made (under argon) in which pressure drop was monitored. The data of Figure 50 summarize the results of these experiments.

In view of our concurrent experience in lithium melting-point studies which has been discussed earlier, it became apparent that immediate plugging of the filters or test section (and possibly the pump and flowmeter) would have occurred if oxygen or nitrogen had been added. Therefore, the loop studies were terminated once the lithium pumping characteristics had been evaluated.

E. Analytical Chemistry

1. Wet Analysis for Chromium, Nickel, Iron, and Alkali Metals

It was not intended to conduct quantitative analysis for all heavy metals. However, it was considered necessary to analyze for those metals most likely to be picked up from Type 316 stainless steel. These include chromium, nickel, and iron. Standard colorimetric methods were available for these metals--for example, nickel by dimethylglyoxime, iron by o-phenanthroline, and chromium by diphenylcarbazide. It also was desirable to run analyses for other heavy metals on the rubidium and lithium as received. The most feasible method for such analyses was by emission spectrography in a commercial laboratory. Although the Institute has the equipment for such analyses, it was not economical to develop the necessary techniques for the relatively small number of samples anticipated.

In the case of other alkali-metal contaminants in lithium and rubidium, the only feasible method was flame photometry, using standard "contaminated" salts of lithium and rubidium. This use of standards eliminated the difficulty caused by the enhancement of line density of one alkali metal by the presence of another, which could amount to more than an order of magnitude. The equipment for such analyses was available at the Institute, as well as personnel with background in these techniques.

a. Sample Preparation

Samples of rubidium and lithium were prepared for analysis as follows:

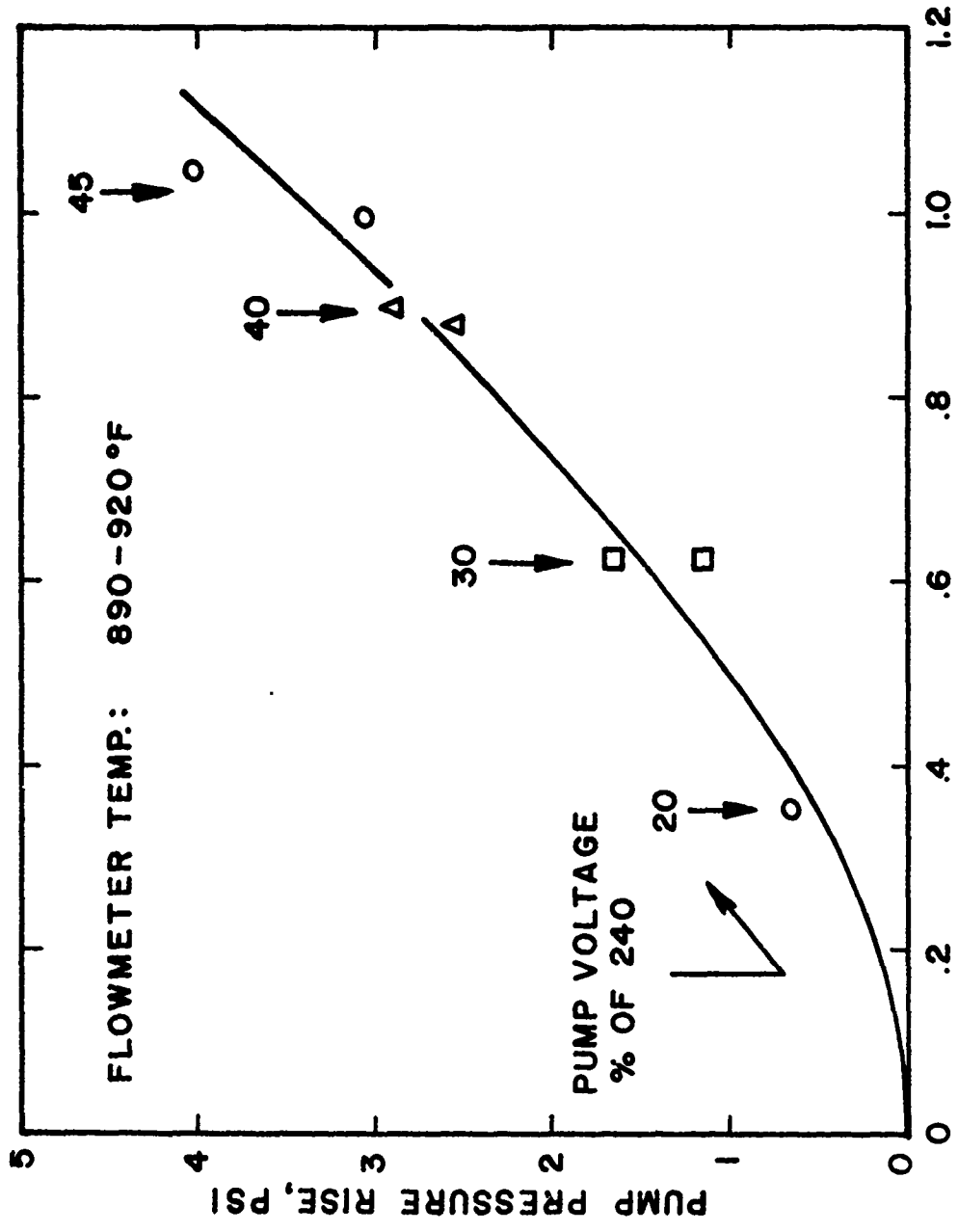

FIGURE 50. ELECTROMAGNETIC PUMPING PERFORMANCE OF REACTOR-GRADE LITHIUM

(1) In a dry box containing argon, the sample was transferred to a screw-cap jar containing mineral oil. The sample was then removed from the dry box.

(2) A one pint plastic bottle was purged with nitrogen while resting on the pan of a Mettler K-7 balance. Small pieces of the alkali metal were removed from the oil, hexane rinsed, and dropped directly into the plastic bottle until 1 gram ± 0.03 gram was obtained.

(3) The plastic bottle was placed in a beaker of ice and the nitrogen flow maintained. Methanol was then added to the rubidium samples. Water was used for lithium samples. Nitrogen purge was removed after reaction had gone to completion.

(4) Concentrated HCl was added to neutralize the base formed and then 1-ml in excess was added.

(5) Rubidium samples were transferred to beakers and the methanol boiled off. After cooling, the sample was transferred to a 250-ml volumetric flask and made to volume. Lithium samples were transferred directly to the 250-ml volumetric flasks.

b. Analysis

A 50-ml aliquot of this solution was required for each of the heavy metals analyses, and the remainder was used for the alkali metals analyses.

Standard colorimetric methods were used employing 1,10-phenanthroline, diphenylcarbazide and dimethylglyoxime as the color producing agents for iron, chromium, and nickel, respectively. *

The alkali metals were determined by flame analysis using the method of standard additions. These analyses were performed by first measuring the emission, at the appropriate wave length, of an equal mixture of sample and distilled water. The emission of an equal mixture of sample plus distilled water containing a known amount of the alkali metal of interest was then measured. Background emission in both cases was determined at a

---

* These methods were adapted from those employed at Foote Mineral Company(59).

wave length differing by approximately 5 mμ from the wave length used to measure the emission of the alkali metal of interest. This technique minimized any enhancement effect which might result from the large concentration of the principal alkali metal[22].

c. Calibration

The wet-chemical methods of analysis for Fe, Cr, and Ni were calibrated, using one gm samples of C. P. potassium. Analyses were conducted on the "as-received" potassium, and known quantities of Fe, Cr, and Ni were added to these samples. The data presented in Table 13 illustrate that recoveries in excess of 90% of the added materials (ranging from 40 to 1000 ppm) were obtained in all cases except one (where the recovery was 43 ppm out of 50 ppm).

TABLE 13. CALIBRATION OF HEAVY METALS ANALYSIS OF POTASSIUM

Sample	Metal	ppm Added	ppm Found	% Recovery
1	Fe	0	3.4	-
2	"	200	189	93
3	"	1000	935	94
4	Cr	0	*	-
5	"	40	*	*
6	"	200	195	97
7	Ni	0	2.6	-
8	"	50	42.8	80
9	"	200	182	91

* Sample lost

2. Oxygen Analysis

In setting up analytical procedures for the principal contaminants in liquid rubidium and lithium, emphasis was placed on analysis for oxygen, in view of its known critical importance in practical corrosion problems. In selecting a method for determining oxygen content, consideration was given to three general classes of methods: mercury amalgamation, reaction with butyl bromide, and neutron activation analysis. In the case of the rubidium, mercury

amalgamation was considered unsuitable (because of a serious question on the solubility of rubidium oxide in mercury); neutron activation analysis was ruled out because it would involve sending samples out for analysis. The butyl bromide method, providing on-site analysis, was therefore selected for rubidium. In the case of the lithium, however, neither the butyl bromide nor the mercury amalgamation method appeared satisfactory. Therefore, lithium samples were sent to the Neutron Activation Laboratory of Texas A & M College for oxygen analysis.

The butyl bromide method was developed by White, Ross and Rowan[95]. This procedure has been used successfully at the Oak Ridge National Laboratories for the oxygen content of both Na and NaK - Method Nos. 1-215871 and 9-00715871. The principle of this method is based on the fact that Rb will react with n-butyl bromide to form RbBr, whereas it was believed that no reaction would occur with Rb_2O. The residual oxides are dissolved in water to form the hydroxide, which is then titrated and the oxygen calculated. This method has proven satisfactory for sodium except in cases where difficulties were suspected because of moisture in the butyl bromide. Therefore, Karl Fischer water determinations were performed on the reagents to minimize this source of error.

a. Apparatus and Procedure

The n-butyl bromide procedure followed was essentially the same as that used at the Oak Ridge National Laboratory for the determination of oxygen in sodium-potassium mixtures. * Two modifications of this procedure were made which warrant discussion in this report. The first modification pertains to the method for breaking the sample bulb in the reaction tube. In the Oak Ridge procedure the sample bulb is broken by striking it with a long glass stirring rod. This method was impractical with the sample bulbs used for this purpose. An extremely hard blow was required, which considerably increased the possibility of breaking the reaction tube.

The difficulty was overcome by fabrication of a sample-bulb crusher, whereby the sample bulb was broken between screw-actuated jaws similar to a vise. The sample-bulb crusher was made entirely of stainless steel. The sample bulb was fastened to the crusher by wrapping wire around the stem of the sample bulb and the supporting arm of the crusher. The photographs of Figure 51 illustrate this apparatus.

---

* Methods Nos. 1-215871, 9-00715871; ORNL Analytical Chemistry Division, Oak Ridge, Tennessee[52].

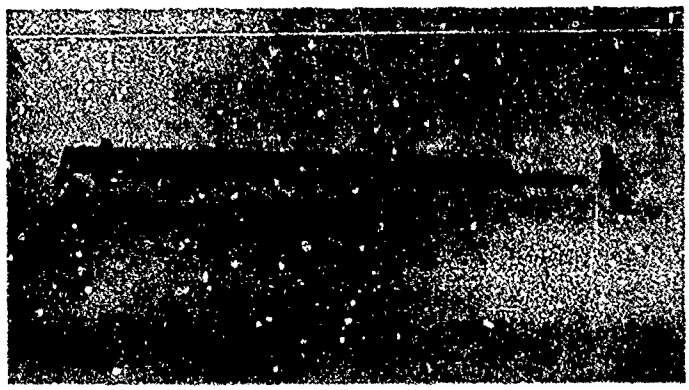

STAINLESS STEEL SAMPLE-BULB CRUSHER
(WITH VISE HANDLE AND RUBIDIUM AMPOULE NOT ATTACHED)

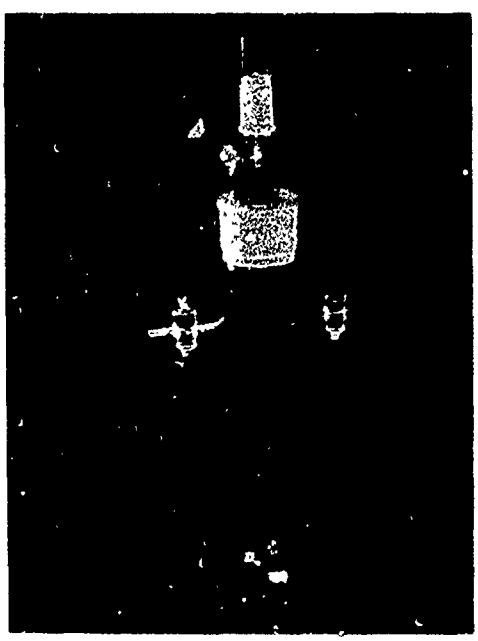

BUTYL BROMIDE REACTION VESSEL
(WITH SAMPLE BULB AND CRUSHER
IN PLACE)

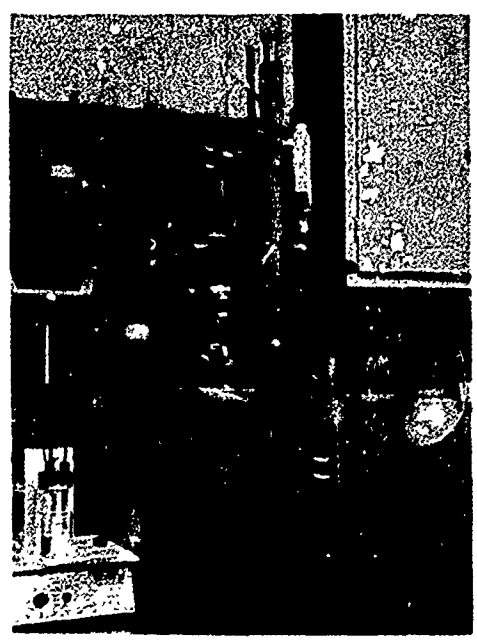

BUTYL BROMIDE REACTION SYSTEM
(WITH TITRATION AND SOLVENT
HANDLING ACCESSORIES)

FIGURE 51. FACILITIES FOR BUTYL BROMIDE METHOD

The second modification in the procedure pertains to preparation of the reaction vessel. The Oak Ridge procedure calls for heating the reaction vessel in a muffle furnace, followed by numerous evacuations and argon fillings of the reaction vessel. Pentane is introduced into the reaction vessel, and then the sample bulb is immersed in the pentane and the bulb broken.

Difficulties were encountered with this procedure. To ensure vacuum tight seals it was necessary to use silicone stopcock grease. Introduction of the pentane carried the silicone grease into the reaction vessel, and this in turn reacted with the rubidium. A teflon-joint seal prevented freezing of the joints but did not give leak-free connections.

The procedure for preparation of the reaction vessel and introduction of the sample bulb was therefore modified so that the teflonized joints could be used and evacuation of the system would not be necessary. The procedure used was as follows:

> The sample bulb was wired to the sample crusher and then rinsed with alcohol and pentane so as to clean and degrease the entire assembly. This assembly was then placed in the reaction vessel, as was a clean and degreased stirring rod. The reaction vessel top was placed in position and then a length of 7-mm glass tubing was inserted clear to the bottom of the reaction vessel. The vessel was placed in a preformed heating mantle (heating tape wound on wire mesh frame) and argon introduced through the 7-mm tubing at 400-500 ml/min. The entire assembly was then removed from the argon flow. The argon purge tube was removed, the argon line attached to one of the side tubes on the reaction vessel, and the stopcock opened so as to again maintain the argon purge. The assembly was then attached to the end of the pentane transfer line and this line purged with the argon flowing from the reaction vessel. The argon flow was then stopped while hexane was transferred from the hexane reservoir to the reaction vessel so as to completely immerse the sample bulb. The assembly was disconnected from the hexane transfer line and the argon flow immediately started again. The reactor top was removed and the sample bulb crushed by turning the extended shaft with the adaptor key. The sample crusher along with the stem of the sample bulb was then removed and the reactor top replaced. Addition of the butyl bromide and the remainder of the procedure was identical to that used at Oak Ridge.

b. Contaminant Exclusion Experiments

Prerequisite to an accurate oxygen determination is the rigorous exclusion of oxygen and moisture from all solvents, reagents, and apparatus

contacting the metal during sampling and analytical operations. Instrumental analysis of the solvent used has confirmed the absence of moisture to within the limits of instrument sensitivity. To further establish the validity of the analytical results, three pure rubidium samples of varying weight were analyzed for oxygen. Any inherent contaminants in the systems would affect the measured oxygen content inversely with the sample size. The results of these studies, which are presented in Table 14 confirm a high degree of success in the efforts to exclude oxygen-containing contaminants.

TABLE 14. BUTYL BROMIDE DETERMINATIONS OF OXYGEN IN PURE RUBIDIUM (Batch 1)

Sample wt, grams	ppm Oxygen
3.0268	580
4.3520	562
11.8721	580

c. Butyl Bromide - Rubidium Oxide Interaction Study

During the study of the influence of added oxygen upon the viscosity of rubidium, considerable doubt began to arise regarding the validity of the n-butyl bromide method for measuring the oxygen content of rubidium samples. Because of the laboratory techniques employed in adding known quantities of gaseous oxygen to a known quantity of rubidium in the viscometer, it was felt that the attained oxygen content should be relatively close to that computed from blending data. As discussed previously, the melting-point-depression data lent confidence to these computed blended values, as was illustrated earlier in Figure 19. However, the data presented in Table 15 illustrate that the oxygen content measured by the butyl bromide method ranged from 520 to 1037 ppm as the quantity of oxygen added varied from 0 to 7000 ppm.

In an effort to explain these discrepancies, a special literature search was conducted. The findings do not completely resolve the anomaly, but they do challenge the suitability of the butyl bromide method for oxygen analysis in rubidium.

Observing that oxides present in high concentration (>1,000 ppm) seem to inhibit spontaneous reaction between the rubidium metal and the

TABLE 15. COMPARISON OF BLENDED AND MEASURED OXYGEN CONTENTS OF RUBIDIUM

O_2 Added, ppm	O_2 Calc'd from ΔT_m, ppm	O_2 Determined by n-Butyl Bromide Method, ppm
0	50	520
1000	840	620
2000	2360	818
7000	≈7000	1037

butyl bromide at room temperature and recalling the unusual amount of heating required to initiate the reaction which then proceeded slower than with samples containing ~ 500 ppm oxide, it was surmised that oxides of rubidium react with butyl bromide at elevated temperatures (~ 80°C) to give the metal halide and dibutyl ether. The literature survey tends to support this theory. It was found that aliphatic halides, eg. C_2H_5I, will react with certain metal oxides, especially Ag_2O, to form diethyl ether and silver iodide. Further, butyl chloride was reported to form the corresponding ether and calcium halide when heated to 250°C in presence of CaO. It may be concluded, speculatively at least, that such reactivity is possible between oxides of rubidium and butyl bromide at much less severe conditions than for CaO and butyl chloride.

A sample of completely oxidized rubidium was prepared and analyzed as before to ascertain the overall merits of the analytical procedure and the reactivity of the oxide toward butyl bromide in this system. The acidified aqueous solution from this analysis was tested for halide ion using ~ 0.1 N $AgNO_3$ solution and gave a positive result. Voluminous solids precipitated upon addition of silver nitrate, indicating that metal bromide salts were present. No attempt was made to determine the total amount of bromide; the fact of its presence was in itself of sufficient significance that further quantification would have contributed nothing to the picture. The observed bromide salt may be the consequence of either the oxide-butyl bromide reaction or elemental metal-butyl bromide displacement. However, negligible quantities of elemental rubidium could have been present in this thoroughly oxidized sample.

In view of the foregoing discussion, it is now believed that oxides of rubidium may react with n-butyl bromide to an appreciable extent. Hence it is tentatively concluded that the butyl bromide method is not applicable to rubidium.

3. Carbon Analysis

A specific method for the determination of carbon (graphite) in rubidium was not uncovered in the literature search. Methods for the determination of carbon in iron, sodium, and lithium have been reported. These methods are all based on the conversion of carbon to carbon dioxide with subsequent determination of the carbon dioxide. Because of the small quantities of carbon involved, gravimetric methods are not suitable for this determination. Other possible approaches involve differential freeze-out (manometric) techniques, absorption of the CO_2 in barium hydroxide solution (and measurement of change in conductivity), and gas chromatography. Of these methods, gas chromatography was chosen for this program. This choice was dictated largely by this laboratory's extensive experience and facilities in this field.

a. Apparatus and Procedure

The method reported here and used only for carbon in rubidium was designed for applicability to any alkali metal, regardless of its reactivity. The method is a modification of that reported by Pepkowitz and Porter(61).

The procedure consists of these integrated steps:

(1) Conversion of the alkali metal to the hydroxide

(2) Oxidation of carbon to carbon dioxide

(3) Measurement of the carbon dioxide

A preferred method for the determination of carbon dioxide is by gas chromatographic techniques. By this technique it is possible to measure carbon dioxide at the one microgram level in the presence of other gases, which is a decided improvement over the manometric method. The following apparatus and procedure were designed for the gas chromatographic method of determination for carbon dioxide.

Figure 52 is a schematic sketch of the apparatus used for the conversion of alkali metal to the hydroxide, and oxidation of the carbon to carbon dioxide. It also shows the traps necessary for collection of carbon dioxide prior to chromatographic analysis. The apparatus is essentially all glass.

The system, AEPQRH, is purged with nitrogen gas from cylinder A and it vents at W. The reactor top, X, is momentarily removed from the reactor, Q, and a previously weighed sample of alkali metal (approximately 0.5 gm) is introduced in the reactor. The reactor top is immediately replaced. For rubidium, one to two ml of distilled water is placed in P by use of a syringe and the serum cap on the side arm provided for this purpose. The assembly, consisting of P, Q, and R, is immersed in a beaker of water, and the water temperature raised to about 50°C. Under these conditions the water carried over by the nitrogen flow from P to Q produces a visible but controlled reaction with the rubidium in Q*. On completion of the reaction a clear liquid pool is obtained. The water bath is removed and the reactor top, X, is removed. The reactor, Q, is immersed in ice water, and sulfuric acid (1:1) is slowly added to produce an acid solution and liberate the carbonate CO_2, which is swept

---

* With lithium, and possibly sodium, the water could be added directly into the reactor, Q. Potassium and cesium would be handled similarly to rubidium.

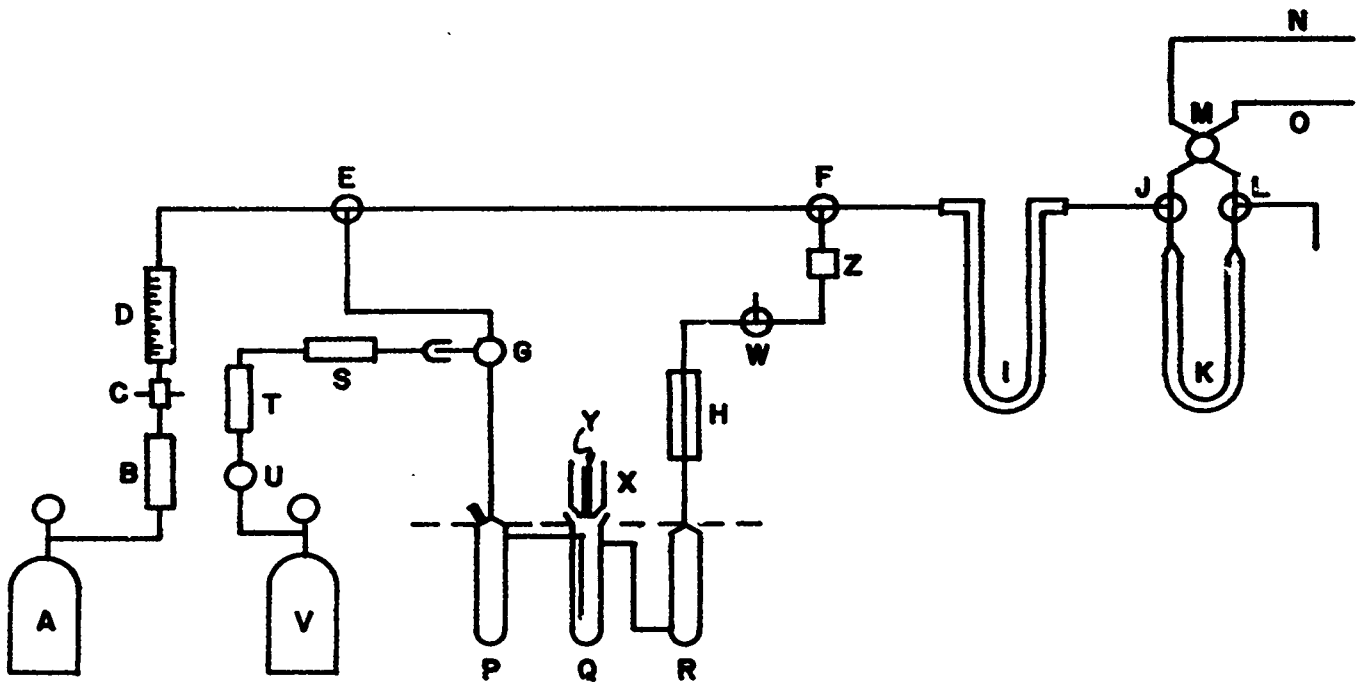

A NITROGEN SUPPLY
B DRYING TUBE
C FLOW CONTROLLER
D FLOWMETER
V OXYGEN SUPPLY
U FLOW CONTROLLER
T CuO
S ASCARITE
H ICEWATER CONDENSER

E,F,G,J,L,M,W - STOPCOCKS
P SATURATOR
Q REACTOR
R WATER TRAP
X REACTOR TOP
Y STOPPER
Z FLOW RESTRICTION
I PRELIMINARY COLUMN (20 % CARBOWAX 1500 ON 30-60 MESH CHROMOSORB)
K TRAP
N,O HELIUM LINES TO & FROM CHROMATOGRAPHIC INSTRUMENT

FIGURE 52. SCHEMATIC DIAGRAM OF CARBON ANALYSIS APPARATUS

from the reactor. Maintaining the nitrogen flow, P and Q are lightly flamed until the salt in Q is near dryness. Oxygen from cylinder V is passed through the copper oxide combustion tube, T, the Ascarite CO_2 absorber, S, and exits around the side arm of the three-way stopcock, G, at approximately 300 ml/min. A vacuum line is attached to the side arm at L so as to draw oxygen thru the system, GPQRFIK, at 100-150 ml/min. The pressure in the system from Z to L is reduced to approximately 100 torr by the flow restriction, Z, so as to prevent condensation of oxygen in the liquid nitrogen trap. The system is purged with oxygen for a few minutes, and then the preliminary column I is immersed in liquid nitrogen. Ten ml of Van Slyke solution is introduced into Q from the reactor top, X, by lifting the stopper rod, Y. Heat from an open flame is applied to Q to oxidize the graphite to CO_2, which is carried over by the oxygen stream and collected in the preliminary column I. The vacuum is then cut off at L, and the pressure in the system, AEFIK, is raised to slightly above atmospheric with nitrogen from tank A. Stopcock, L, is then positioned so that the nitrogen flow vents at L. The trap, K, is immersed in liquid nitrogen. The liquid nitrogen is removed from the preliminary column, which is then warmed by a water bath to about 40°C. The CO_2 is then swept from the preliminary column and collected in trap, K, whereas water which was collected on the preliminary column is held by the polar coating of the preliminary column. The trap, K, is then isolated by proper positioning of the stopcocks, J and L. The bulk of the nitrogen is evacuated from the trap, K, and the trap is then warmed. Rotation of the four-way stopcock, M, allows helium from the chromatographic instrument to flow through the trap and carries the CO_2 to the chromatographic column. Conventional methods of gas chromatographic analysis are then used to obtain quantitative data on the carbon dioxide, which is readily calculated as ppm graphite in the original sample.

b. Analysis of Rubidium

Using the above procedure, three blank determinations were made which gave 35.2, 32.8, and 33.8 micrograms carbon respectively, for an average of 33 micrograms carbon. These results are in good agreement with the work reported by Pepkowitz. A sample of rubidium was run in triplicate. The individual samples were found to be 172, 125, and 60 ppm carbon for an average of 119 ppm carbon. Pepkowitz also found a wide variation in duplicate samples and explained this variation by the non-uniformity of carbon distribution in alkali metals.

It should be mentioned here that, with refinements of the described procedure, it appears possible that carbide carbon, carbonate carbon, and elemental carbon could each be determined on the same sample of alkali metal.

4. Nitrogen Analysis

In the case of lithium, analysis for nitrogen content was considered as the most important. Well-established and detailed analytical methods were available, based on modifications of the Kjeldahl procedure using Nesslerization and colorimetric analysis. One such method is described in detail in the Foote analytical manual[59] and it was used without essential change in our work.

5. Analysis of As-Received Rubidium and Lithium

Analyses of the as-received rubidium and lithium are presented in Tables 16 and 17. Component concentrations were certified by the supplier and were measured and in this laboratory(and for this laboratory by commercial laboratories). Comparison of measured concentrations (or estimated limits of detection) among the three sources of data reveal satisfactory agreement, except for sodium and silicon. The excess of these latter constituents found by this laboratory probably reflects slight contamination resulting from contact of the samples with glass during the preparation of salts for subsequent analyses.

TABLE 16. ANALYSES OF AS-RECEIVED RUBIDIUM

Batch:	Cyl. No. 1			Cyl. No. 2		
Analysis Source:	Supplier	This Work		Supplier	This Work	
		In-House	Commercial		In-House	Commercial
Nominal Purity, wt %:	99.5+	--	--	99.9+	--	--
Constituent, ppm:						
Al	--	--	<7	8	--	40
B	--	--	<70	<49	--	<70
Ba	--	--	--	<5	--	--
Ca	--	--	31	6	--	45
Cu	--	--	7	4	--	9
Cr	--	<3	<3	1	<3	<3
Fe	--	<5	<7	24	12	<7
Mg	--	--	9	<2	--	9
Mn	--	--	--	4	--	--
Ni	--	<3	<6	<2	<3	<6
Pb	--	--	--	<2	--	--
Si	--	--	250	31	--	950
Sn	--	--	--	<10	--	--
Sr	--	--	--	<2	--	--
Ti	--	--	--	<2	--	--
Tl	--	--	--	<5	--	--
Li	--	30	--	<49	20	--
Na	--	110	900	<196	680	900
K	--	200	<1400	<196	200	<1400
Cs	~4000	3100	--	216	300	--
O_2	--	--	--	--	50	--
C	--	--	--	--	119	--

TABLE 17. ANALYSES OF AS-RECEIVED REACTOR-GRADE LITHIUM

Analysis Source:	Supplier	This Work	
		In-House	Commercial
Nominal Purity, wt %:	99.98		
Constituent, ppm:			
Al	10*	--	42
Ca	10*	--	183
Co	10*	--	--
Cu	10*	--	3
Cr	10*	<3	<6
Fe	10*	31	51
Mg	--	--	10
Ni	10*	3	<18
Si	10*	--	49
Na	30*	110	920
K	45*	<200	--
Cl	41*	--	--
N_2	31*	215	--
O_2	--	--	3200 ± 750**

* Typical values

** Duplicate neutron activation analyses performed gratis by Texas A&M College

IV. CONCLUSIONS

As a result of this experimental investigation, several conclusions may be drawn regarding the thermophysical properties of rubidium and lithium and the anticipated role of contamination in applications involving these fluids.

Experimental vapor pressure data for pure rubidium were found to agree with recently reported values. Melting point determinations on pure rubidium and reactor-grade lithium give values of 102.9°F and 359.2°F, respectively. The rubidium melting point is the highest value ever reported and, hence, represents the melting point of the purest rubidium sample for which a melting point has been determined.

Experimental studies of the depression of the melting point of rubidium by oxygen contaminant and of lithium by nitrogen contaminant have revealed significant information regarding these phenomena. In the case of rubidium, oxygen contaminant appears to exist as soluble rubidium monoxide for oxygen contents up to at least 7000 ppm. The solubility of nitrogen in lithium has been confirmed to be quite limited. In fact, the results of this study suggest that much of the conflicting published information on the solubility of nitrogen in lithium may stem from the fact that lithium nitride precipitates from supersaturated lithium solutions at relatively slow rates. Accordingly, it is now believed that effective cold-trapping techniques can be developed for removing nitrogen (as well as oxygen) from lithium provided that adequate precipitation time is allowed.

The kinematic viscosity of pure and oxygen-contaminated rubidium have been measured in a specially-designed capillary viscometer at temperatures from 200 to 1200°F for pure rubidium and from 100 to ~500°F for each oxygen-contaminated sample. Each of these rubidium samples yielded linear relationships between the logarithm of kinematic viscosity and the reciprocal absolute temperature. Although prior theoretical treatments have been based on such a linear relationship for the absolute viscosity, similar theoretical arguments could be applied in favor of such a relationship for the kinematic viscosity rather than the absolute viscosity. In any event, these viscosity results demonstrate that the contamination of rubidium by oxygen can lead to significant viscosity increases, especially in the region of the normal melting point. However such influences become less pronounced at higher temperatures.

The experimental studies of this program have revealed that the electromagnetic-pumping characteristics of rubidium may be seriously impaired

by the presence of significant quantities of oxygen contaminant. Although the mechanism of this impairment is not immediately apparent, the effect appears to be real and significant and suggests the need for further investigation.

During the analytical chemistry phase of this program, a combination of wet oxidation and gas chromatography was adapted for the analysis of carbon in rubidium. This method should be applicable to all alkali metals with only minor modifications. The validity of the n-butyl bromide method for the analysis of oxygen in rubidium has been shown to be open to serious question. This study has indicated the possibility of reactivity between rubidium oxides and n-butyl bromide. On the basis of the results and observations of this experimental program, the following relatively simple and straightforward method is recommended for the analysis of oxygen in rubidium (and possibly other alkali metals). After adding a rubidium sample to a melting-point apparatus containing appropriate hot-gettering material, the initial melting point should provide an index of the extent of contamination. Following a subsequent hot-gettering procedure, the final melting point will reveal the exact melting-point depression experienced by the original sample. Assuming that oxygen contaminant is present as rubidium monoxide, as indicated by the results of the present study, the oxygen content may then be computed directly. This analytical procedure would be time consuming because of the hot-gettering step. However, because of its inherent simplicity, a multiple-unit melting-point device could be employed easily on a routine basis.

The overall results of this program have pin-pointed certain features of liquid rubidium and liquid lithium systems which bear further discussion. The low melting point, relatively low ratio of surface tension to density, high contaminant solubility, and general ease of handling and disposal of rubidium provide strong arguments in favor of the use of rubidium rather than lithium as the working fluid for alkali-metal systems. The contrasting high melting point, extremely high ratio of surface tension to density, limited contaminant solubility, and general difficulty of handling and disposal of lithium suggest that the use of lithium as a working fluid can be justified only on the basis of criteria such as the higher system temperatures attainable at reasonable pressures. In fact, similar arguments can be made, but to a lesser degree, in favor of the use of rubidium in preference to potassium or sodium. It is recognized that other criteria must enter into the selection of suitable working fluids for space-power applications; however, it is believed that the foregoing appraisal of fluid characteristics, based on laboratory observations, could be applied to estimates of overall system reliability in alkali-metal applications.

V. REFERENCES

1. Addison, C. C., Kerridge, D. H., and Lewis, J., J. Chem. Soc., 1954, 2861.

2. Arabian, R. V., and Young P. F., "Rubidium Corrosion Capsule Program," Quarterly Tech. Report, AGN-8051 (Nov. 1961 - Jan. 1962).

3. Arabian, R. V., Young, P. F., and Deutsch, D. E., "Rubidium and Cesium Evaluation Program," Aerojet-General Nucleonics Quarterly Tech. Report (Aug. 1 - Oct. 31, 1961).

4. Azbiter, W., and Lazerus, S., "Purification of Lithium by Vacuum Distillation," Nuclear Development Corp. of Amer., Rept. No. NDA-39 (Del.) (75-15) (June 14, 1957).

5. Berthold, C. E., "Rubidium and Cesium-Where Are They Going?", J. Metals, 14, 355-8 (1962).

6. Bonilla, C. F., Sawhney, D. L. and Makansi, M. M., "Vapor Pressure of Alkali Metals. Rubidium, Cesium, and Sodium-Potassium Alloy (NaK) Up to 100 psi," Trans Am. Soc. Metals, 55, 877-890 (1962).

7. Brotherton, T. D., Cole, N. O., and Davis, R. E., "Properties and Handling Procedures for Rubidium and Cesium Metals," Trans. AIME, 224, 287-93 (1962).

8. "Cesium and Rubidium Metals," Technical Data, Amer. Potash Chem. Corp., Dec. 1961.

9. Champeix, L., Darras, R., and Duflo, J., "Determination of Oxygen in Sodium. The Mercury Method: Its Use in the Case of Very Low Concentrations," Centre études Nucléaires Saclay, Gif-Sur-Yvette, France, J. Nuclear Materials, 1, 113-19 (1959) (In French).

10. Cleary, R. E. and Kapelner, S. M., "Alkali Metal Physical Properties Program at Pratt & Whitney Aircraft-Canel," AEC Contract AT (30-1)-2789.

11. Cochran, D. L., "Rubidium-Cesium Evaluation Program Thermodynamic Property Measurement," Aerojet-General Nucleonics, San Ramon, Calif., presented at the 2nd Annual Meeting on High-Temperature Liquid-Metal Heat Transfer Technology, Brookhaven National Lab., May 17-18, 1962.

12. "Compendium of Data on Lithium and Selected Compounds of Lithium," Lithium Corporation of America, Inc., Feb. 1958 (Rev. July 1959).

13. Douglas, T. B., Epstein, L. F., Dever, J. L., and Howland, W. H., "Lithium: Heat Content from 0 to 900; Triple Point and Heat of Fusion, and Thermodynamic Properties of the Solid and Liquid," J. Am. Chem. Soc., 77, 2144 (1955).

14. Edgerton, J. H. and Davis, H. G., "Determination of Microgram Quantities of Carbon by Low-Pressure Combustion," ORNL-2211 Jan. 29, 1957.

15. Ellis, J. F., "A Data Sheet for Lithium," UKAEA Industrial Group, R&DB(CA)TN-154, 1958.

16. Epstein, L. F. and Howland, W. H., "The Distillation of Lithium Metal, "Knolls Atomic Power Lab., AECH-1549, Jul. 2, 1961.

17. Eremenko, V. N., "Surface Tension of Liquid Metals," Ukr. Khim. Zh., 28, 427-40 (1962) (In Russian).

18. Ewing, C. T., Grand, J. A., and Miller, R. R., "Viscosity of the Sodium-Potassium System," J. Amer. Chem. Soc., 73, 1168 (1951).

19. Ewing, C. T., Grand, J. A., and Miller, R. R., "Viscosity of the Sodium-Potassium System," J. Phys. Chem., 58, 1086 (1954).

20. Ewing, C. T., Stone, J. P., Spann, J. R., Kovacina, T. A., and Miller, R. R., "High Temperature Properties of Sodium," NRL Memo Report 1069, 1159, 1165, 1236, 1263, 1312; 1960 and 1962.

21. Farquhar, M. C., "Cesium Analyses," Amer Potash and Chem. Corp., TRM-62055, Apr. 16, 1962.

22. Farquhar, M. C. and Hill, J. A., "Analysis of Cesium and Rubidium Salts and Metals," Anal. Chem., 34, 222-224 (Feb. 1962).

23. Fedorov, T. F. and Shampay, F. I., "Refining Metallic Lithium," Izvest. Akad. Nauk, SSSR, Otdel. Tekh. Nauk, Met. I. Topl., No. 6, 56-60 (1960). (ASTIA No. AD-261794).

24. Ferrari, A., "Nitrogen Determination by a Continuous Digestion and Analysis System," (Technicon Instrument Corp., Chauncey, N. Y.), Ann. N. Y. Acad. Sciences, 87, 792-800 (1960).

25. Fontana, P., Jr., "The Determination of Nitrogen by the Kjeldahl Method," (Inst. Oswaldo Cruz, Rio Janeiro, Brazil), Mem. Inst. Oswaldo Cruz, 51, 277-88 (1953).

26. Fraser, J. W. and Holzmann, R. T., "Micro Determination of Carbon in Metals," Calif. University, Livermore Lawrence Radiation Lab., June 1960.

27. Friedrich, M., "Metall," Tech Hochschule Karlsruhe Ger., 15, 1173-80 (1961).

28. Gill, W. N. and Walker, E. J., "Mass Transfer in Liquid Lithium Forced-Convection Systems," WADC BPS No. 7-(1-3048) 30193, OMCC-HEF-169, Dec. 16, 1958.

29. Goldberg, G., "Determination of Oxides and Nitrides in Lithium Metal . . . ," Anal. Chem., 34, 1343-4 (1962).

30. Grosse, A. V. "The Relationship between the Surface Tensions and Energies of Liquid Metals and Their Critical Temperature," J. Inorg. Nucl. Chem., 24, 147-56 (1962).

31. Hampel, C. A., "Rare Metals Handbook," New York, Reinhold Publishing Corp., 1954.

32. "Handling and Uses of the Alkali Metals," "Advances in Chemistry Series 19," Washington, D. C., American Soc., 1957.

33. Hedgcock, F. T., "Magnetic Susceptibility of Rubidium and the Electrical Resistance Anomaly," Can. J. Phys., 34, 1164-67 (1956).

34. Hoffman, E. E., "The Solubility of Nitrogen and Oxygen in Lithium and Methods of Lithium Purification," ASTM Special Technical Publication No. 272, pp. 195-206, 1959.

35. Hoffman, E. E., "Corrosion of Materials by Lithium at Elevated Temperature," Oak Ridge National Laboratory, ORNL-2924, Oct. 27, 1960.

36. Hoffman, E. E. and Jansen, D. H., "Lithium Symposium - Analytical Procedure and High Temperature Corrosion - Reading List," Oak Ridge National Laboratory, ORNL 57-10-6, Aug. 7-8, 1957.

37. Hoffman, E. E. and Trotter, L. R., "Corrosion and Mass Transfer by Lithium at Elevated Temperature," Oak Ridge National Laboratory, Metallurgy Information Meeting, Ames Lab., Iowa State College, Feb. 1957.

38. Jackson, C. B., Editor, "Liquid Metals Handbook, Third Ed., Sodium (NaK) Supplement," Washington, Atomic Energy Commission - Dept. of the Navy, 1955.

39. Jahns, W. and Weidmann, G., "The Determination of Low Oxygen Concentrations in Sodium," (Siemens-Schuckertwerke Ag., Erlangen Ger.), Nukleonik, 1, 189-90 (1959). (In German).

40. Jeschke, D., Z. Ver. Deut. Ing., 69, 1526 (1925).

41. Kapelner, S. M., "The Electrical Resistivity of Lithium and Sodium Potassium Alloy," PWAC 349 (June 15, 1961).

42. Kapelner, S. M. and Bratton, W. D., "The Electrical Resistivity of Sodium, Potassium, Rubidium, and Cesium in the Liquid State," PWAC-376 (June 28, 1962).

43. Kelly, K. J., "Liquid Metal Corrosion Research," NASA-TN-D-769, pp. 27-31.

44. Kutateladze, S. S., Borishanskii, V. M., Novikov, I. I., and Fedynskii, O. S., "Liquid-Metal Heat Transfer Media," Atomnaia Energiia, Supp. No. 2, 1958.

45. Lemmon, A. W., Jr., "Engineering Properties of Potassium," 1st through 9th Quarterly Report on NASA Contract No. 5-584, Battell Memorial Institute, Oct. 1960-Dec. 1962.

46. Leavenworth, H. W. and Cleary, R. E., "The Solubility of Ni, Cr, Fe, Ti, and Mo in Liquid Lithium," Acta Metallurgica, 9, 519 (1961).

47. "Lithium Metal," Foote Mineral Company, Technical Data, Bulletin 101, Apr. 1959.

48. Lyon, R. N., Editor, "Liquid-Metals Handbook," Second Ed., Washington, AEC - Dept. of the Navy, 1952.

49. Malikova, E. D. and Turovtseva, Z. M., "Determination of Oxygen in Alakli Metals and Their Alloys by Mercury Extraction," Trudy Komissii Anal. Khim., Akad. Nauk SSR, Inst. Geokhim. i Anal. Khim., 10, 91-6 (1960).

50. Markowitz, M. M., "Delineating Lithium," Foote Mineral Company, Technical Data, Bulletin 106, May 1960.

51. Markowitz, M. M. and Boryta, D. A., "Study of Lithium Metal-Gas Reactions," Foote Mineral Co., 1962.

52. "Master Analytical Manual-Section 1, Ionic Methods," ORNL, TID-7015 (Sect. 1), April., 1958.

53. McCoy, H. E. and Hoffman, E. E., "Handling Techniques for Rubidium," Contract No. W-7405-Eng-26, Dec. 12, 1955.

54. McFarlane, E. F. and Tompkins, F. C., "Kinetics of Oxidation of Lithium," Trans. Faraday Soc., 58, 1177-86 (1962).

55. McGlothlan, C. K., "Summary of the Properties of Lithium," Oak Ridge National Laboratory, USAEC, 1958.

56. McKee, J. M., "Liquid Metal Research," Nuclear Development Corp. of America, NASA-TN-D-769, 41-2.

57. Mencik, Z., "The Influence of Capillary Curvature on the Flow Characteristics of a Capillary Viscometer," "Collection Czech. Chem. Commun.," 27, 147-54 (1962).

58. Minushkin, B., "Determination of the Solution Rate of Metals in Lithium," NDA 44 (NDA 2075-22), June 30, 1958.

59. "Official Methods of Analysis Lithium Metal, Lithium Hydride," Foote Mineral Company, 1962.

60. Pepkowitz, L. P., "The Micro Detection of Carbon," Knolls Atomic Power Lab., KAPL-636, June 4, 1951.

61. Pepkowitz, L. P. and Porter, J. T., II, "The Determination of Carbon in Sodium," KAPL-1444, Nov. 28, 1955.

62. "Physikalisch-chemische Tabellen," Landolt-Bornstein-Roth, Verlag Julius Springer, Berlin, 1927, 1936.

63. Plisushchev, V. E. and Shako, I. V., "Development and Recent Status of Technology of Rubidium and Cesium and Their Compounds," Translated for Los Alamos Scientific Lab., from USPekHI Khim., 26, 944-64 (1957).

64. Poindexter, F. E., Phys. Rev., 27, 820 (1926).

65. Poindexter, F. E. and Kernzghan, M., Phys. Rev., 33, 837 (1929).

66. Potts, J. R. and Hobart, E. W., "The Determination of Carbon in Lithium," USAEC Contract AT (11-1)-229, presented at 4th Conference on Anal. Chem. in Nuclear Reactor Technology, Oct. 13, 1960.

67. Quarterman, L. A. and Primak, W. L., J. Am. Chem. Soc., 72, 3035 (1950).

68. "Rubidium and Cesium Evaluation Program," AGN-8039, USAEC Contract AT(04-3)-368.

69. Sax, N. I., Chu, N. Y., and Miles, R. H., "Determination of Nitrogen in Lithium," NDA-38 (75-14), June 1957.

70. Sax, N. I. and Steinmetz, H., "Determination of Oxygen in Lithium Metal," Oak Ridge National Lab., ORNL-2590.

71. Schreck, A. E., "Lithium, A Materials Survey," US Dept. of the Interior, Bureau of Mines, 1961, Information Circ. 8053.

72. Schulek, E., Burger, D., and Feher, M., "The Direct Alkalimetric Determination of Ammonia in the Kjeldahl Method," (Eötvös Lóránd Tud. Egyetem, Budapest, Hung.). "Magyar Kem. Folyóirat 66," 1960, p. 250-1.

73. Shamrai, F. I., "Lithium and its Alloys,"(Litii i Ego Splavy) translated from a publication of the Academy of Sciences, USSR, Moscow, 1952.

74. Silverman, L. and Shideler, M., "Experimental Techniques for the Determination of Oxygen in Sodium and in NaK by the Butyl Bromide Method," NAA-SR-1509, Atomics International Division, North Amer. Aviation, Inc., Canoga Park, Calif., June 15, 1956.

75. Smith, C. R. F., "The Determination of Oxygen in Sodium--A Critical Review of Analytical Methods," Atomics International Division, North Amer. Aviation, Inc., NAA-SR-Memo-2061.

76. Stahlhuth, P. H., Bjerklie, J. W., Doolittle, R. G. and Boyer, R., Jr., "High Temperature Inorganic Lubricant Study," CDRD-61:4014, Sundstrand Aviation-Denver, Aug. 1961.

77. Stone, J. P., Ewing, C. T., Spann, J. R., Steinkuller, E. W., Kovacine, T. A., and Miller, R. R., "High Temperature Properties of Sodium," NRL Memo. Report 1312, April 1962.

78. Stratton, R., Phil. Mag., 44, 1236 (1953).

79. Strauss, S. W. (Naval Res. Lab.), "The Surface Tensions of Liquid Metals at Their Melting Points," Nuclear Sci. and Eng., 8, 362-3 (1960).

80. Strauss, S. W., "Parameters Controlling Solubility in Dilute Liquid Metal Systems," NRL Memo. Rept. 1203, Sept. 1961.

81. Suttle, J. R., "The Alkali Metals," "Comprehensive Inorganic Chemistry," Sneed, M. C. and Brasted, R. C. (Ed.), Vol. VI, New York, D. Van Nostrand, 1957.

82. Taylor, J. W., AERE M/R 1247, Dept. of Atom. Energy, Harwell, 1953.

83. Taylor, J. W., "The Surface Tension of Liquid Metals and Alloys," AERE N/TN 24, Dept. of Atom. Energy, Harwell, 1954. (ASTIA No. 139433).

84. Taylor, J. W., "The Surface Energy of the Alkali Metals," Phil. Mag., 46, 867-76 (1955).

85. Taylor, J. W., Metallurgia, 50, 161 (1954).

86. Tepper, F., Murchison. A., Zelenak, J., and Roehlich, F., "Thermophysical Properties of Rubidium and Cesium", ASD-TDR-63-133, MSA Research Corp., Feb. 1963.

87. Timofeevicheva, O. A., "Dual Gas Instrument for Measuring the Surface Tension of Liquids," Zh. Fiz. Khim., 35, 1140-1 (1961).

88. Timofeevicheva, O. A., Lazarev, V. B., and Pershikov, A. V., "The Surface Tension of Cesium as a Function of Temperature," Dokl. Akad. Nauk, SSSR, 143, 618-20 (1962).

89. Trans. Aluminum-Magnesium Inst. (Russian), 14, 99 (1937).

90. Weatherford, W. D., Jr., "Recent Data on the Thermophysical Properties of Alkali Metals," presented at 1963 USAF Fluids and Lubricants Conferences, San Antonio, Texas, April 16-19, 1963.

91. Weatherford, W. D., Jr., Tyler, J. C. and Ku, P. M., "Properties of Inorganic Energy-Conversion and Heat Transfer Fluids for Space Applications," WADD TR 61-96, Southwest Research Institute, Nov. 1961.

92. Wegener, H., Z. Phys., 143, 548 (1956).

93. White, C. M., "Streamline Flow through Curved Pipes," Proc. Roy. Soc., A-123, 645 (1929).

94. White, J. C., "Procedure for the Determination of Oxygen in Sodium and NaK by the Distillation Method," Oak Ridge National Lab., April 5, 1956.

95. White, J. C., Ross, W. J., and Rowan, R., Jr., "The Determination of Oxygen in Sodium," Anal. Chem., 26, 210 (1954).

96. Williams, D. D., Grand, J. A., and Miller, R. R., "Determination of the Solubility of Oxygen Bearing Impurities in Sodium, Potassium, and Their Alloys," J. Phys. Chem., 63, 68 (1959).

97. Williams, D. D. and Miller, R. R., Modified Apparatus for Determination of Sodium Monoxide in Sodium," Anal. Chem., 23, 1865, (Dec. 1951).

98. Worthington, A. M., Phil. Mag., 20, 51 (1885).

99. Young, P. F. and Deutsch, D. E., "Rubidium Evaluation Program," AGN No. 8007, 8016, 8023, 8027; USAEC Contract AT (04-3)-251, Reports No. 3, 6, 9, 12.

100. Zadumkin, S. N., Izv. Akad, Nauk SSSR, Otdel Tekh, Nauk, Met. i Toplivo, 1961, 55.

101. Zeratsky, E. D. (Ansul Chemical Co.), "Special Dry Powder Extinguishing Agents," Vol 54, Oct. 1960.

APPENDIXES

APPENDIX A

NOMENCLATURE FOR DETAILED HANDLING PROCEDURES

In order to clarify the sketches that accompany the detailed handling procedures enumerated in this Appendix, the following nomenclature list is presented:

√-A: Refers to vacuum-argon cycling. The system is first evacuated to < 1 torr and leak checked via a mercury manometer. Once it is established that no leaks are present, 20 psi argon is introduced into the system. The argon is pressure retained for approximately two minutes, then the vacuum pump is started to vent the argon and pump down to < 1 torr.

 : Indicates the direction of flow in a valve; the pressure being against the seat. If a valve is not installed in the direction shown on the sketches, decontamination of the valve end would be time consuming, impractical, and nearly impossible insofar as removing all of the alkali metal trapped in the bellows.

 : This symbol signifies valve number one.

T/C: Signifies thermocouple. Whenever normally solid alkali metal is to be transferred, it is most desirable to monitor the temperature, especially in the case of lithium, m.p. 359°F; for NaK or rubidium this is not so important. Chromel-alumel thermocouples were potted into one of the mounting holes in the valve body for temperature measurement.

$A_1A_3A_2$: Refers to the viscometer valve manifold; A_1 being the receiver valve, A_3 the pressure equalizing valve, and A_2 the reservoir valve. This manifold is preassembled and leak checked prior to installing on the viscometer apparatus.

Decontaminate:

Refers to the reacting of unwanted alkali metal, whether it be located in a sample line, the entire valve or side of the valve exposed to the atmosphere, etc., generally where relatively small quantities of alkali metal are presented. The main danger in decontaminating is the formation and ignition of hydrogen. Therefore, decontamination should be done in a well-ventilated area. Secondary fires can arise from the addition of alcohol-water to the alkali-metal.

NaK (78): NaK (78) can be safely reacted by the addition of small quantities of alcohol. Since NaK is liquid at room temperature (m.p. 12°F), the alkali metal is easily reacted. Once all apparent metal is gone, distilled water may be applied to the part to finish the reaction. The part should then be thoroughly dried in an oven (over 212°F) for several hours or with heat applied by its built-in heater in the case of a system such as the loop or viscometer apparatus.

Na: Sodium with a melting point of 208°F is not extremely reactive at room temperature. A 50-50 mixture of alcohol-distilled water can be used. A syringe with a 4-inch long needle, bent at 90 degrees was used throughout for valve decontamination. This proved to be very useful in that the needle could reach almost to the seat of the valve, thereby expediting the reaction. After nearly all the sodium is reacted, distilled water is used to react the remaining traces of sodium.

Rb: Rubidium, being more reactive than NaK, can be reacted safely with 50-50 alcohol and distilled water. Alcohol itself may not start the reaction, depending on the amount of oxide formed on the surface as well as the temperature of the rubidium. Liquid rubidium will react with alcohol. Final flushing with distilled water will react the remaining rubidium very rapidly.

Li: The techniques developed for decontaminating NaK, Na, and Rb cannot be used for lithium. With its high melting point (359°F), lithium is fairly stable at room temperature. In order to decontaminate the end of a valve line, one must remove the bulk of the lithium from the valve end. A successful method is to use an auger to hand drill the lithium from within the tube. The alkali metal remaining on the auger can be reacted by immersing it in pan of hot water. Repeated use of the auger can remove most of the metal. Then hot water dispensed from the syringe can be used for the final reaction. It has become evident that the bellows side of a valve cannot be completely decontaminated, therefore, selecting the direction of flow (arrow on valve) is most critical. Lithium was the most time consuming material to work with insofar as handling and decontamination was concerned.

APPENDIX B

TRANSFER OF ALKALI METAL FROM ONE CONTAINER TO ANOTHER
(Method Monitors Weight During Transfer)

PURPOSE: 1. To transfer liquid alkali metal from one vessel to another.

2. To monitor the weight during transfer.

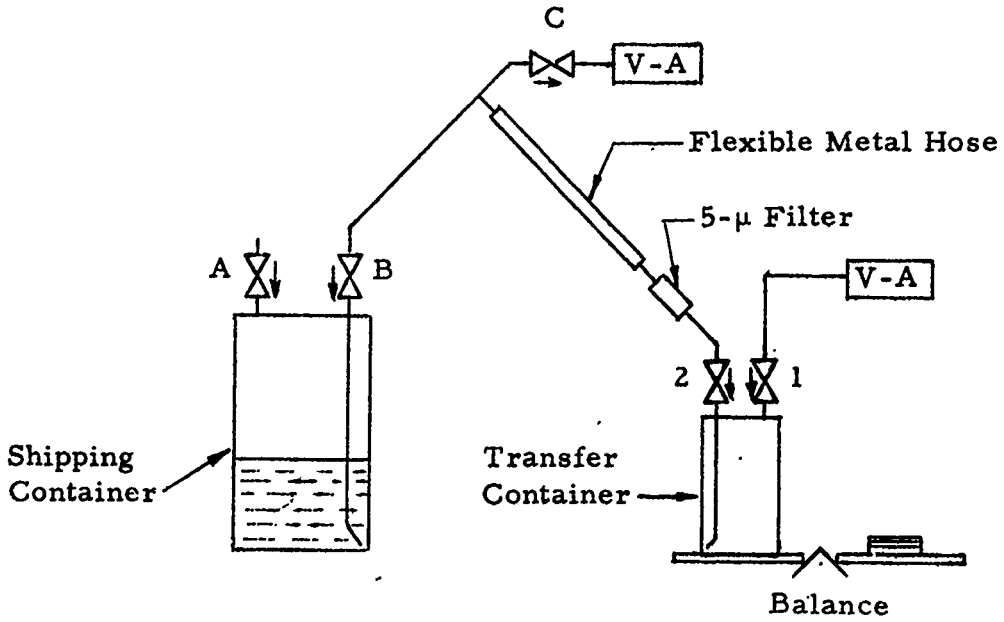

PROCEDURE:

1. Attach shipping container to transfer container as shown.
2. A, B, C closed; 1 and 2 open.
3. V-A cycle 3 times to C.
4. Finish with 20 psi to C.
5. V-A cycle 3 times through 1 and 2 to B and C.
6. Finish with vacuum to 1 and close 1 (2 remains open).
7. Zero in torsion balance (note tare on scale).
8. Crack B (fill transfer container to desired volume, i.e., by weight determination), then close B.
9. Crack C until bubbling is heard in transfer container.
10. Continue until bubbling stops at which time there is 20 psi argon pressure over the alkali metal. Close C and 2.
11. Decontaminate trapped alkali metal in flexible hose, filter, line B-C and on atmosphere side of B and 2.

TRANSFER OF NORMALLY-SOLID ALKALI METAL

STEP I.

PURPOSE: 1. Adjust pressure in container to a known value.

2. Insure a full dip tube for subsequent transfers.

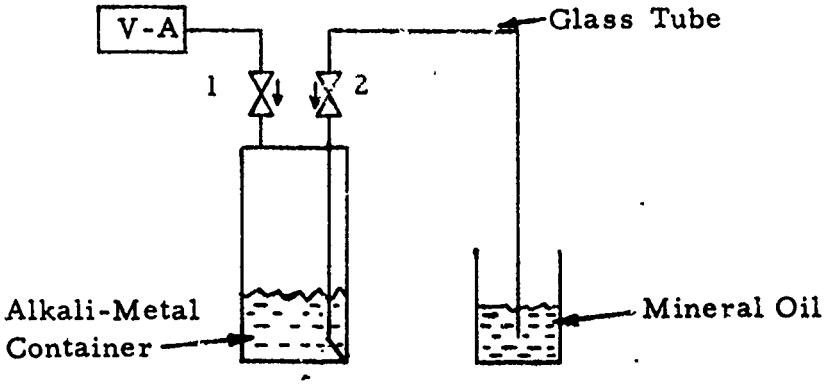

PROCEDURE:

1. Connect as shown.
2. Heat container and valves to melt alkali metal.
3. V-A cycle 3 times to 1.
4. Finish with 20 psi to 1.
5. Open 1.
6. Crack 2 until liquid metal can be seen in glass tube.
7. Close 2.
8. Remove glass tube and fitting at 2.
9. Decontaminate trapped alkali metal on atmosphere side of 2.
10. Keep alkali-metal container upright at all times (this prevents inert gas from entering dip tube which would otherwise yield a false sample volume).

NOTE: All active portions of system including valve bodies wrapped with electrical heating tape.

STEP II.

PURPOSE: To fill a sample tube of known volume with alkali metal.

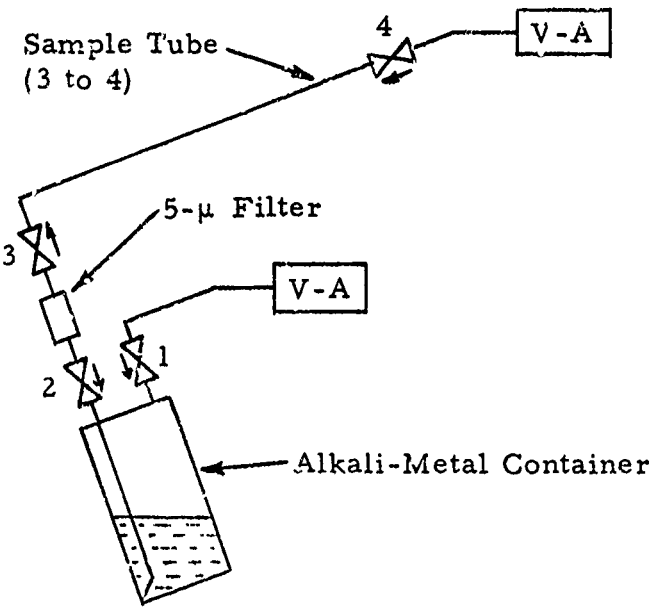

PROCEDURE:

1. Connect as shown (tilted); filter may be used for cold trapping.
2. Heat all lines, valves, and alkali-metal container to desired value.
3. Valves 1, 2 closed; valves 3, 4 open.
4. V-A cycle 3 times to 4.
5. Finish with vacuum to 2 and close 4 (3 remains open).
6. V-A cycle 3 times to 1.
7. Finish with 20 psi to 1.
8. Open 1, crack 2, and listen for sample tube to fill.
9. Close 1, 2, and 3.
10. Disconnect between 3 and filter and 2.
11. Decontaminate trapped alkali metal in filter and on atmosphere side of 2 and 3.

NOTE: All active portions of system including valve bodies wrapped with electrical heating tape.

STEP IIIa (ALTERNATE)

PURPOSE: To load a pressurized apparatus from sample tube of known volume

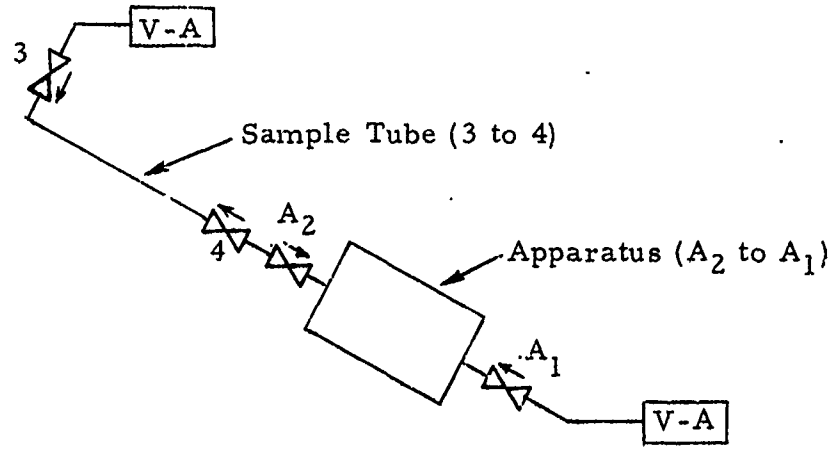

PROCEDURE:

1. Heat apparatus, valve manifold, and all lines to desired value.
2. Energize liquid level gage.
3. Close 3 and 4; sample tube full.
4. Open A_1, A_2.
5. V-A cycle 3 times through A_1 and A_2 to 4.
6. Finish with 5 psi to 4; close A_1.
7. Remove V-A line from A_1; attach bleed line to A_1 (for bleeding gas under oil).

NOTE: All active portions of system including valve bodies wrapped with electrical heating tape.

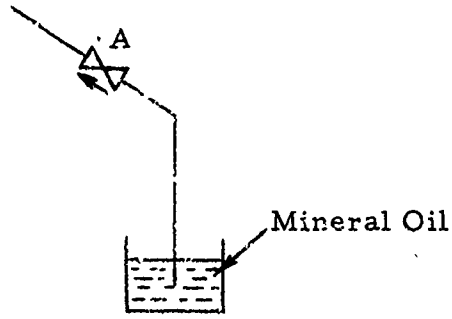

8. V-A cycle 3 times to 3.

9. Finish with 20 psi to 3.

10. Crack A_1 to start bleed.

11. Open 3 and then crack 4 (liquid being displaced from sample tube). Monitor liquid level gage during fill.

12. When transfer completed, close A_1 (pressurizing at 20 psi from 3 to A_1). Close 3, 4, and A_2.

13. Disconnect between A_2 and 4.

14. Decontaminate trapped alkali metal in sample tube and on atmosphere side of A_2.

STEP IIIb (ALTERNATE)

PURPOSE: To load an evacuated apparatus from sample tube of known volume.

NOTE: Same sketch as on STEP IIIa (ALTERNATE)

PROCEDURE:

1. Heat apparatus, valve manifold, and all lines to desired value.

2. Energize liquid level gage.

3. Close 3 and 4; sample tube full.

4. Open A_1, A_2.

5. V-A cycle 3 times through A_1 and A_2 to 4.

6. Finish with vacuum to 4; close A_1.

7. V-A cycle 3 times to 3.

8. Finish with 20 psi to 3.

9. Open 3.

10. Crack 4 (liquid being displaced from sample tube). Monitor liquid level gage during fill.

11. When transfer complete, close A_2, 3 and 4. (Apparatus now contains alkali metal at 20 psi; gas pressure.)

12. Disconnect between A_2 and 4.

13. Decontaminate trapped alkali metal in sample tube and on atmosphere side of A_2.

APPENDIX C

MELTING POINT-BOILING POINT APPARATUS OPERATING PROCEDURE

1. The apparatus is initially under 5 psig argon pressure.
2. Actuate recording potentiometer.
3. Turn on clam-shell heater transformer to about 40%.
4. Monitor alkali metal temperature rise with recording potentiometer.
5. When melting point plateau is first reached switch to bench potentiometer and take several readings.
6. Once the alkali metal is completely melted, the temperature will rise.
7. Turn heater voltage to zero.
8. Remove the apparatus from the heater housing (monitor recording potentiometer for freezing point).
9. Read freezing point plateau with bench potentiometer.

NOTE: For boiling point determination: Install a bleed line to the gas valve and continually bleed apparatus to atmospheric pressure during run.

NOTE: Record Barometric Pressure.

VISCOMETER OPERATING PROCEDURE

Note: Refer to schematic diagram of viscometer in text for nomenclature

1. Energize all instruments (loaded apparatus is vertical and under positive pressure).

2. A_1, A_2, A_3 closed.

3. Heat apparatus and valve manifold to desired temperature.

4. Attach bleed line to A_1 and bleed under oil to atmosphere.

5. Close A_1 and transfer bleed line from A_1 to A_2. Attach flexible V-A line to A_1.

6. V-A cycle 3 times to A_1.

7. Rotate apparatus ccw to predetermined angle.

8. Apply 5 psi to A_1 (recorder should show reservoir filling).

9. Close A_1 when reservoir full.

10. Rotate viscometer cw to vertical and immediately open A_3 to start run.

11. As soon as reservoir is empty, rotate ccw to angle-stop, bleed under oil through A_2 with A_3 open.

12. Close A_3 and A_2.

13. Repeat items 8 through 12 for subsequent runs.

VISCOMETER DECONTAMINATION PROCEDURE

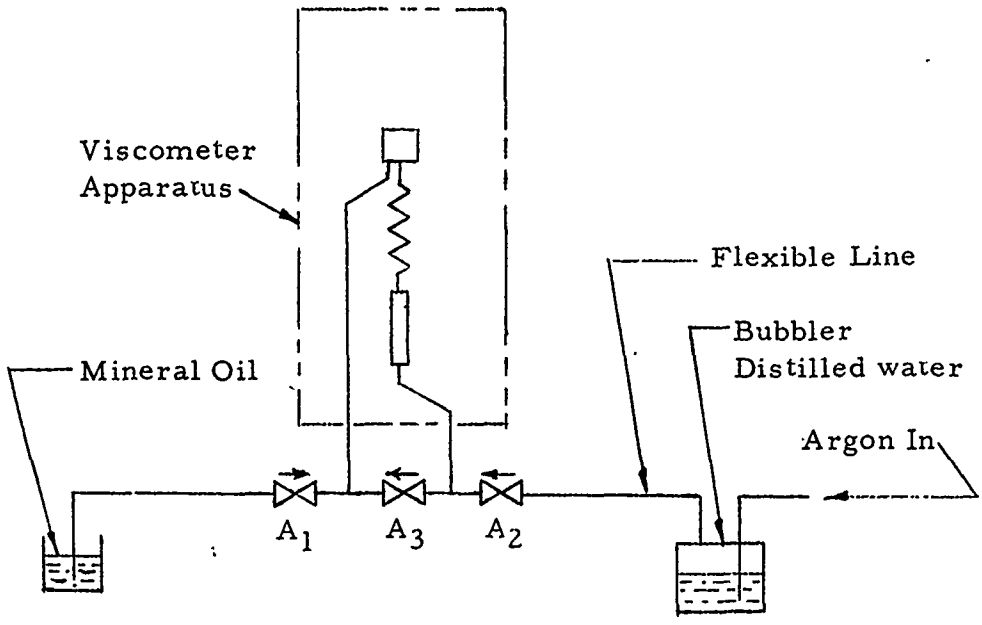

1. Alkali metal previously flushed out of apparatus.
2. Attach as shown. A_1 open; A_3 closed; A_2 open.
3. Bubble moist gas through apparatus; monitor temperature.
4. If temperature does not rise after 4 hours, proceed to step 5; if temperature rises, continue bubbling until nearly all alkali metal has reacted.
5. Invert bubbler to allow small amount of water into apparatus.
6. Repeat 5 times until reaction decreases, then add large quantities of water.
7. Close A_1 and A_2; disconnect oil line and bubbler.
8. Rotate apparatus to upright position.
9. Remove manifold; decontaminate manifold.
10. Attach flexible line to bypass and attach drain line.
11. Circulate water through viscometer until water clears.
12. Drain water from apparatus under argon pressure.
13. Dry apparatus with heat and argon flowing.
14. Leave under 20 psi argon; turn off heat and cap ends.

ALKALI METAL LOOP OPERATING PROCEDURES

1. Turn on main power switches.

2. Turn on temperature indicator and temperature recorder.

3. Make sure pump transformer is set at zero.

4. Turn on loop line heaters to desired value.

5. As loop is heating, adjust transformers to provide uniform temperature throughout the loop.

6. Once the alkali metal is well above its melting point, the pump transformer may be actuated. Caution must be exercised not to accelerate the pump too rapidly otherwise alkali metal may be forced into the gas lines.

7. Once the pump is started, the temperatures throughout the loop will begin to merge.

8. Monitor the liquid level gage and flow meter occasionally.

9. Increase the pump transformer to about half of the maximum desired flow. (The temperatures will converge more rapidly as the flow increases).

10. Turn on balanced-pressure detector indicator lamps.

11. Decrease the flow to zero. Calibrate both suction and discharge balanced-pressure detector at no flow from 0 to 50 psig at 10 psi increments.

12. Increase the flow to 10% and record suction and discharge pressures from 0 to 50 psig at 10 psi increments.

13. Increase the flow to 20% and record pressures as in step #12.

14. Repeat, increasing flow until highest desired flow is attained.

15. Repeat step #11.

NOTE: Throughout the entire run, the temperature of the flow meter should be recorded.

NOTE: The loop should be left under 20 psig argon pressure when run is complete.

APPENDIX D

SAMPLING FROM TRANSFER CONTAINER OR APPARATUS

PURPOSE: To fill a sample bulb with alkali metal; weight of sample is determined by difference.

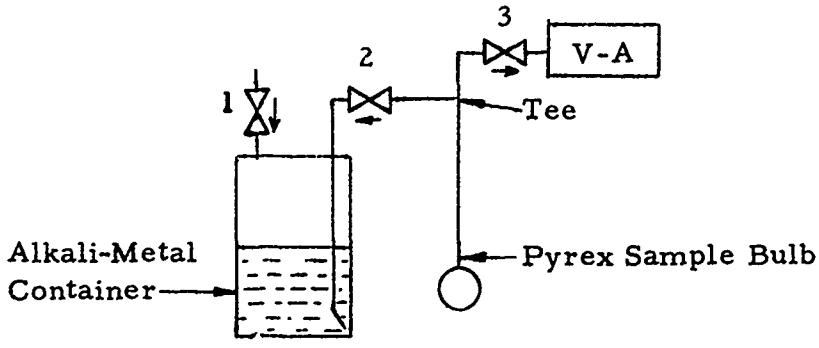

PROCEDURE:

1. Accurately weigh sample bulb.
2. Connect as shown.
3. Heat alkali-metal transfer container, valves and tee.
4. Valves 1 and 2 closed (container under 20 psi).
5. Valve 3 open.
6. V-A cycle 3 times to 2. During each vacuum cycle apply heat (heat gun) to sample bulb and stem.
7. Finish with vacuum to 2 (closed 3).
8. Crack 2; alkali metal enters sample tube; close 2.
9. Start vacuum pump and crack 3.
10. Finish with vacuum to bulb; close 3.
11. Heat seal sample bulb stem with torch.
12. Remove the glass stem attached to tee; decontaminate and dry.
13. Weigh stem and sample together.

NOTE: All active portions of system including valve bodies wrapped with electrical heating tape.

SAMPLING FROM TRANSFER CONTAINER OR APPARATUS
(For Li)

PURPOSE: To fill a plastic tube with alkali metal.

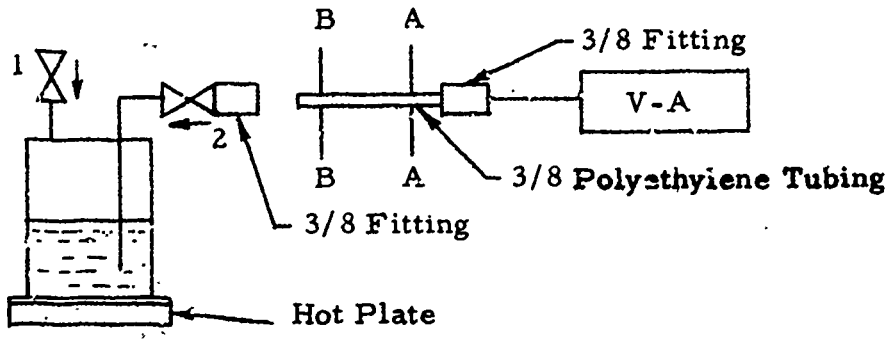

NOTE: Figure 17 in text illustrates sampling.

PROCEDURE:

1. Heat alkali metal transfer container and valves (monitor temperature of container to insure melting).

2. Once the lithium is completely melted, slip the polyethylene tubing into the valve fitting and tighten.

3. V-A cycle 3 times to 2.

4. Finish with vacuum to 2.

5. Use a conventional refrigeration pinch-off tool to pinch off polyethylene tubing at A-A.

6. Cut tubing to the right of pinch-off tool.

7. Heat seal flattened tubing at A-A with pinch-off tool in place.

8. Crack 2 and close 2 when desired quantity of alkali-metal enters tube and immediately apply liquid freon to cool sample.

9. Pinch off at B-B (semi-soft lithium will be displaced).

10. Cut tube to left of B-B with pinch-off tool still attached.

11. Remove exposed lithium, decontaminate, and argon dry prior to heat sealing B-B.

Aeronautical Systems Division, Dir/Aeromechanics, Aero Propulsion Lab, Wright-Patterson AFB, Ohio.
Rpt Nr ASD-TDR-63-413. CONTAMINATION EFFECTS ON LIQUID RUPIDIUM AND LIQUID LITHIUM SYSTEMS. Final report, May 63, 138p. incl illus., tables, 101 refs., appendixes.

Unclassified Report

A research program directed toward the goal of developing an improved understanding of contamination effects on liquid rubidium and liquid lithium system. is described. Experimental measurements were conducted on the vapor pressure of pure rubidium, the melting point of pure and oxygen-contaminated rubidium, and the melting point of

(over)

UNCLASSIFIED

1. Contamination (Abstract concepts)
2. Liquid metals
3. Lithium
4. Rubidium
I. AFSC Project 8169, Task 816902
II. Contract AF 33(657)-8657
III. Southwest Research Institute, San Antonio, Texas
IV. W. D. Weatherford, et al.
V. Aval fr OTS
VI. In ASTIA collection

UNCLASSIFIED

Aeronautical Systems Division, Dir/Aeromechanics, Aero Propulsion Lab, Wright-Patterson AFB, Ohio.
Rpt Nr ASD-TDR-63-413. CONTAMINATION EFFECTS ON LIQUID RUBIDIUM AND LIQUID LITHIUM SYSTEMS. Final report, May 63, 138p. incl illus., tables, 101 refs., appendixes.

Unclassified Report

A research program directed toward the goal of developing an improved understanding of contamination effects on liquid rubidium and liquid lithium systems is described. Experimental measurements were conducted on the vapor pressure of pure rubidium, the melting point of pure and oxygen-contaminated rubidium, and the melting point of

(over)

UNCLASSIFIED

1. Contamination (Abstract concepts)
2. Liquid metals
3. Lithium
4. Rubidium
I. AFSC Project 8169, Task 816902
II. Contract AF 33(657)-8657
III. Southwest Research Institute, San Antonio, Texas
IV. W. D. Weatherford, et al.
V. Aval fr OTS
VI. In ASTIA collection

UNCLASSIFIED

pure and nitrogen-contaminated lithium. A capillary viscometer was designed and constructed and extensive viscosity data were measured for pure and oxygen-contaminated rubidium from less than 200°F to about 1200°F. Pumping experiments in an isothermal loop revealed that oxygen contamination is quite deleterious to the electromagnetic pumping characteristics of rubidium. A new method was developed for the analysis of carbon in rubidium, and it was shown that the butyl bromide method for oxygen analysis is not applicable to rubidium. An alternate oxygen-analysis procedure for rubidium, based upon melting-point measurements, is proposed.

pure and nitrogen-contaminated lithium. A capillary viscometer was designed and constructed and extensive viscosity data were measured for pure and oxygen-contaminated rubidium from less than 200°F to about 1200°F. Pumping experiments in an isothermal loop revealed that oxygen contamination is quite deleterious to the electromagnetic pumping characteristics of rubidium. A new method was developed for the analysis of carbon in rubidium, and it was shown that the butyl bromide method for oxygen analysis is not applicable to rubidium. An alternate oxygen-analysis procedure for rubidium, based upon melting-point measurements, is proposed.